İSTANBUL TECHNICAL UNIVERSITY ★ INSTITUTE OF SCIENCE AND TECHNOLOGY

SUBSTRUCTURAL EVOLUTION DURING SEVERE PLASTIC DEFORMATION OF ULTRA LOW CARBON STEEL

M.Sc. Thesis by

Fatih UYSAL, B.Sc.

Department :Metallurgical and Materials Engineering

Programme :Materials Engineering

JUNE 2008

İSTANBUL TECHNICAL UNIVERSITY ★ INSTITUTE OF SCIENCE AND TECHNOLOGY

SUBSTRUCTURAL EVOLUTION DURING SEVERE PLASTIC DEFORMATION OF ULTRA LOW CARBON STEEL

M.Sc. Thesis by
Fatih UYSAL, B.Sc.
(506061405)

Date of submission : 5 May 2008

Date of defence examination: 9 June 2008

Supervisor (Chairman): **Prof. Dr. Eyüp Sabri KAYALI**

Members of the Examining Committee **Prof.Dr. Hüseyin ÇİMENOĞLU (İ.T.Ü)**

Prof.Dr. Mehmet KOZ (M.Ü)

JUNE 2008

İSTANBUL TEKNİK ÜNİVERSİTESİ ★ FEN BİLİMLERİ ENSTİTÜSÜ

ULTRA DÜŞÜK KARBONLU ÇELİĞİN AŞIRI PLASTİK DEFORMASYONU ESNASINDA OLUŞAN ALTYAPISAL DEĞİŞİMLERİN İNCELENMESİ

YÜKSEK LİSANS TEZİ

Met. Müh. Fatih UYSAL

Tezin Enstitüye Verildiği Tarih : 5 Mayıs 2008

Tez Danışmanı : **Prof. Dr. Eyüp Sabri KAYALI**
Diğer Jüri Üyeleri **Prof.Dr. Hüseyin ÇİMENOĞLU (İ.T.Ü.)**
Prof.Dr. Mehmet KOZ (M.Ü.)

HAZİRAN 2008

ACKNOWLEDGEMENTS

Firstly I would like to thank my supervisor, Prof.Dr. Eyüp Sabri KAYALI, at Istanbul Technical University. His experiences and comments helped me a lot in adapting a new research environment and improving my skills. As well, I am grateful to Prof. Dr. Hüseyin ÇİMENOĞLU, for his support, guidance and incredible help.

Many thanks go out to the staff and students at Istanbul Technical University`s Department of Metallurgical and Materials Engineering. I would also like to thank Prof. Bert VERLINDEN and Prof. Marc SEEFELT from the Catholic University of Leuven, Department of Metallurgy and Materials Engineering (MTM), Heverlee, Belgium where I performed a big part of my experimental study. They shared their invaluable experience and knowledge in the severe plastic deformation area.

Assoc. Prof. Erdem ATAR was very helpful during my study in Istanbul Technical University. He kindly facilitated his extensive knowledge and different perspective in every aspect of my research. I would also like to thank Özgür ÇELİK for his help to understand indentation test device. Dr. Vanessa VIDAL and Liang Zhu are thanked for their help in orientation imaging microscopy and specimen preparation.

My classmates Gökhan BÜYÜKSARI and Eng. Ferhat OMAÇ were both great friends and great colleagues. Their existence eased the difficulties and helped to develop a productive research group. We discussed many issues together and helped each other through difficulties.

Finally, my family and my wife specially thanked for their continuous courage, confidence and love. They have been my strongest supporter during my study.

June, 2008 Fatih UYSAL

TABLE OF CONTENTS

ABBREVIATIONS

ECAP : Equal Channel Angular Pressing
ULC : Ultra Low Carbon
Th : Homologous Temperature
EBSD : Electron Backscatter Scanning Diffraction
UFG : Ultra Fine Grain
HPT : High Pressure Torsion
SPD : Severe Plastic Deformation
TMP : Thermo Mechanical Processing
GDR : Geometric Dynamic Recrystallization
ARB : Accumulative Roll Bonding
MAC/F : Multi-Axial Compression/ Forging
RCS : Repetitive Corrugation and Straightening
PM : Powder Metallurgy
RD-ECAP : Rotate Die Equal Channel Angular Pressing
PC : Parallel Channel
CSPD : Continuous Severe Plastic Deformation
C2S2 : Continuous Confined Strip Shearing
IDB : Incidental Dislocation Boundaries
GNB : Geometrical Necessary Boundaries
DB : Deformation Bands
MOA : Misorientation Angle
SB : Shear Bands
MB : Micro Bands
DDW : Dense Dislocation Wall
CB : Cell Blocks
LB : Laminar Boundaries
FCC : Face Centered Cubic
BCC : Based Centered Cubic
HAB : High Angle Boundary
LAB : Low Angle Boundary
ED : ECAP Direction
TD : Transverse Direction
OIM : Orientation Imaging Microscopy

LIST OF TABLES

Page No

LIST OF FIGURES

Page No

LIST OF SYMBOLS

σ_e : Flow stress
σ_i : Stress the resistance to a dislocation movement
k : Slip transition mechanism constant
d : Grain size
T_m : Melting temperature
θ : Die angle
 : Arc of curvature
N : Number of ECAP pass
ε_N : Equivalent strain
Hv : Vickers Hardness
Kv : Kilovolts
mN : Milinewton
h_c : Contact Depth

ULTRA DÜŞÜK KARBONLU ÇELİĞİN AŞIRI PLASTİK DEFORMASYONU SIRASINDA OLUŞAN ALTYAPISAL DEĞİŞİMLERİN İNCELENMESİ

ÖZET

Son on yılda, aşırı plastik deformasyona maruz kalan malzemelerin teknolojisi ve bilimi büyük bir evrime uğramıştır. Bu zaman diliminde görülen önemli gelişmeler, nano yapılı malzemeleri, Malzeme Biliminin önemli bir dal haline getirmiştir.

Malzemelerde aşırı plastik deformasyon metodunu uygulamak amacı ile özel metodlar geliştirilmiştir. Farklı metodların içerisinden eşit kesitli kanal içinde açılı presleme olarak bilinen (ECAP) teknik, herhangi bir artık porozite içermeyen, numune boyutunda herhangi bir değişim olmadan ultra-ince taneli malzeme üretime yeteneği ile diğer aşırı plastik deformasyon tekniklerine göre üstünlük sağlamıştır.

Ultra düşük karbonlu çelik numuneler 172 °C sıcaklıkta sırasıyla 1,2,3,4,5 ve 8 paso olmak üzere rota Bc metodunu kullanarak ECAP kalıbından geçirilmiştir. Preslenen her malzemeden mekanik ve mikroskobik karakterizasyon incelemelerinde kullanılmak üzere 3 adet numune belli standartlara göre kesilerek belli bir prosedürde numune hazırlama yöntemleriyle hazırlanmıştır.

Mekanik karakterizasyon aşamasında numunelere basma ve sertlik testleri, sertlik testleri mikro sertlik ve mikro indentasyon olmak üzere iki farklı yöntemle yapılmıştır. Mikroyapısal karakterizasyon kapsamında ise optik mikroskop çalışması ve taramalı elektron mikroskobi yöntemi olan EBSD tekniği kullanılarak OIM analizi yapılmıştır.

Bu çalışmada, düşük karbon içerikli çelik malzemenin aşırı deformasyon işlemi esnasında göstermiş olduğu yapısal değişimini incelemenin yanı sıra mekanik özelliklerde meydana gelen değişimlerin belirlenerek bu tekniğin düşük karbonlu çelik için uygulanabilir olduğunun gösterilmesi amaç edinilmiştir.

SUBSTRUCTURAL EVOLUTION DURING SEVERE PLASTIC DEFORMATION OF ULTRA LOW CARBON STEEL

SUMMARY

The science and the technology of materials subject to severe plastic deformation (SPD) has evolved largely during the past decade. In this period nano structured materials changed the status of material science.

Special methods are developed to apply SPD to metallic materials. Among these methods, ECAP process has advantages with the capability of producing relatively large, porosity free, fully-dense samples having ultra fine grain size in sub-micrometer or nanometer range. Throughout the ECAP/ECAE process there is a no change in sample size.

Coarse-grained billets of Ultra Low Carbon (ULC) steel has been pressed through an ECAP die at a homologous temperature $T_h = 0.25$ for 1, 2, 3, 4, 5 and 8 passes via route B_c. Each pressed billet is cut in three parts to investigate the strength in a compression test and to investigate the microstructure in two perpendicular sections using the OIM technique.

Microstructure and mechanical properties of successfully extruded billets were reported using optic microscopy, Electron Back Scattered Diffraction (EBSD) technique, compression tests and micro hardness measurements.

The ultimate goal of this study is to produce stabilized end microstructures with improved mechanical properties, demonstrate the applicability of ECAP on ULC steel and investigate substructural evolution of ULC steel.

1. INTRODUCTION

Materials with grain sizes smaller than 1 μm have received much attention in the past decade. These materials have been classified as ultra fine grain (UFG) materials (grain size 100 to 1000 nm) and nano-materials (grain size < 100 nm) depending on the grain size [1]. In the late 1990s, a lot of research projects performed to develop the new types of low carbon steel for the structural use to prepare the replacement of existing infrastructures and the construction of more gigantic infrastructures in the near future [2]. Accordingly, two categories of methods were developed, namely, the "bottom-up" and the "top-down" approaches. In the first method, fine grain materials are fabricated by assembling individual atoms or by consolidating nano particulate solids [3]. In the "top-down" method, the ultrafine-grained (UFG) material is obtained by deforming a bulk material with a relatively coarse grain size and processing it using severe plastic deformation (SPD), such as equal-channel angular pressing (ECAP), high-pressure torsion (HPT), multi-directional forging, twist extrusion and so on [4].

Several methods have been developed to obtain UFG materials through severe plastic deformation. Among them, the equal-channel angular pressing (ECAP) technique has been proved to be an effective method for the fabrication of various bulk UFG materials without residual porosity. In performing ECAP, a material is subjected to intense plastic straining by pressing a sample repeatedly through a die containing two channels, with equal cross-sections, intersecting at an angle [5].

It is now well established that processing through the application of severe plastic deformation is especially effective in refining the grain size of bulk polycrystalline solids [6]. Typically, a process such as equal-channel angular pressing (ECAP), in which a sample is pressed through a die constrained within a channel bent through an abrupt angle, is capable of producing a submicrometer grain size in a wide range of materials.

Furthermore, ECAP is an attractive procedure because it can be scaled up fairly easily to produce relatively large bulk samples [7].Compared to the other SPD techniques, ECAP has some more advantages;

- ✓ It can be applied to fairly large billets,
- ✓ It is relatively simple procedure,
- ✓ It can be applied to materials with a different crystal structures, alloys, intermetallics and metal-matrix composites,
- ✓ And deformed material is reasonably homogeneous.

The present research was designed to extend the results by conducting experiments using an ultra low-carbon steel. Specifically, the objectives were investigate the grain refinement and substructure evolution achieved by ECAP and evaluate the mechanical properties of the steel in the initial condition and as-pressed condition.

2. ULTRAFINE GRAINED MATERIALS

Ultrafine grained materials (UFG) usually refer to materials with grain sizes of ~1 μm or sub micrometer level by comparison to coarse-grained materials. In some cases, ultrafine-grained materials also refer to nano crystalline materials with grain sizes in the range of 10-100 nμ. Currently considerable interest is focusing on fabrication of ultrafine-grained materials and extensive research work has been conducted to evaluate the characteristics of UFG materials. The increasing interest in UFG materials arises mainly for two reasons. Firstly, it is known that in all alloys the Hall-Petch effect contributes to the strengthening at room temperature by the relationship;

$$\sigma_e = \sigma_i + kd^{-m} \tag{2.1}$$

Where σ_e is the flow stress, σ_i is the stress characterizing the resistance to dislocation movement within the grain, k is a constant depending on the mechanism of slip transition through the grain boundary, d is the grain size and m is an exponent approximately equal to 0.5 depending on the nature of the alloy [8].

It is thus possible to conclude that UFG materials have larger strengths than coarse-grained materials. Secondly, it has been established that the retention of ultrafine grain sizes at high temperatures, typically sizes of 0.01-10 μm at temperatures >0.5 Tm, where Tm is the absolute melting point, favors flow in the form of a grain boundary sliding accommodating diffusion-controlled processes and thus offers a potential of achieving superplastic ductilities [9].

Moreover, the rate of flow is inversely proportional to the square of the grain size in the regime of superplastic flow [10]. Accordingly, UFG materials have the potential for high strain-rate superplasticity as well.

2.1 Methods of fabrication of ultrafine grained materials

Several methods have been developed to attain ultrafine-grained materials and nanocrystalline materials. Traditionally, small grain sizes are obtained using appropriate thermomechanical processing (TMP) methods, where a continuous recrystallization process termed as geometric dynamic recrystallization (GDR) is usually observed [11].

However, TMP methods can only produce materials with grain sizes in the range of 1-10 μm and the refinement of grain sizes is achieved by specific processing route involving specially designed heat treatments which lead to an increase in the expense. Therefore, the TMP methods are not suitable for the production of UFG materials.

Later, inert gas condensation [11, 12], high-energy ball milling [13] and sliding wear [14] were developed to produce UFG materials. These methods are very effective to refine grain sizes, even to the nanometer level, and avoid extensive heat treatment procedures. However, all these methods involve the compaction of nano-powders to attain a solid sample and thus are not capable of producing bulk samples in a fully-dense condition.

Therefore these methods are not sufficiently ready to explore industrial applications of UFG materials. The techniques based on powder metallurgy and rapid solidification all lead to flaws, pores and impurities in the material that have a profound negative influence on the mechanical properties. Furthermore, they are not economical methods to produce large quantities of material. As for the traditional thermo mechanical treatments, they take a long time to develop and implement.

Recently, methods of severe plastic deformation (SPD) were introduced in producing ultrafine-grained materials [6, 15]. Unlike conventional plastic deformation methods, such as cold rolling or drawing, methods of SPD can readily attain very refined micro structures at low temperatures with the imposition of a high pressure, and the structures consist of a large number of high angle boundary grains in the sub micrometer range giving dramatic changes in properties.

Furthermore, methods of SPD are capable of producing bulk samples in a fully-dense condition, therefore showing a potential for use in industrial applications.

Severe plastic deformation processes can be defined as those processes that induce very high plastic strain in a metal in order to cause grain refinement. Though such processes have been around for many decades, there has been a recent upsurge in a new class of SPD processes which generally have one characteristic feature, namely the size and shape of the work-piece remains unchanged after SPD processing.

Older techniques, such as forging, extrusion or rolling, used either singly or in combination, result in a product shape substantially different from the starting billet. Extrusion, for example, can impart very large strains by reductions in area of 100:1 or greater. But the extrudate is generally longer and of smaller cross section than the starting billet.

2.1.1 Severe plastic deformation (SPD) processes

The new SPD processes, such as equal channel angular extrusion or pressing (ECAE/P), high pressure torsion (HPT), accumulative roll bonding (ARB) and multi-axial compression/forging (MAC/F) all aim to keep the starting and finishing work piece shapes the same. ECAE/P, on which the current project is based on, is discussed below, followed by some of the other processes. Among the processes discussed, some like ECAE/P, MAC/F, and HPT introduce severe plastic deformation on bulk materials, while others like ARB, RCS, and Con-shear work on sheet materials.

2.1.1.1 High pressure torsion (HPT)

Severe plastic deformation by high pressure torsion involves in the deformation of discs by pure shear between two anvils in which one anvil rotates against the other anvil holding the material as shown in Figure 2.1 [16, 17]. This method is limited to small discs. The deformation induced during HPT is non uniform from the center to the outside diameter [16].

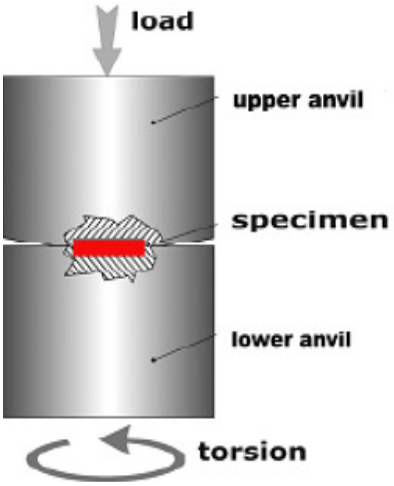

Figure 2.1: Schematic of High Pressure Torsion [16]

2.1.1.2 Multi-axial compressions/forgings (MAC/F)

Multi-Axial Compressions/Forgings involves the deformation of a rectangular cross section samples through a series of compressions so that the initial dimensions of the billet are retained. The loading direction is changed through 90º between successive compressions [18, 19]. A schematic of one step multiple compression/forging is shown in Figure 2.2. Multi-Axial Compression/Forgings are effective in producing fine grain structure, but are deficient due to the non-uniform strain distribution along the billet cross-section. However this non-uniformity can be eliminated by very good lubrication of the billet and through a large number of compression/forgings steps.

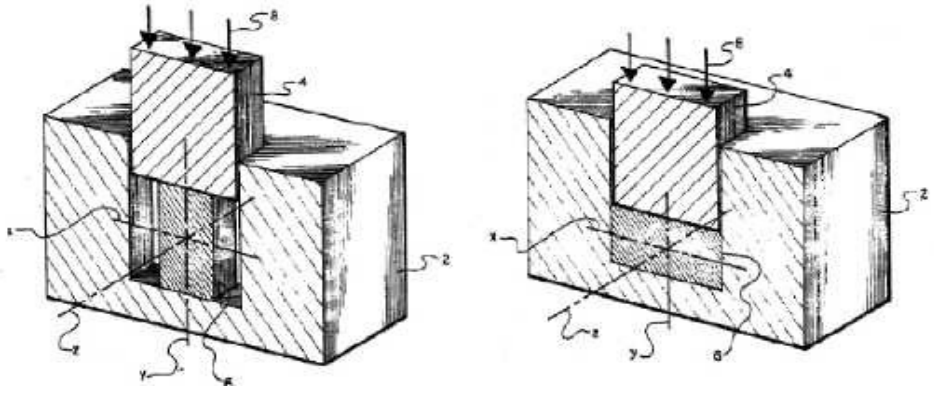

Figure 2.2: One step of the MAC/F Process [18]

2.1.1.3 Accumulative roll bonding (ARB)

Accumulative Roll Bonding (ARB) involves deforming a stack of two sheets of equal thickness to 50% reduction in thickness by plane strain rolling. This amount of reduction usually causes the sheets to bond together.

The rolled sheet is cut in half and stacked up to the initial thickness and rolled again to accumulate more strain. The sample dimensions are not changed during the processing, allowing the accumulation of large plastic strains [20]. A schematic of the ARB processes is shown in Figure 2.3.

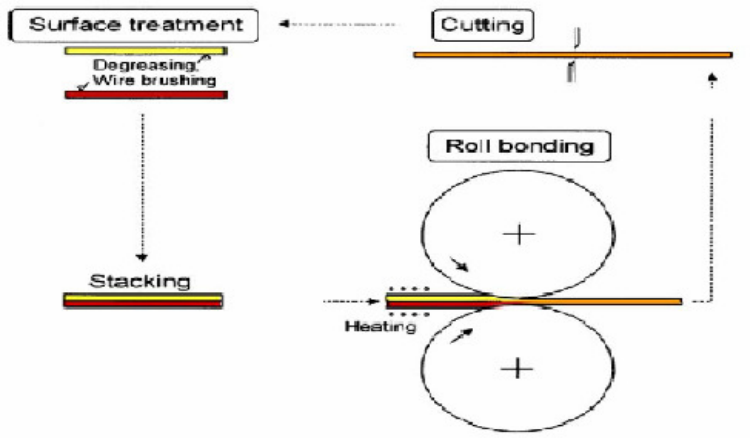

Figure 2.3: Schematic of the Accumulative Roll Bonding process [20]

2.1.1.4 Repetitive corrugation and straightening (RCS)

During the RCS process, the work piece undergoes repetitive bending and straightening, as shown in Figure 2.4. By this process, large strains are accumulated while maintaining the initial work piece shape [16]. This process can be either continuous or discontinuous, the work piece is flattened out by flat dies in the case of discontinuous process and smooth rolls in the case of continuous process.

2.1.1.5 Con-shearing process

The con-shearing process is a continuous pure shear deformation process. During the process, the sheet material is guided to an equal channel die by a large center roll, small satellite rolls, and guide shoe as shown in Figure 2.5. The material undergoes pure shear deformation as it passes through the equal channel die [21].

Since the die has equal channels, the thickness of the sheet is not changed, which allows multiple passes to accumulate more stain in the material.

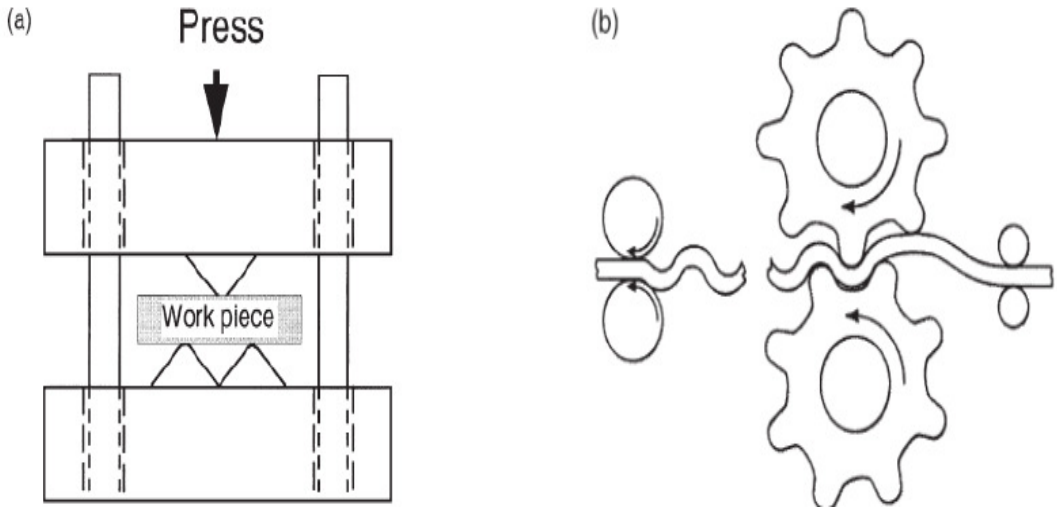

Figure 2.4: Schematic of Repetitive Corrugation and Straightening [16]; (a) Discontinuous and (b) Continuous

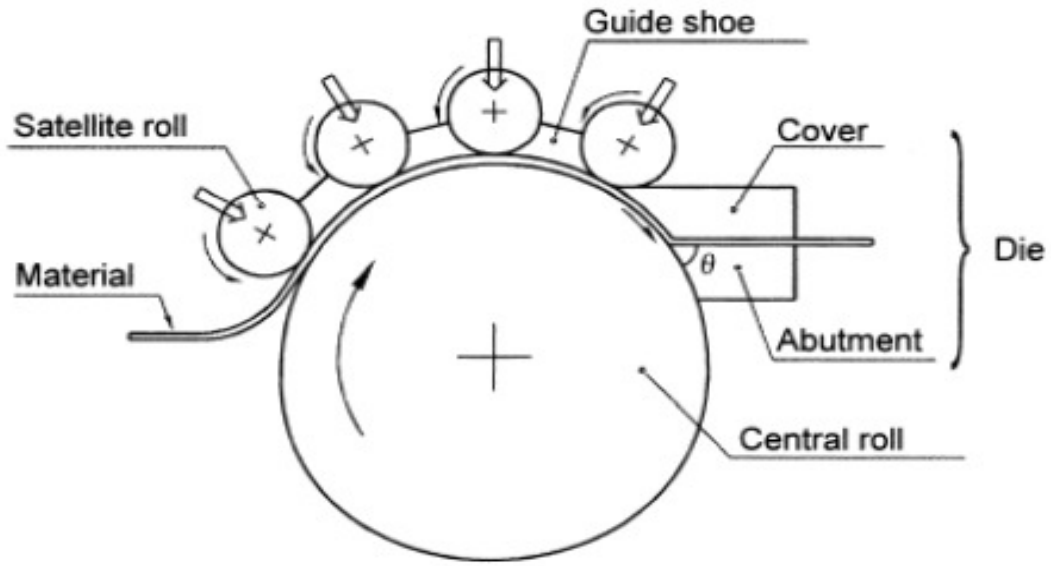

Figure 2.5: Schematic of Con-shear process [21]

3. OVERVIEW OF EQUAL CHANNEL ANGULAR PRESSING (ECAP)

3.1 Principle of ECAP

Although several of the SPD methods developed to date have been shown to be capable of achieving ultrafine-grained structures, the ECAP method is most attractive among all of them because of the large size of the sample which is capable of scale-up and the relatively simple process. As shown in Fig. 3.1, the basic principle of the ECAP process is to press a sample through a die having two intersecting channels, where the two channels have identical cross-sections so that the cross-section of the sample experiences no change during pressing. On passage through the die, the sample undergoes straining by simple shear as illustrated schematically in Fig. 3.2. The simple shear is imposed at the shearing plane of the sample between two adjacent segments labeled 1 and 2. Simple shear is considered a "near ideal" deformation method for structure and texture formation in metal working [22-24] and it enables the sample to be subjected to a large amount of strain without the damage that occurs in conventional metal working such as rolling. Also, the unchanged cross-section of the sample makes it possible for the sample to be processed by ECAP repetitively and thus to accumulate very large shear strains.

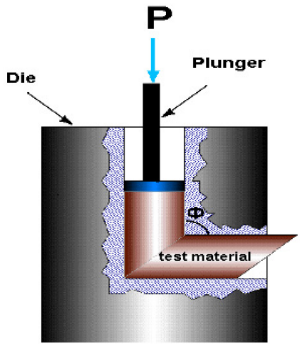

Figure 3.1: The Principle of ECAP [22]

As shown in Fig. 3.1, a specially-designed die is used in ECAP and two internal angles Φ and Ψ are defined as the curvature associated with the two channels where Φ corresponds to the angle between the two intersecting channels and Ψ is the angle at the outer arc of curvature of the two intersecting channels. In spite of two angles Φ and Ψ, the dimensions of the two channels are also important parameters of the die. Although it is theoretically defined that the two channels have identical cross-sections, the entrance channel is sometimes designed to be slightly larger than the exit channel to make the reinsertion of the sample into the channel easier. However, the allowance of the difference between two channels is quite small, usually less than 5%, otherwise the sample may be bent during pressing and this will result in straining other than simple shear and a reduction in the imposed shear strain. Moreover, inhomogeneous deformation is introduced in that case.

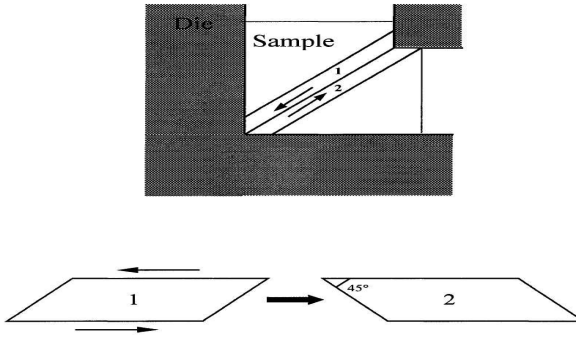

Figure 3.2: The principle of shearing in the sample during ECAP [23]

So far there are mainly two kinds of dies used in ECAP according to the different fabrications of two channels: split dies and solid dies [25]. In the split die, the channels are cut from a steel plate and the die is manufactured by combining the plate having channels with another flat plate by bolts; whereas the solid die is made by drilling a single channel of L-shape in a block of steel. The split die allows varying shape of channels and easy control of the two internal angles, but in practice, the sample pressing through the split die easily forms a thin sheet along the interface between the two combined plates. The formation of a thin sheet at the sides of the sample makes the sample unable to fit in the entrance channel without polishing and thus this is inefficient for repetitive pressing.

The solid die solves the problem of the material extruding between the two plates under high pressure and simplifies the repetitive pressing process. But in practice it is difficult to fabricate channels with polygonal shaped cross sections or a sharp corner with □ = 0°, and this limits the variance of the shape of the sample and optimization of the angle □. Recently, a rotary die was designed for continuous ECAP process as well [26].

3.2 History of Equal-Channel Angular Pressing

Equal Channel Angular Pressing (ECAP) was invented in the former Soviet Union by Vladimir Segal in 1977, for which he obtained an Invention Certificate of the USSR, similar to a patent [27]. Researchers in the Texas A&M University's (TAMU) Deformation Processing Laboratory in the Department of Mechanical Engineering have been conducting research on the ECAE process since 1992. Dr. V. Segal was a research associate in the Lab from 1992 to 1995. ECAP is an innovative process capable of producing uniform plastic deformation in a variety of materials, without causing significant change in geometric shape or cross section. Multiple extrusions of billets by ECAP permit severe plastic deformation in bulk materials. By changing the orientation of the billet between successive extrusions, complex microstructures and textures can be developed. Many advantages were found with ECAP; a variety of microstructures, and equiaxed, laminar, and fibrous textures for many of the materials that were investigated at TAMU [28].

3.3 Advantages of ECAP Process

This technique has numerous advantages over the procedures previously described.

3.3.1 Possibility to introduce very large strains

The first and main advantage of the technique is that there are no major geometrical changes in the billet while it goes through the die, allowing the same billet to be processed several times and therefore the introduction of a very high level of strain inside the material. This is clearly a critical gain over traditional deformation techniques such as rolling or extrusion.

3.3.2 Homogeneous deformation

The deformation occurs by simple shear and therefore it is very homogeneous. This was confirmed in microstructural investigations and through finite element analysis.

3.3.3 Limited issues with porosity and impurities

In this procedure, bulk pieces of material are deformed in the solid state, and therefore there are no problems associated with porosity and also the impurity level remains low. Both are critical gains over PM techniques and rapid solidification.

3.3.4 Large billet size

The size of the deformed pieces is limited only by the size of the ECA die and the pressing capability of the press. Even with a small die. The pieces are easily larger than those commonly produced through PM or TS.

3.3.5 Low tensile stresses

Since the billet is in compression between the tool walls and the plunger while it is sheared, few areas are under tensile stresses and the structural damage to the billet is reduced during deformation, as in the classical case of deformation under hydrostatic pressure. Note that the ability to introduce a very large amount of homogeneous strain in conditions where tensile stresses are low can be used to understand the work hardening behavior at large strains, the so-called stage IV of work hardening [29].

3.4 Limitations of ECAP Process

Conventional ECAP involves pushing a billet through two channels that meet at an angle Φ is shown Figure 3.1. For an ideal rigid plastic material, once the applied force reaches a critical value, the billet material undergoes plastic deformation, and the process continues without further increase in load. To produce long pieces of processed material, one simply needs to take a longer starting stock. Some experimental results using soft thermoplastic materials reported in literature to confirm this is possible, and the accumulated strain is additive [30].

However when a metal billet is used, due to elastic deformation and the Poisson effect, there is a lateral expansion of the billet in the entrance channel, and very high frictional forces develop between the work-piece and the channel walls.

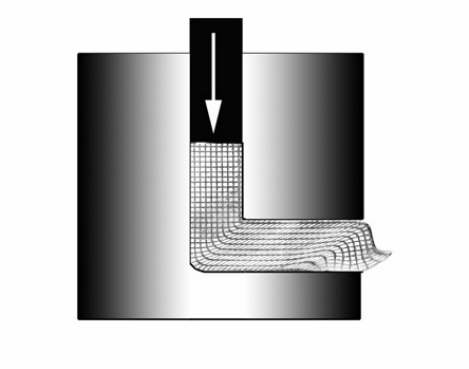

Figure 3.3: Principally sketch of ECA pressing [30]

The force required to press a billet through the die increases very rapidly with the length of the billet. Correspondingly, there is also a large increase in stresses experienced by the die. These two factors limit the length of the billet that can be practically processed by ECAP.

3.5 Applications of ECAP Technique

One of widely used SPD method ECAP can serve as a gateway to nanotechnology for traditional industry working with conventional materials and will boost the unrivalled innovation and competitiveness of European industry. Since most technical alloys show a positive response to ECAP, its impact on industries producing and using these new materials will be considerable and will increase further when commercialization brings additional momentum.

Markets targeted include:

- Automotive,
- Aircraft,
- Implants,
- Sports & Leisure and
- Energy storage.

Bolts, fasteners and screws can be readily manufactured from the billets available at ARC [31].

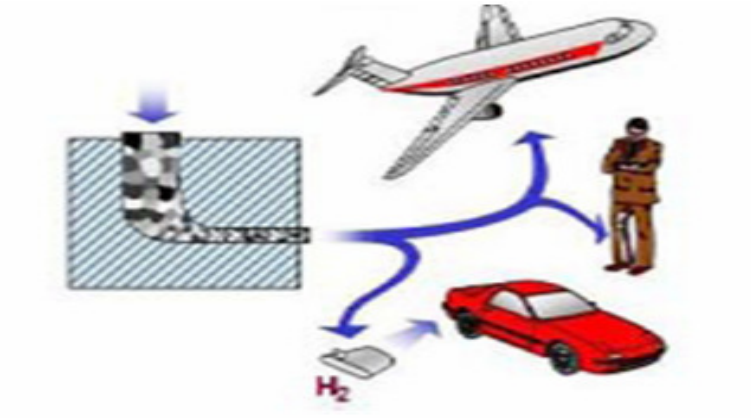

Figure 3.4: Applications of ECAP [32]

Substantially improved fatigue lifetimes and increased damage tolerances will pave the way for industrial applications. Safe working conditions can be guaranteed due to the absence of potentially hazardous nano particles in the production process. With regard to medical usage, SPD-strengthened pure alloys have improved biocompatibility and may even be soluble (as in the case of stents). Storing hydrogen in nano scale magnesium is predicted to have an extremely beneficial impact on the environment and the automotive industry expects SPD materials to further increase passenger comfort and safety by the use of lightweight structures.

3.6 ECAP Developments

Being the most popular process, ECAP has experienced several alterations or modifications. Modifications of the outlet channel will increase the process force and decrease the tool life. Using small slenderness of the billet or increasing the angle between consecutive channels in the die can help reduce the force. Most small design alterations have only a limited impact on improving the processing conditions. Thus modifications which improve the performance of the ECAP method are of considerable importance to industry.

3.6.1 Outer channel modifications

To deal with friction Segal invented movable walls in the channels (Fig. 4a). Stecher and Thomson (Fig. 4b) introduced a die equipped with a cylindrical surface in the form of a rotatable roll to avoid friction. Markushev et al. patented an unequal channel extrusion in which the billet changes its cross-section in the outlet channel (Fig. 4c) [33].

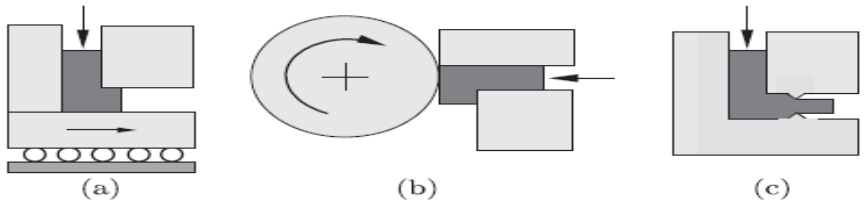

Figure 3.5: Modifications of ECAP: a) movable wall, b) rotatable roll, c) profiled output channel [43]

3.6.2 Rotary die ECAP process

We have developed the new ECAP (Equal channel angular pressing) process termed RD (Rotary-Die) ECAP. In current ECAP, a billet is repeatedly passed through two channels of equal cross-section intersecting at an angle. Then, intense plastic strain is introduced in a material without changing the cross-sectional area. RD-ECAP is differentiated from current ECAP by the following characteristics.

- ✓ Billet removal and re-insertion between passes are not required.
- ✓ The ECAP time is reduced by more than 75% compared to ordinary ECAP.
- ✓ The ECAP temperature can be precisely controlled and altered for different passes.

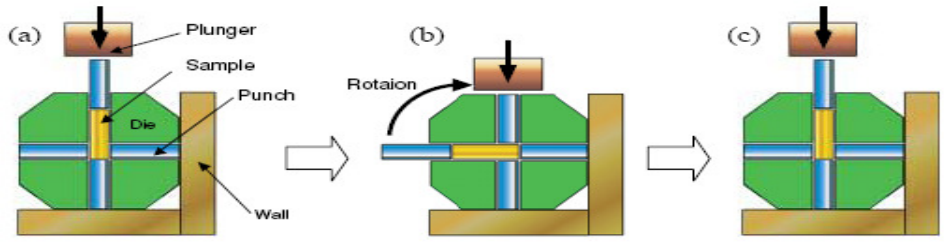

Figure 3.6: The ECAP process using a rotary-die; (a) initial state, (b) after one pass and (c) after 90° die rotation [34]

3.6.3 Developing ECAP with parallel channels

The distinctive feature of ECAP in parallel channels is the fact that during one processing cycle as much as two shear events take place. This can result in a considerable reduction in the number of cycles at UFG structure formation. In theory, a billet does not change its initial shape and it is very important to put this condition into practice. However, the value of channels displacement *K*, and the angle of channels intersection, Φ, can influence the flow pattern, strain–stress state and power characteristics of ECAP process [35].

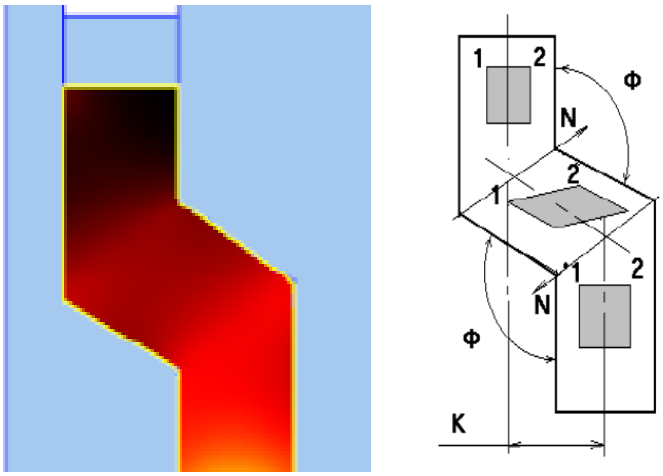

Figure 3.7: The ECAP process with parallel channel [35]

3.6.4 Continuous processing by ECAP

Several techniques for producing ultrafine grained materials are currently being investigated. These techniques are limited in their ability to produce the size and quantities of material needed for commercial use. One technique to produce ultrafine grained materials is the Equal Channel Angular Pressing (ECAP) process.

This technique is a multi-step batch process that produces small cross-section, short-length stock, which severely limits its commercialization. The Continuous Severe Plastic Deformation (CSPD) process will overcome the limitations of ECAP by producing large cross-section, continuous-length stock.

3.6.4.1 Continuous confined strip shearing (C2S2)

A process was developed using a rolling facility combined with the principles of ECAP. This process was variously designated continuous confined strip shearing (C2S2). The material is in the form of a thin strip and it is fed into the facility between two rolls, extruded slightly to reduce the thickness from 1.55 to 1.45 mm, and then it flows into the outlet channel where the original thickness of 1.55 mm is restored. The terminology C2S2 arises therefore because of the small difference in the thickness associated with the passage into the outlet channel [36].

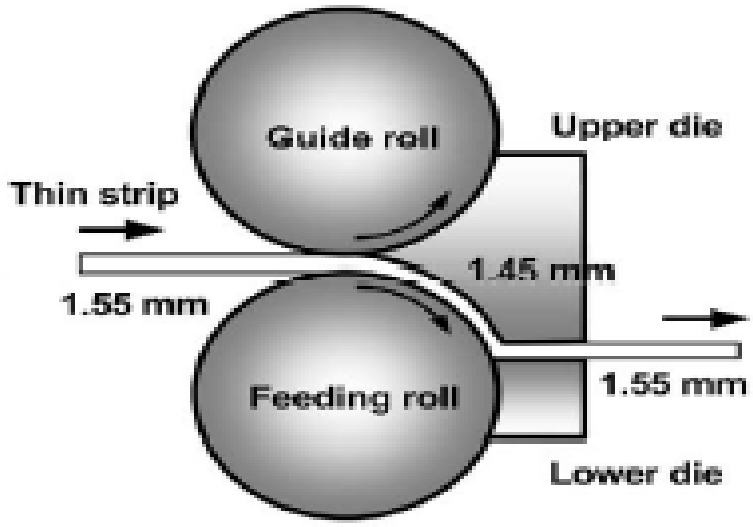

Figure 3.8: The ECAP process with parallel channel [36]

3.6.4.2 The ECAP-conform process

The conform extrusion process was developed over thirty years ago for the continuous extrusion of wire products but in recent time it has been combined with equal channel angular pressing in the ECAP-conform process. The designed ECAP-conform set-up is shown schematically in Fig. 3.9. As shown, a rotating shaft in the center contains a groove, into which the work-piece is fed. The work-piece is driven forward by frictional forces on the three contact interfaces with the groove, which makes the work-piece rotate with the shaft.

The work-piece is constrained to the groove by a stationary constraint die. The stationary constraint die also stops the work-piece and forces it to turn an angle by shear as in a regular ECAP process. This set up effectively makes ECAP continuous [37].

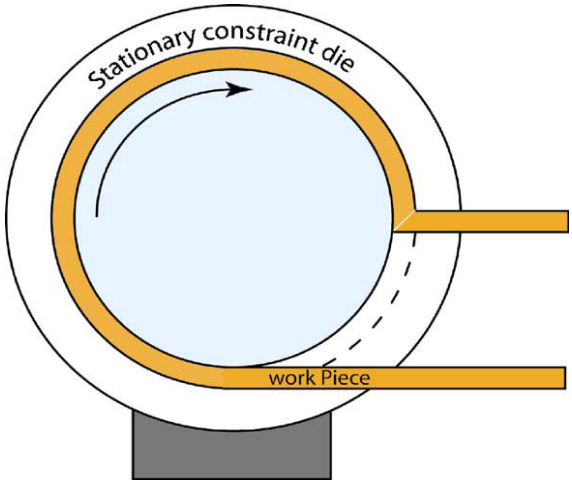

Figure 3.9: A schematic illustration of an ECAP–Conform set up [37]

3.7 Fundamental Parameters in ECAP

3.7.1 The strain imposed in ECAP

For every passage through the ECAP die, an abrupt strain is imposed on the sample. The precise value of the Von Mises equivalent strain is dependent on the channel angle Φ and the arc of the curvature Ψ. Since the cross sectional dimensions of the sample remain unchanged with a single passage through the die, the sample may be pressed repetitively through the die in order to achieve a very high strain. The total strain accumulated through a series of repetitive pressings, ε_N, is given by Eq. 3.1, where N is the total number of passes through the die [38].

$$\varepsilon_N = \frac{N}{\sqrt{3}}\left[2\cot\left(\frac{\Phi}{2}+\frac{\Psi}{2}\right)+\Phi\cos ec\left(\frac{\Phi}{2}+\frac{\Psi}{2}\right)\right] \quad \textbf{(3.1)}$$

From this equation, it is clear that the strain in every passage has the same value. Fig.3.10. shows how the equivalent strain imposed by single passes changes with Φ and Ψ.

When the channel angle is equal to 90° which is most frequently used, the Von Mises strain is around 1 and it is not largely influenced by the arc of the curvature Ψ. Therefore, the strain is close to N for a total of N passes through the die. It is important to mention that the Von Mises strain has an accumulated value, not taking the different processing route into account.

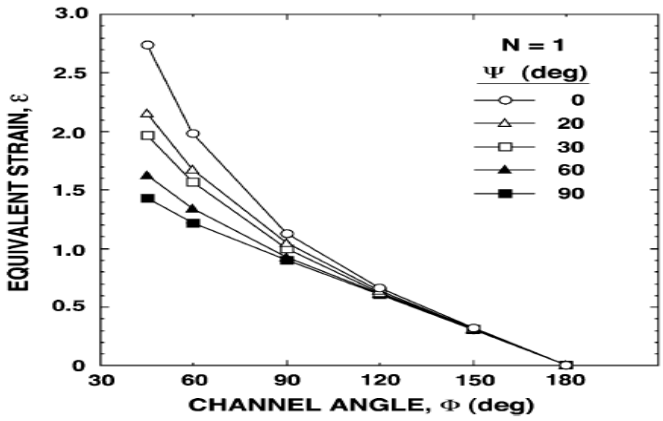

Figure 3.10: Variation of the equivalent strain, ε, with the channel angle, Φ, over an angular range of Φ from 45° to 180° for the angle of the arc of curvature, Ψ, form 0° to 90° ; the strains are shown for a single pass where N=1 [38]

3.7.2 The processing routes in ECAP

There are mainly four basic processing routes in ECAP [38]. These routes activate different sets of slip systems during the pressing operation so that they lead to significant differences in the microstructures produced by ECAP. The four different processing routes are summarized schematically in Fig.3.11. In route A the sample is pressed without rotation, in route B_A the sample is rotated around the X-axis by 90° in alternate directions between consecutive passes, in route B_C the sample is rotated by 90° in the same sense (either clockwise or counter clockwise) between each pass and in route C the sample is rotated by 180° between passes.

Various combinations of these routes are also possible, such as combining routes B_C and C by alternating rotations through 90° and 180° after every pass, but in practice the experimental evidence obtained to date suggests that these more complex combinations lead to no additional improvement in the mechanical properties of the as-pressed materials [39].

Accordingly, for the simple processing of bars or rods, attention is generally devoted exclusively to those four processing routes.

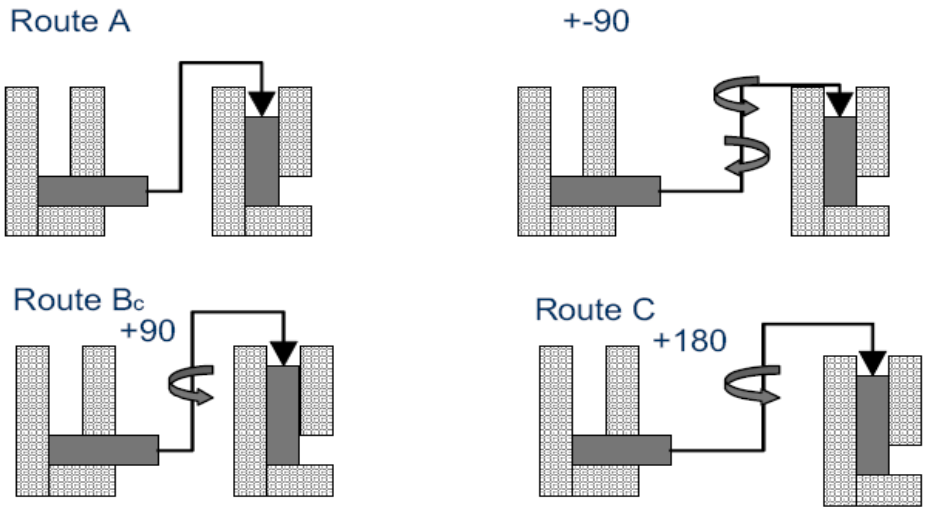

Figure 3.11: The four fundamental processing routes in ECAP [38]

The four classical ECAP routes A, C, B_A and B_C have a significantly different impact on the grain refinement. Route C is distinctly less efficient than the other routes, while route B_C yields the most homogenously refined and equiaxed microstructure.

3.7.3 Slip systems and shearing pattern

The different slip systems associated with these various processing routes are depicted schematically in Fig.3.12.(a) where the X, Y and Z planes correspond to the three orthogonal planes and slip is shown for different passes in each processing route. The planes labeled 1 through 4 correspond to the first 4 passes of ECAP.

In route C, the shearing continues on the same plane in each consecutive passage through the die but the direction of shear is reversed on each pass. As a result, route C is termed a redundant strain process and the strain is restored after every even number of passes. It is apparent that route B_C is also a redundant strain process because slips in the first pass is cancelled by slip in the third pass and slip in the second pass is cancelled by slip in the fourth pass [38]. By contrast, routes A and B_A are not redundant strain processes and there are two separate shearing planes intersecting at an angle of 90° in route A and four distinct shearing planes intersecting at angles of 120° in route B_A.

In routes A and B_A, there is a cumulative build-up of additional strain on each separate pass through the die.

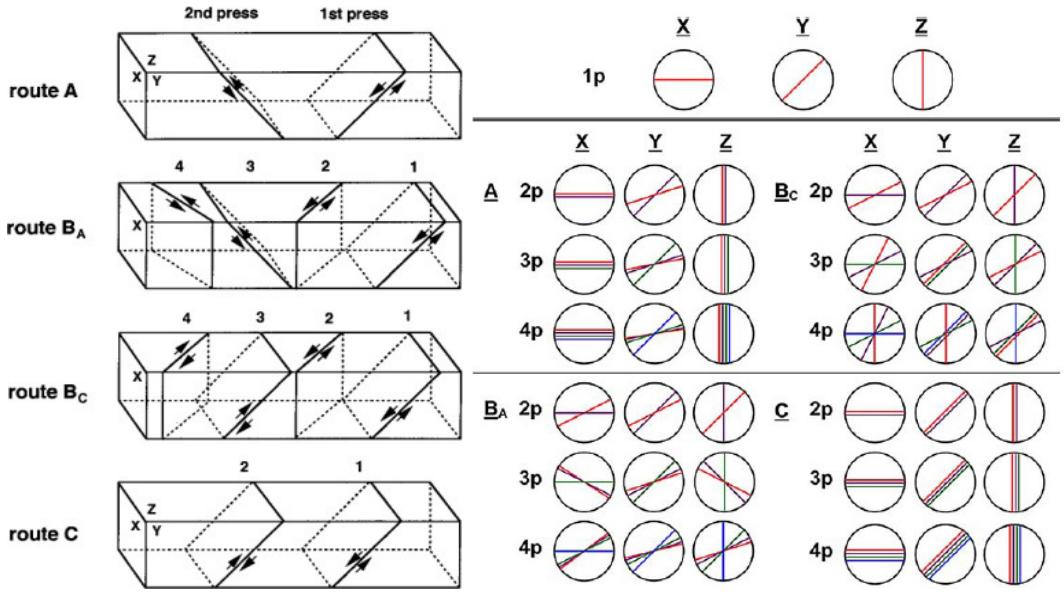

Figure 3.12: The Slip systems and shearing patterns for different ECAP routes a) The slip systems b) the distortions introduced into cubic elements when viewed on the X, Y, Z planes for consecutive passes using processing routes A, B_A, B_C and C [38]

In order to understand the grain refinement during ECAP, it is necessary to examine the theoretical shearing patterns that develop on the various planes of section. When a sample is pressed through an ECAP die, the material is deformed by simple shear which is parallel to the intersection of two parts of the channel. Assume that a cubic element is deformed by a ECAP die with Φ=90°, Ψ=0°.

As a result, it is sheared into the rhombohedral shape depicted within the exit channel. Individual inserts are given for the X, Y and Z planes showing the distortions of the grains in the shaded outlines and the operative slip system within each grain.

The second passage through the die may be undertaken either with no rotation of the sample (route A) or with rotations of 90° (route B) or 180° (route C). These three situations are shown in Fig.3.13. Respectively, together with illustrations of the deformation associated with each plane.

Inspection shows that route A leads to an elongation of the grains in the Y plane at an angle of ~ 15^{o} to the x axis, route B to elongations of the grains on each orthogonal plane, whereas route C restores the cubic element.

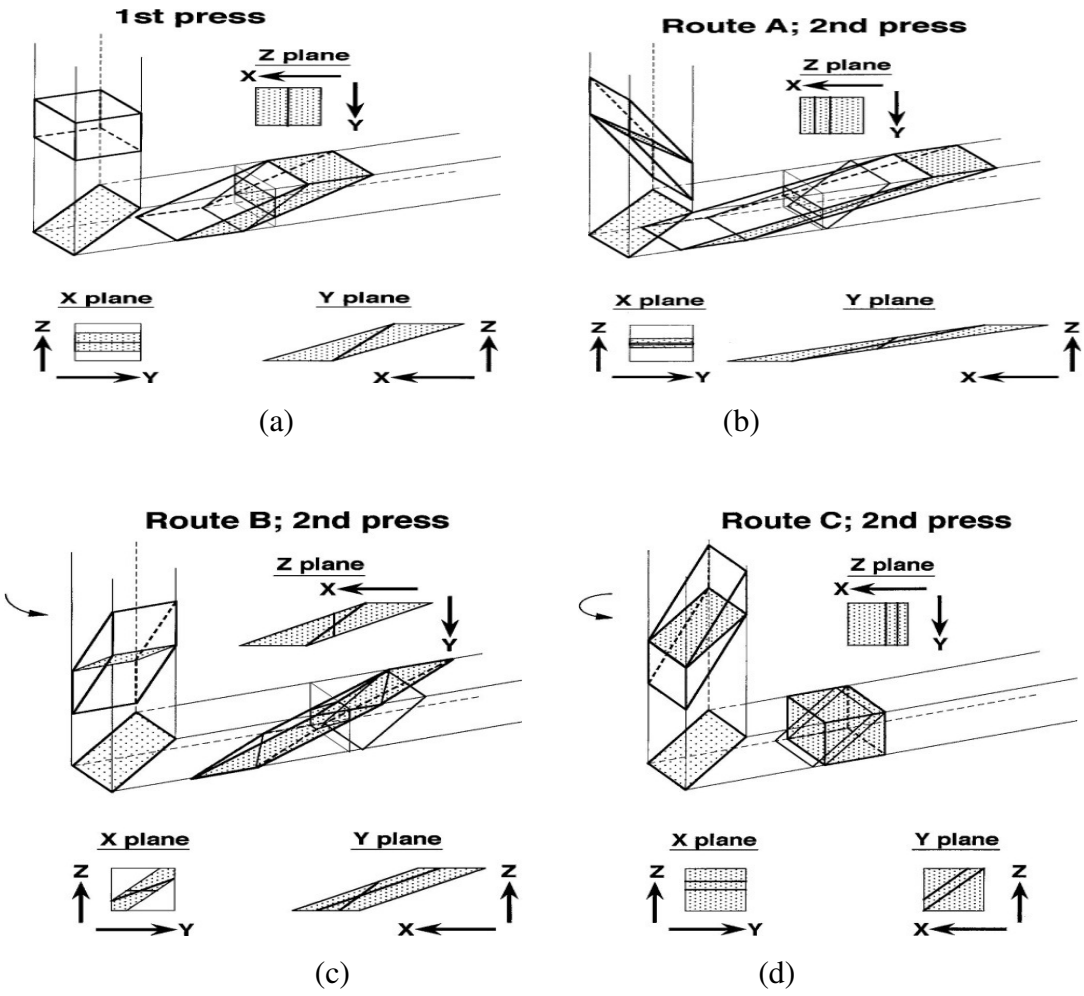

Figure 3.13: The macroscopic shearing of a cubic element in a) 1^{st} pass, b) 2^{nd} pass through route A, c) 2^{nd} pass through route B, d) 2^{nd} pass through route C [40]

For pressings in excess of two passes through the die, it is necessary to consider separately the implications for routes B_A and B_C. The predictions for the 3^{rd}, 4^{th} and 5^{th} passes are illustrated in Fig.3.14. for routes A, B_A, B_C and C, respectively. It is apparent that the shearing characteristics of routes A and B_A are similar and they both lead to increasing distortions of the original cubic element, whereas routes B_C and C are also similar with a restoration of the cubic element after totals of 4n and 2n passes for routes B_C and C, respectively.

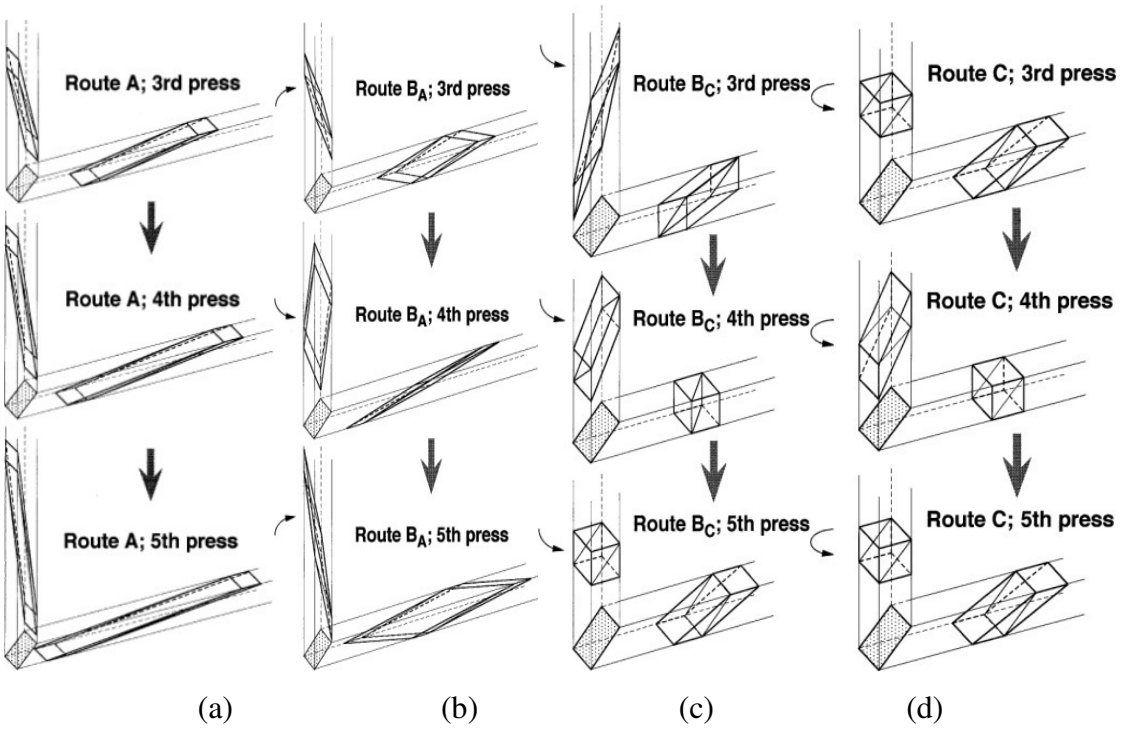

Figure 3.14: The 3rd, 4th and 5th passages through an ECAP die when using a) route A, b) route B_A, c) route B_C, d) route C [40]

As shown in Fig.3.12 (b), shearing patterns for different processing routes up to a total of 4 passes have been predicted by examining the macroscopic characteristics in Fig.3.13. and Fig.3.14. For the first passage, these patterns are in excellent agreement with the experimental results [38, 41]. These lines provide a useful summary of the main characteristics of how the slip patterns rotate around three axes when the sample is ECAPed. A parameter, angular angle η, is developed to describe the range of slip for each plane and each processing route. The angle gives the range of the angles containing slip traces when viewed on each separate plane. The individual values of η for each plane and each set of passes is summarized in Table 3.1. It is obvious that the route B_C yields the largest angular range with values of 90°, 63° and 63° after 4 passes on the X, Y and Z planes respectively.

Since slip over a wide angular range is an important prerequisite for achieving the rapid development of an equiaxed ultrafine grained microstructure [41], the processing route B_C is expected to be the most efficient processing route to subdivide the material.

Table 3.1: Angular ranges for slip using different processing routes [38]

Processing route	Number of passes	Total angular range, η		
		X	*Y*	*Z*
A	2p	0°	27°	0°
	3p	0°	34°	0°
	4p	0°	37°	0°
B_A	2p	27°	18°	45°
	3p	33°	27°	63°
	4p	37°	31°	72°
B_C	2p	27°	18°	45°
	3p	63°	18°	63°
	4p	90°	63°	63°
C	2p	0°	0°	0°
	3p	0°	0°	0°
	4p	0°	0°	0°

It is concluded that three conditions favor the production of an optimum microstructure consisting of essentially uniform and equiaxed grains separated by high-angle grain boundaries.

These conditions are;

- the development of slip traces over large angular ranges on each of the three orthogonal planes within the sample,
- a regular and periodic restoration of the equiaxed structure during consecutive pressings the occurrence of deformation on all three orthogonal planes.
- This criterion is fulfilled most readily when using route B_C with a die angle of 90° [42].

3.8 Experimental factors influencing ECAP

3.8.1 Significance of the channel angle (Φ)

The channel angle, Φ, is the most significant experimental factor since it dictates the total strain imposed in each pass. A series of detailed experiments on pure aluminium, using dies having values of Φ ranging from 90° to 157.5°, showed that an ultra-fine microstructure of essentially equiaxed grains, separated by grain boundaries having high angles of misorientation, was obtained most easily when imposing a very intense plastic strain with a value of Φ very close to 90°.

By contrast, when the channel angle is increased, the microstructure becomes less regular and the SAED patterns show that there are higher fractions of boundaries having low angles of misorientation. These results demonstrate that the total cumulative strain is not the important factor in determining the microstructure in ECAP but rather it is important to ensure that a very high strain is imposed on each separate pass [38]. This means in practice that a similar microstructure cannot be attained with other techniques, as in conventional extrusion using multiple passes, where small incremental strains are imposed in each separate pass. However, too small Φ (for example 60°) requires high extrusion pressure. Therefore, Φ=90° is the optimum choice for an ECAP die.

3.8.2 Influence of the angle of curvature (Ψ)

This angle plays only a minor role in determining the strain imposed on the sample, as shown by the estimates of equivalent strain given in Fig. 3.10. However, it is important to investigate the influence of this angle in the production of ultra-fine grained materials. From a practical point of view, the conventional split die is easily constructed with Ψ=0°, but the arc of curvature of the solid die need to be larger than 0°. Obviously, it is easy to press the material through an ECAP die with a larger arc of curvature.

Therefore, a die with a round corner or right corner was attempted and simulated by finite element analysis [43]. When Ψ=0°, homogeneous shear deformation takes place on the whole cross section of the sample, but a small "dead zone" or corner gap is formed which means that the billet no longer remains in contact with the die wall at the sharp outer corner where the two channels intersect. As Ψ=90°, the shear deformation at the upper part of the sample is found to be comparatively uniform whereas the deformation at the lower part of the specimen becomes smaller. This results in inhomogeneities in the as-pressed sample [38].

For compromise, the arc of the curvature is chosen to be 20° [43], it is also reported the optimum value of Ψ is 20-30°. Therefore, it is reasonable to conclude that the most promising approach is to construct a die with a channel angle of 90°, with an outer angle of curvature of around 20-30°.

3.8.3 The influence of pressing speed

Usually, the material is ECAPed using high-capacity hydraulic presses that operate with relatively high ram speeds. Typically, the pressing speeds are in the range of ~1-20 $mm.s^{-1}$. At lower pressing speed, recovery occurs more easily. Consequently, more equilibrated microstructures are produced.

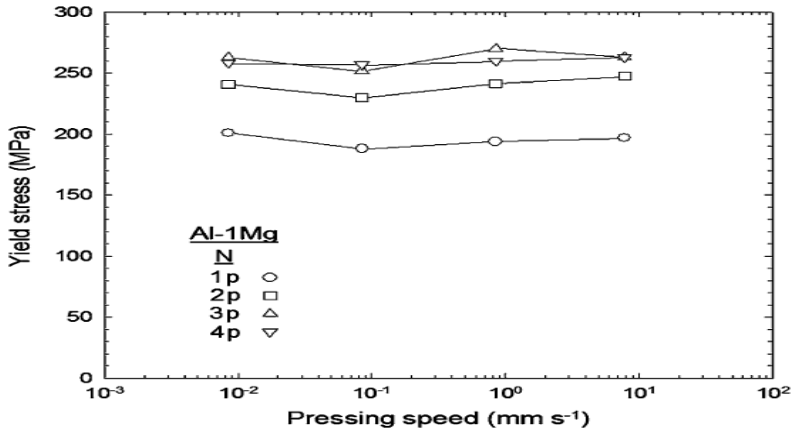

Figure 3.15: Variation of the yield stress with the pressing speed for an Al-1%Mg alloy after ECAP through 1-4 passes, data recorded at room temperature using a strain rate of 0,1 s-1 [38]

In Fig. 3.15, the yield stress in subsequent tensile testing at room temperature using a strain rate of $0.1s^{-1}$ is plotted against the pressing speed during ECAP. It is clear that the strength of the material only increases with increasing passes of ECAP deformation rather than increasing pressing speed. In addition, for higher pressing speed, a high quality of the ECAP die is required and abrupt heating of the sample during pressing must be considered.

3.8.4 The influence of pressing temperature

The pressing temperature also influences the results of ECAP. First, there is an increase in the equilibrium grain size with increasing temperature as shown in Fig. 3.16 for three different materials. Second, the fraction of high angle grain boundaries decreases with increasing temperature. It is probably due to the faster rates of recovery at higher temperatures which leads to an increasing annihilation of dislocations within the grains and a consequent decrease in the numbers of dislocations absorbed into the subgrain walls.

This also means that a higher fraction of high-angle boundaries forms at lower temperatures. Therefore, optimum ultrafine grained microstructures will be attained when the pressing is performed at the lowest possible temperature as long as the pressing operation does not introduce any significant cracking in the sample.

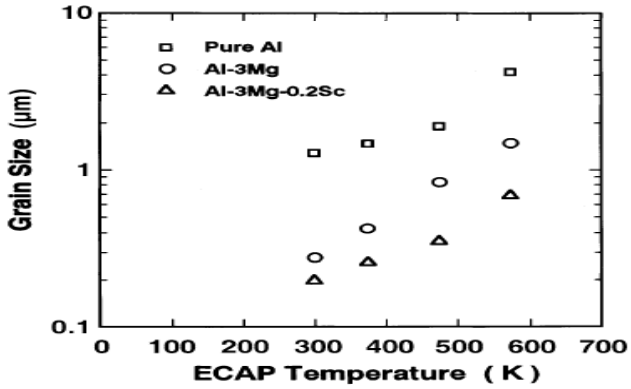

Figure 3.16: Grain size after ECAP versus the pressing temperature for 3 materials [38]

3.8.5 The influence of back pressure

Since the beginning of the design of a facility for ECAP, back pressure has been considered as a useful auxiliary tool to convenience the ECAP procedure. However, most of current experiments on ECAP applied no back pressure during the process because the difficulty to realize the design. It is estimated that a back pressure is capable of reducing the friction between the sample and die walls in the exit channel. Also, a back pressure may retain the flow of the sample and thus eliminate the dead zone and reduce the area of deformation zone. Although it is expected that careful control of back pressure is capable of achieving a homogeneous microstructure.

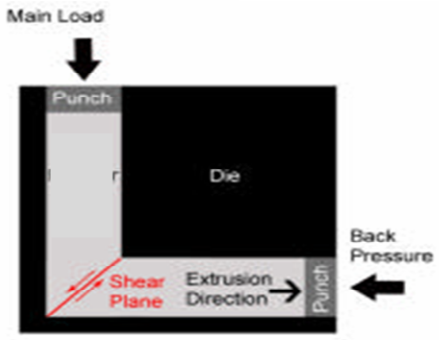

Figure 3.17: Principally sketch of ECAP with back pressure [44]

3.9 Origin of Structural Changes in Materials produced by ECAP

3.9.1 Grain refinement by ECAP

According to the general framework [45, 46], dislocation structures organize incidental dislocation boundaries (IDBs) and geometrical necessary boundaries (GNBs). When strain increases, GNBs evolve in a few steps: (I) reorganization into deformation bands (DBs), (II) decrease of spacing to a cell size, (III) rotation to a total flow direction and (IV) increase in misorientation angles (MOA) [47]. Simultaneous changes in microstructure and texture during such an evolution lead to material hardening or softening. Depending on the material and deformation mode, hardening may extend continuously to large strains while softening may interrupt that by localized flow at moderate strains.

If softening becomes predominant, continuous evolution is substituted by flow localization in shear bands (SBs). Shear bands are planar thin material layers accommodating strains which are significantly larger than in the surrounding areas. The average distance between bands approximates to the cell size outside the bands. Crystallographic multi-slip activity in SBs results in gradually increased MOAs along their boundaries. SBs have non crystallographic orientations that always follow to continual principal shears and they may penetrate a few grains without noticeable deviation. Upon origination, SBs substitute pre-existing structures and define the final structure of heavily deformed metals.

The number of active slip systems at each location is generally lower than the five predicted by the Taylor theory as this is energetically favorable. Thereby, the grain starts to subdivide into volume elements. Within one element the slip pattern is different from that in the neighbouring elements, but collectively they fulfill the Taylor assumption for strain accommodation. The volume elements correspond to an experimentally observed feature denoted *cell block* (CB) which, as the name indicates, consists of a number of adjacent cells. The boundaries between neighbouring CBs arise out of geometrical necessity, as the selection of slip systems is different on either side of them. Hence, they are termed geometrically necessary boundaries (GNBs).

Several types of GNBs are described, e.g. dense dislocation walls (DDWs), observed at small to moderate strains, and laminar boundaries (LBs), separating flat elongated CBs at large strains. Microbands (MBs) are plate-like zones bounded by dislocation sheets which tend to develop from the DDWs, and thereby separate CBs. Within the CBs there are cells separated by cell boundaries. These boundaries are formed through mutual trapping of mobile and stored dislocations, and thereby they are termed incidental dislocation boundaries (IDBs). A schematic illustration of the cells, cell blocks, GNBs and MBs at a moderate strain level is given in Figure 3.18.

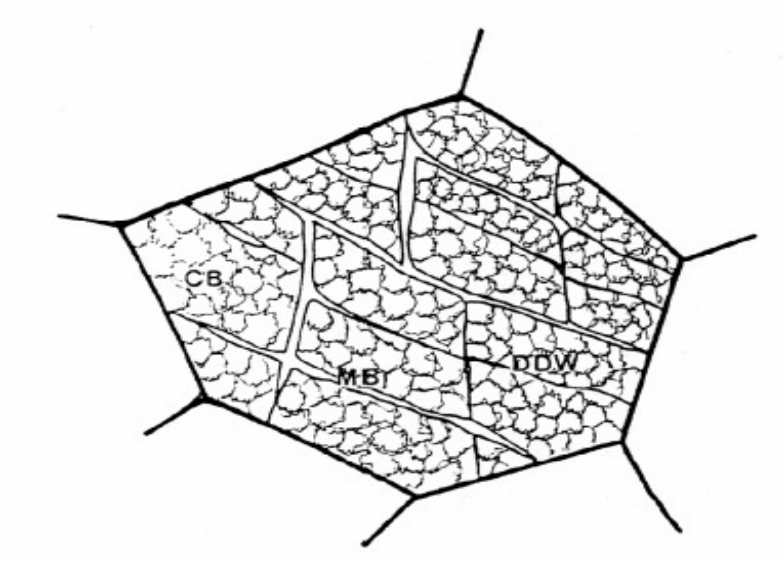

Figure 3.18: Schematic drawing of the early deformation structure in a cell-forming metal [48]

Iwahashi et al. seem to be the first to make a detailed systematic research on the microstructural evolution during ECAP in 1997. They conducted detailed experiments on pure (99.99%) aluminium in order to investigate the development end evolution of the ultra fine grains during ECAP for the routes A and C.

It was shown [49] that pure Al with an initial grain size of ~1.0 mm could obtain grain structures at the micrometer level (~4 μm) after a single pass through the die with an introduced effective strain of ~1.05. The microstructure after the first press consists of bands of elongated sub-grains. There is a rapid evolution with further pressings into an array of equiaxed grains.

The initial massive reduction in grain size is achieved in the first passage through the die because the original grains break up into bands of sub grains. These sub-boundaries subsequently evolve with further pressings into high angle grain boundaries, giving ultimately a reasonable equiaxed microstructure.

When samples of pure Al, with a coarse grain size, are cold rolled to reductions of ~15% to 30%, the grains become divided into bands of elongated sub grains and the average size of these sub grains is typically of the order of ~1 - 2 μm. These sub grain bands appear to be the precursor of the well-defined and regular band structure, which is visible also in ECA pressed samples, after a single passage through the die to a strain of ~1,05. In order to understand the nature of grain refinement at the high strains associated with ECA pressing, and in particular the influence of the processing route, it is necessary to examine the shearing patterns which develop within each sample during repetitive passages through the die.

As a result of this duality in the shearing directions, sub grain bands are developed on repetitive pressings along two separate and intersecting sets of planes and this leads rapidly to an evolution in the boundary structure into a reasonably equiaxed array of high angle boundaries. It is known that route B_C is the preferable procedure for use in ECAP experiments. By contrast, route A has two shearing planes intersecting at 90° and route C repeats shearing on the same plane. It is confirmed in an earlier investigation [49], that route C is preferable to route A in developing an array of high angle boundaries.

Although the reason for this observation has not been established in detail, it probably arises because route C permits the shear to build continuously on a single set of planes whereas in route A the extent of shearing is divided equally between two sets of orthogonal planes. Valiev et al [50] proposed a model for the formation of non-equilibrium grain boundaries as shown in Fig. 3.19 where the grain boundaries are featured with extrinsic dislocations of high density. The model can explain the granular structure observed in ultrafine-grained materials by ECAP and the evolution of high angle boundaries during repetitive ECAP passes [51, 52].

Because of the excess of grain boundary energy of non-equilibrium grain boundaries, the stability of grains is very important for the ultrafine-grained structures obtained by ECAP.

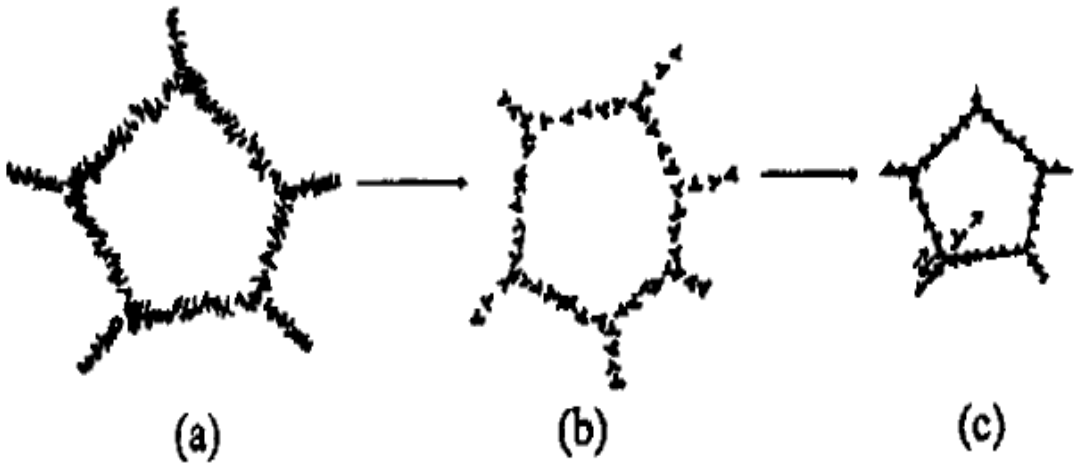

Figure 3.19: Schematic model of dislocation evolution at different stages during ECAP; a) initial cellular structure (sub-grains) containing many dislocations, b)cell experiencing partial annihilation of dislocations at the boundaries, c)granular structure achieved with high angle boundaries [51]

3.9.2 Evolution of BCC deformation

Compared to FCC material, much less attention has been given to BCC metals although they have equal industrial importance. Therefore, less is known about microstructure evolution during deformation in BCC metals.

Recently, BCC materials such as IF-steel have been studied. According to these investigations, some rough ideas have been acquired. The deformation microstructures consist of similar features to those already identified in several FCC metals, namely cell blocks showing a pattern of subdivision and cellular structures. The deformed microstructures also show a significant dependence on the initial crystal orientation. The formed band structure is parallel to the trace of the primary slip system.

However, there are some important differences. Local shear or strain localization was found to be prevalent in deformed BCC materials. According to [53] even at low strains, localized shearing takes place. With increasing rolling reduction up to 50%, local shearing is extensively developed into two types.

First, local shearing results in very narrow regions of micro-shearing across the formed GNBs, giving rise to a characteristic "S-band" appearance of the GNBs. Second, local shearing may be further developed into narrow regions of at least one dislocation cell width. Both types of localized shearing can be seen in Fig.3.20. One set of GNBs (inclined to RD by -35°) intersected by widely spaced localized shear bands (inclined to RD by 28°), the initial GNBs become S-shaped.

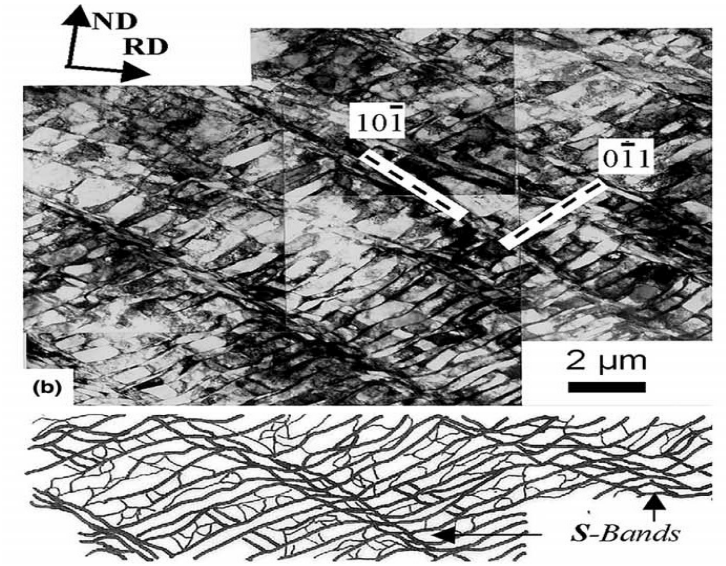

Figure 3.20: Deformation microstructure after 50% cold reduction, one set of GNBs intersected by widely spaced localized shear bands [53]

The deformed bands (extended dislocation boundaries) and micro-shear traces in BCC metals are crystallographic. The former is most coincident with {110} slip plane and the latter is most commonly parallel to {112} trace [62]. This indicates that there are 18 possible slip planes for BCC metals (assuming slip on {110} or {112} planes), compared to just four {111} slip planes in FCC metals. It is testified that nearly all the planar boundaries are within 15° of either a {110} or {112} plane. This means for BBC metals there is a larger possibility that any given plane will be near to a slip plane.

4. EXPERIMENTAL PROCEDURE

4.1 Experimental Route

Grain refinement and strengthening mechanisms during Equal Channel Angular Pressing (ECAP) of an ultra low-carbon (ULC) steel were explored by a careful analysis of mechanical tests and microstructural characterization techniques.

The experimental route of the research is shown below in Fig. 4.1. The aim of the research is to understand the substructural evolution during ECAP processing. EBSD analysis is the most important part of this research because this technique provides important information about how substructures evolve during ECAP.

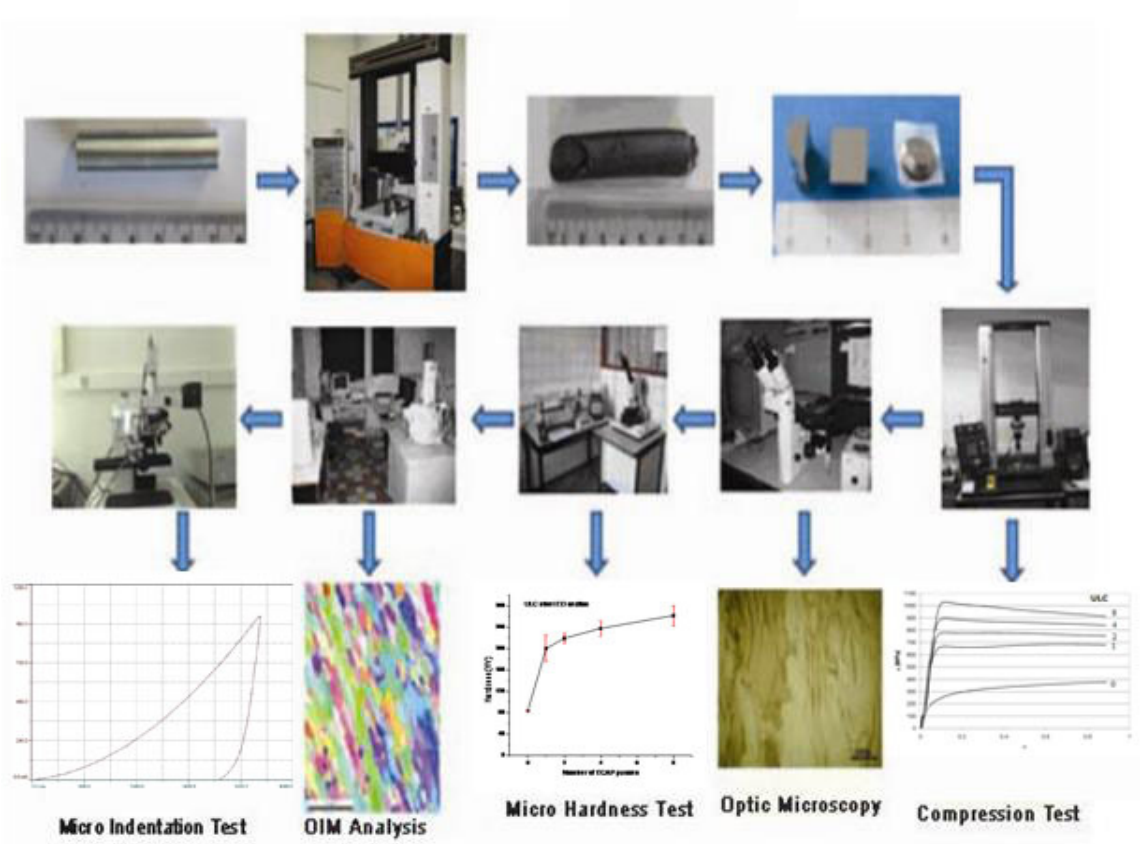

Figure 4.1: Summary of experimental methods utilized throughout this research.

In summary, the initial material were observed and tested for comparison purposes. They were then ECAPed at one specific temperature and for a specific number of passes. 3 and 5 Passes were performed at later to get the information between 2-4 and 4-8 passes. The microstructures were observed via Optical microscopy and Orientation Image Microscopy (OIM) is the automation of the orientation measurement process using EBSD, with an emphasis on the substructures, misorientations across the grain boundaries. Mechanical properties were observed by Compression Tests and Micro hardness tests, performed in 2 different types to have an idea about how hardness is changing with increasing ECAP pass.

4.2 Starting Material

This research material was chosen to investigate the effect of ECAP on microstructure and the resulting mechanical behavior of ULC steel. The starting material was received and used in as cast condition. The grain size was about 1mm. The main impurities are: 24ppm C, 17 ppm N, 100 ppm S, 0.079wt% Mn and 0.021 wt% Al. The as cast material was machined into billets with a diameter of 12mm and a length of 50 mm for ECAP processing.

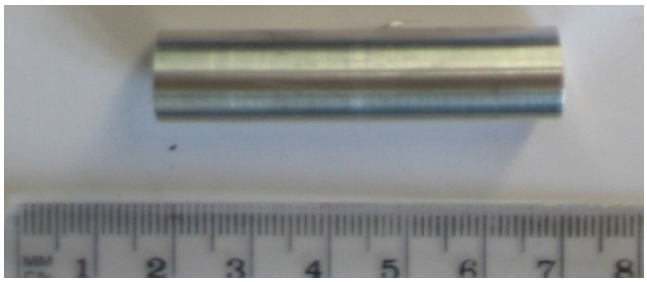

Figure 4.2: ECAP sample machined out of a block of as received material.

4.3 ECAP Process

The Instron 1196 is used as pressing tool for the ECAP process. The ECAP processing was performed using a solid die containing an L-shaped channel with an angle of 90^0 and an angle of 0^0 at the outer arc of curvature where the two parts of the channel intersect. This creates an equivalent true stress of 1.15 for each pass.

The initial grain size was around 1mm. All billets were coated with a lubricant MoS_2 and then pressed through the die at 172^0 C using a pressing speed of 10 mm s^{-1}. The billets were rotated by 90^0 in the same sense between consecutive passes. This processing scheme is generally denoted as route B_c.

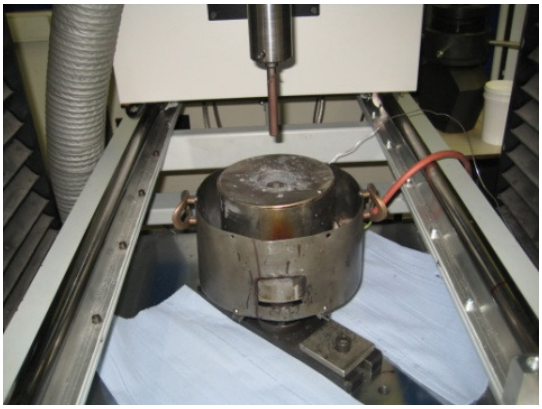

Figure 4.3: A picture of the ECAP die and the plunger.

From literature it is known that four classical ECAP routes A, C, B_A and B_C have a significantly different impact on the grain refinement. Route C is distinctly less efficient than the other routes, while route B_C yields the most homogenously refined and equiaxed microstructure. And a channel with an angle 90°creates a higher deformation strain with an outer arc of 0°.

As discussed in chapter 3, an ultra-fine microstructure of essentially equiaxed grains, separated by grain boundaries having high angles of misorientation, was obtained most easily when imposing a very intense plastic strain with a value of Φ very close to 90°. Because of this reason Route B c and a die with a 90° angle, is chosen as an ECAP test parameter.

4.4 Sample Preparation

Each pressed billet is cut in three parts to measure the strength with mechanical tests and to analyse the microstructure in two perpendicular sections using the EBSD technique. A schematic illustration of the parts for observation is shown in Fig. 4.4.

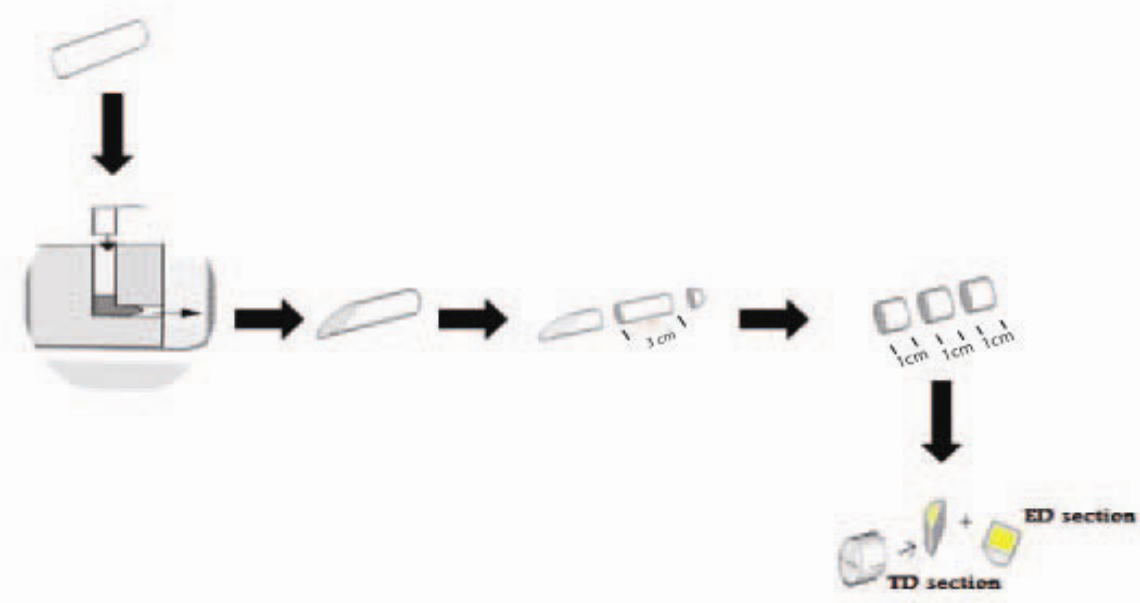

Figure 4.4: Schematic illustration of sampling for testing.

The first step in collecting data for microscopic work, is preparing the specimens. Different routes were followed but there were several problems to find the optimum conditions for this ULC steel. Finally specimens have been prepared with a Jeanwirtz Pressair E TF 250 automatic machine which is given in Fig. 4.5. The sample preparation procedures are given in Table 4.1.

Table 4.1: The route which is followed to prepare the samples

Grinding	**SiC Paper**	**Cycles (min^{-1})**	**Time (min.)**	**Pressure (bar)**
1	800#	150	2	2.5
2	1200#	150	2	2.5
3	4000#	150	2-5	2.5
Polishing	**Diamond Paste**	**Cycles (min^{-1})**	**Time (min.)**	**Pressure (bar)**
1	3 µm	150	10	2.5
2	1 µm	150	10-20	2.5
Final Polishing	**OPS**	**Cycles (min^{-1})**	**Time (min.)**	**Pressure (bar)**
1	0,15 µm	200	2-10	2.5

Figure 4.5: Automatic grinding and polishing machine.

For electro polishing, several solutions and in different conditions were tried out but it didn't give good results for ULC steel: Firstly samples were electro polished at -30^0 C using a perchloric acid/methanol electrolyte (5:95) with stainless steel anode and 10V dc for 1-2 min. Later the samples were electro polished in a different way, at room temperature in a mixture of perchloric acid and acetic acid (10:90) at 10V for 2 min.

4.5 Mechanical Tests

4.5.1 Compression test

ULC steel is investigated in an INSTRON compression machine. A sheet of Teflon is placed in between the sample and the stamps to reduce the friction. An extensometer is not used, only the displacement of the clamps of the machine is measured. This result in a strain measurement with poor accuracy, especially in the elastic regime, but no other option was possible.

Figure 4.6: A picture of the Instron compression machine.

4.5.2 Micro hardness tests

4.5.2.1 Conventional micro Vickers test

The working principle of micro hardness testing is forcing a diamond indenter of specific geometry into the polished surface of the samples. The procedure for testing is very similar to that of the standard Vickers hardness test, except that it is done on a microscopic scale with higher precision instruments. The measurements were performed to metallographic finished samples; because of the reason the smaller the load used, the higher the surface finish was required. Precision microscopes are used to measure the indentations with a magnification of around X500 and measure to an accuracy of $\pm$0.5 micrometers, is given in Fig.4.7.

In order to examine the effect of ECAP passes, the micro hardness was measured using a Vickers device prior and after the ECAP process on the plane perpendicular to the extrusion direction and on the plane perpendicular to the transverse direction. A 50g load is applied for 10s. The hardness values were taken as the average of a minimum of 5 measurements.

Figure 4.7: Conventional micro hardness test device.

4.5.2.2 Depth-Sensing Micro Vickers Hardness Test

Once a indentation machine has collected load-displacement data, a number of different analyses can be used to determine the mechanical properties of the sample from the data. A significant advantage of using the "depth sensing indentation" approach is that one can obtain much more information than just hardness. However the results obtained depend on the analysis model chosen and can be very sensitive to the details of the analysis.

Hardness tests were carried out with a Vickers V-F 34 pyramid indenter, using a CSM micro-hardness tester, is shown in Fig. 4.8. During tests, load–indentation depth–time data were recorded. Hardness measurements are performed under six different indentation loads, ranging from 50-500g, is applied to the samples with a 5s pause between loading and unloading parts. The hardness values were taken as the average of a minimum of 5 measurements.

The aim of the study is to investigate the effect of ECAP passes and the effect of loading on indentation hardness values. The results are compared which were obtained from conventional micro hardness method.

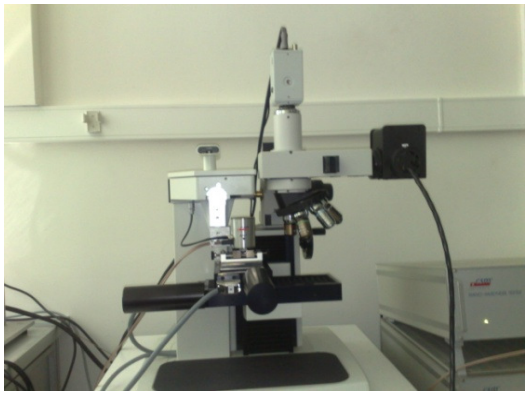

Figure 4.8: Depth sensing micro indentation test device.

4.6 Microstructural Characterization

4.6.1 Optical microscopy

The microstructure of processed and as-received samples was examined with a Nikon 200 light optical microscope which is given in Fig. 4.9. Optical microscopy samples of ECAPed ULC steel were prepared following the steps of sectioning, mounting, polishing, and etching. Sectioning was done with a Struers Secotom-10 cut-off machine using a bor based lubricant. The sectioned samples were mounted in fast cure epoxy. Grinding of samples was performed by abrasive removal of material from the material surface. The purpose of grinding and polishing is to produce a suitable surface for microstructural evaluation by means of step-by-step removal of deformed material; therefore silicon carbide papers of 800, 1200 and 4000 Grit were sequentially applied.

As a final step, polishing of samples using 3μ, 1μm diamond paste and colloidal silica (OPS) on a special cloth was performed. Etching of ULC steel is performed with %2 Nital solutions for 10-20 seconds. The microstructure of the ULC steel as a function of ECAP pass number, examined in both ED and TD sections.

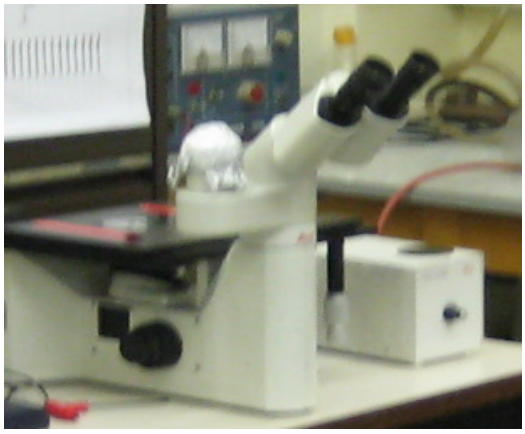

Figure 4.9: Nikon 200 Light optical microscope.

4.6.2 Electron backscatter diffraction (EBSD) analysis

EBSD is an SEM based technique that provides crystallographic orientation data necessary to understand the microstructure –property relationships. EBSD patterns, consisting of Kikuchi bands, are formed when a stationary electron beam interacts with a crystalline lattice in a highly tilted sample, while mounted in the SEM. The geometrical relationships of the bands hold information about the crystal lattice in the diffracting volume.

Orientation Image Microscopy (OIM) is the automation of the orientation measurement process using EBSD. OIM data are collected by moving the electron beam to points on a regular grid, defining an area of interest for the sample. At each point an EBSD pattern is acquired and automatically indexed to obtain the orientation information. It is impossible to determine the crystallographic orientation using Optic microscopy.

Orientation image microscopy vie electron backscattered analysis is used to overcome this problem. The advantage of this technique is that it is excellently suitable to swiftly determine the dimensions of large volumes of (sub-) grain structures and for the determination of the orientation of individual crystals.

Even the orientation of spots within a crystal can be determined so that orientation gradients can be recorded and can be mapped. This also enables the determinations of the orientation relationship between two points in adjacent crystals. The processed samples were examined with a Philips XL 30 SEM-microscope equipped with an EDAX (TSL) OIM system which is shown in Fig. 4.10.

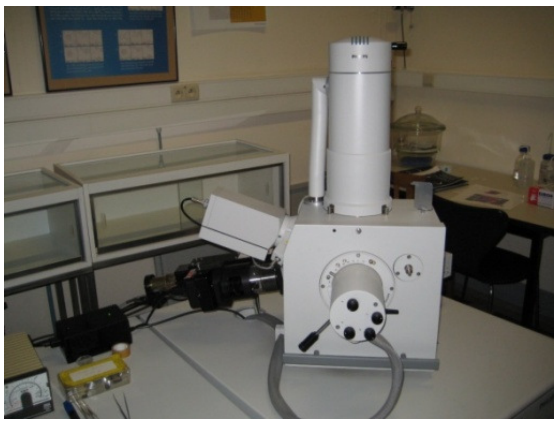

Figure 4.10: Philips XL 30 SEM Microscope with EBSD detector.

OIM was applied to the samples, which were ECAPed for 0, 1, 2, 3, 4, 5 and 8 passes. Careful polishing was essential, since orientation image mapping can only be carried out accurately on samples with strain-free surfaces. Sample preparation is performed by the way which is given in section 4.4. The samples were analysed in two cross sections. The first cross section is perpendicular to the ED direction and the second cross section is perpendicular to the TD direction of the ECAP die.

5. RESULTS AND DISCUSSION

5.1 Mechanical Tests

The mechanical properties of the ECAP processed samples were evaluated using micro hardness and compression tests. For comparison, micro hardness tests performed in two different method by using conventional micro Vickers tester and depth sensing micro indentation testing. The increase in the strength and the hardness is caused by (1) strain hardening, i.e. the built-up of a dense dislocation network and subsequent entanglement of dislocations, and (2) grain boundary strengthening, i.e. the formation of a barrier in the movement of the dislocations. At higher strains, the dislocation density increases only moderately until reaches a maximum. During subsequent deformation, the misorientation between the lattices of adjacent sub-grains tends to increase further, thereby forming a barrier in the movement of dislocations that is increasingly harder to overcome. Consequently, the generation of new dislocation and their subsequent movement throughout the crystal lattice is the reason of the origin of strengthening after deformation. The larger fraction of the ferrite allows a considerably larger amount of dislocations to be formed. Due to this, the mechanical properties of the ULC steel continue to increase gradually with increasing ECAP pass.

5.1.1 Compression tests

Figs. 5.1 and 5.2 show the stress-strain response of ULC steel. The maximum true compression stress and compressive yield strengths of ULC steel increase with ECAP deformation: the higher the deformation pass, the higher the yield strength. Two parameters are calculated to show the strengthening of the ULC steel; an approximate (compressive) yield stress and the maximum true compression test (TCS) in case of softening. Both parameters show a tendency to increase with the number of ECAP passes Fig. 5.2 gives an overview of the evolution of the yield stress for ULC steel.

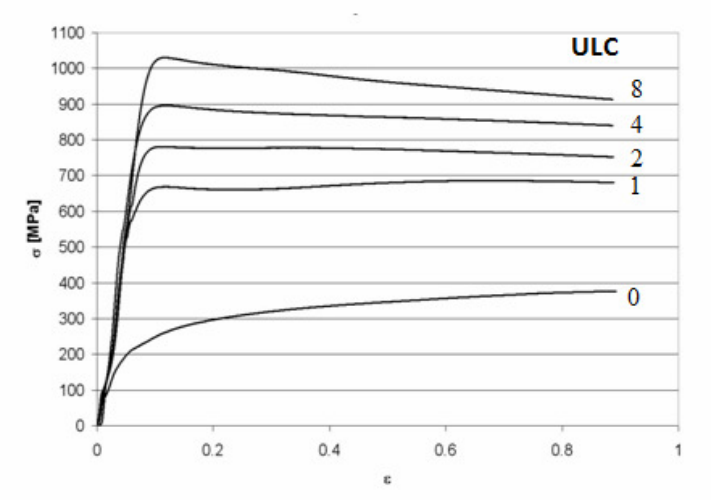

Figure 5.1: True stress-true strain curves of the compression tests carried out at room temperature on samples of ULC steel. The evolution of strength is indicated for increasing ECAP passes.

It is apparent from Fig. 5.1 that the strength increases with increasing numbers of passes and there is a very high strength of >1 G Pa after 8 passes of ECAP where this is nearly three times higher than for as-received condition. The yield strength of the ULC steel is initially around 200 Mpa. After a single pass, the yield strength quickly rises to a value of about 450 Mpa. At higher levels of deformation, the yield stress of the steel progressively increases, although at a much lower rate than after the first pass.

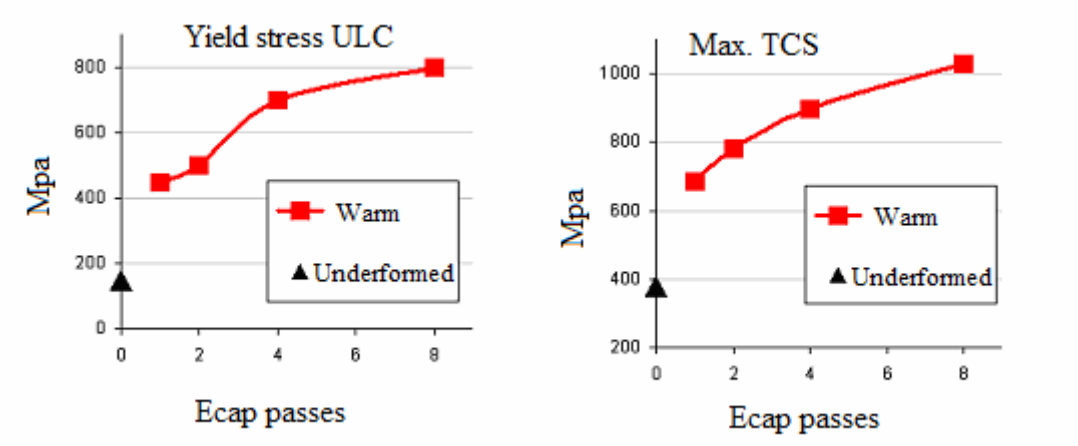

Figure 5.2: Evolution of the measured yield stress and maximum true compression stress (TCS) for the ULC steel samples. The vertical axis is the stress in MPa and the horizontal axis represents the number of ECAP passes. The square symbols are the samples deformed at T_h = 0.246, and the triangles are the undeformed samples. T_h is the homologeous temperature (T/T_{melt}).

5.1.2 Micro hardness tests

5.1.2.1 Conventional micro hardness tests

It is obvious that from micro-hardness tests there is a huge increase of hardness value between 0 and 8 passes but the big increasing is in between 0-1 pass. The reason of the big hardness increase between pass 0 and 1, is the uniform matrix before ECAP where the mean free path of the dislocations is very long.

Between the values of deviation at 1st pass and 4th pass in both cross sections is the matter of microstructural heterogeneity. The results are stated in Table A.1 and the hardness variation with increasing passes of ECAP is plotted in Figure 5.3.The micro hardness of the ULC steel increases from ~90 HV in the initial condition to just under the 270 HV after 8 passes.

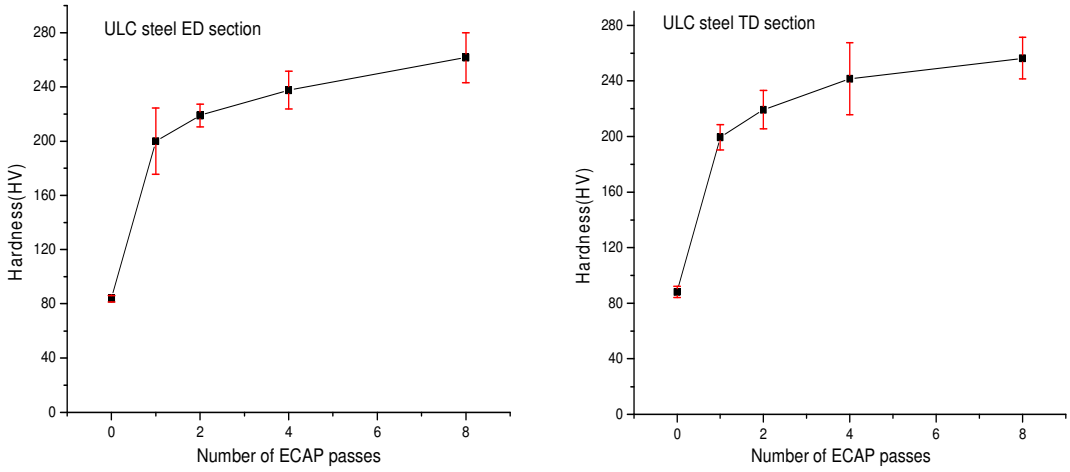

Figure 5.3: The variation of hardness with increasing passes of ECAP over ED and TD sections.

5.1.2.2 Depth sensing micro indentation test

It is apparent from Fig. 5.4 that the hardness increases with increasing numbers of passes and there is kind a high strength of >340 Vickers after 8 passes of ECAP where this is almost three times higher than initial condition. The results are given in Table A.2 and the hardness variation with increasing passes of ECAP is plotted in Figure 5.4.

The measurements are performed on ED section of samples in the load range from 500 to 5000 mN. It is found that the degree of the micro hardness anisotropy decreases for higher indentation test loads. The examined material exhibits the behavior of indentation size effect (ISE), i.e., the apparent hardness increases with decreasing indentation load.

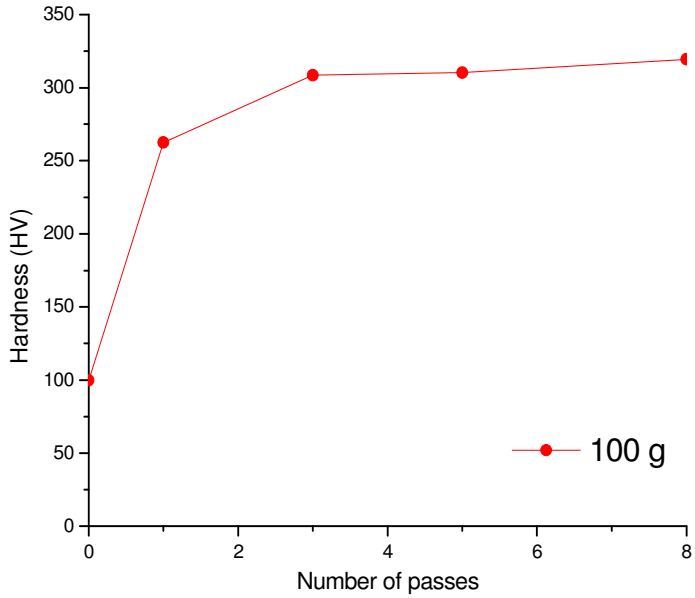

Figure 5.4: Hardness variations with increasing ECAP passes under 1000 mN indentation load.

The hardness values which are calculated from plastic energy method are given in Table A.3. The values are compared for both methods in different graphs to see the correlation between the two methods. HV numbers of the ULC steel calculated using the load and energy methods are plotted in Fig. 5.5 with respect to h_c, depending on the value of P_{max} (500-5000 mN).

At a first glance, Fig. 5.5 shows that the HV numbers of the ECAPed ULC steel obtained from the load method decrease with increasing indentation depth and the energy method gives almost the same HV numbers. Especially at low h values, the HV numbers calculated using the conventional load method are higher than those of the energy method.

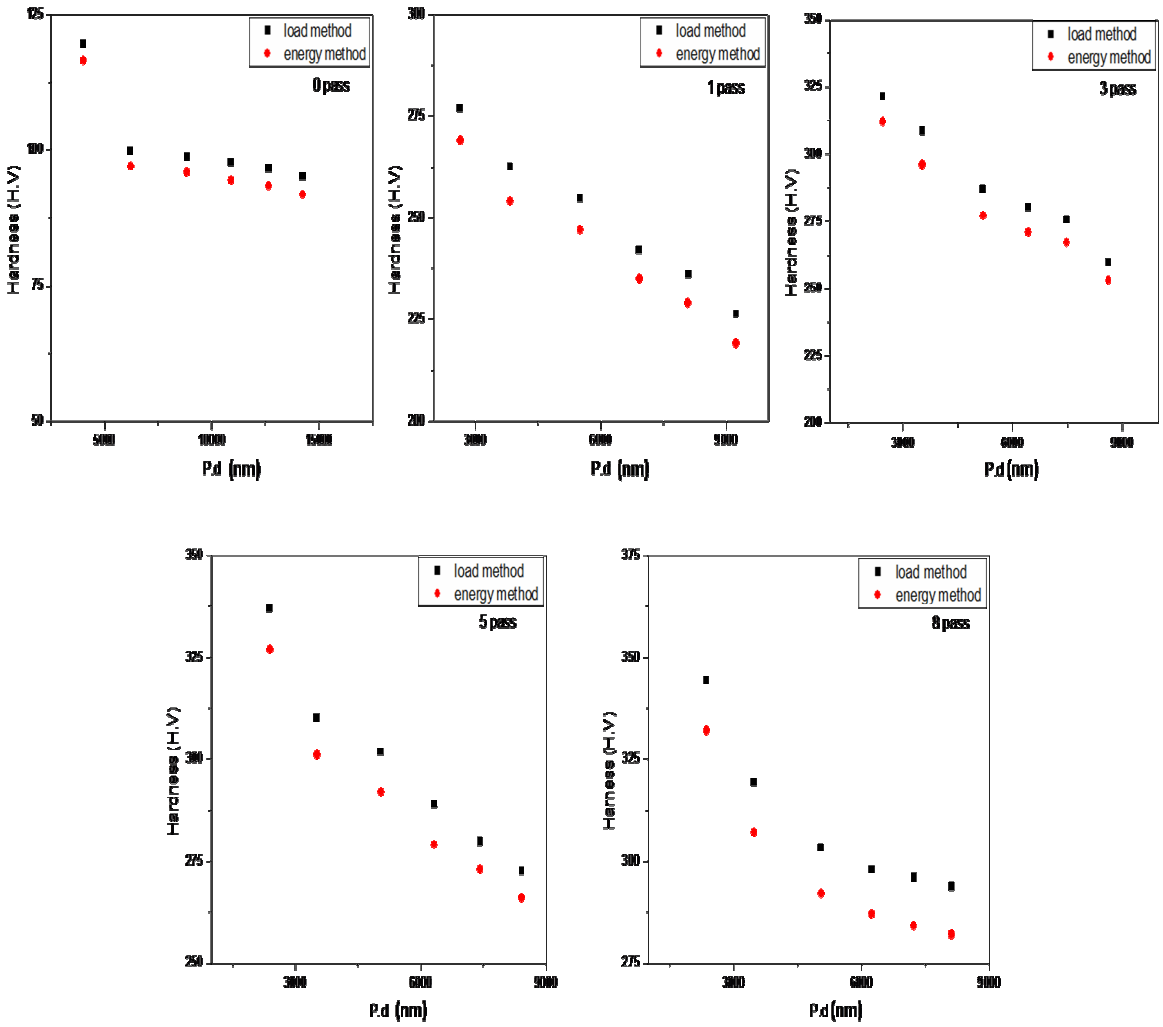

Figure 5.5: HV numbers of the ECAPed ULC steel obtained from the load and energy methods for ECAPed ULC steel in a load a) 50g , b) 100g , c) 200g ,d) 300g, e) 400g , f) 500g.

5.2 Microstructural Characterization

5.2.1 Optical Microscopy

The microstructure of the ULC steel as a function of ECAP pass number, viewed both in ED and TD sections, is shown in Fig. 5.6 and Fig. B.1. It can be obtained from the Figs. microstructures is close to each other for both section. It is clearly shown that the initial equiaxed grains of the as-received sample, with a size of ~ 1mm, are elongated after the first ECAP pass.

The subsequent ECAP pass resulted in smaller and more irregular equiaxed grains as compared with the as received microstructure. Further passes brought similar morphological changes; there is no clear direction of elongation after four passes. At the end of the 8 passes the grains become finer and are restored to their equiaxed shape.

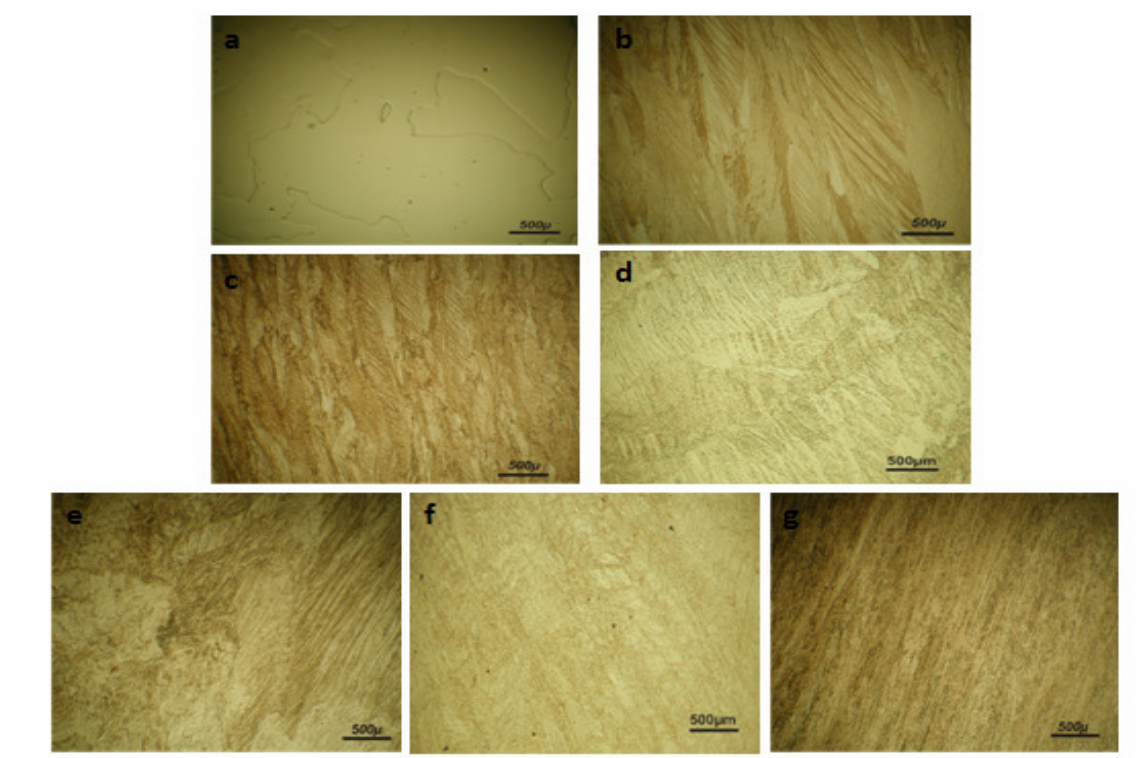

Figure 5.6: Microstructure, obtained by optical microscopy on the ED section of the samples a) As received ULC steel b) 1 pass ECAP ULC steel c) 2 pass ECAP ULC steel d) 3 pass ECAP ULC steel e) 4 pass ECAP ULC steel f) 5 pass ECAP ULC steel g) 8 pass ECAP ULC steel.

5.2.2 Electron backscatter diffraction (EBSD) analysis

Mechanical testing revealed that the main change occurs during the first pass, where as slowly increase occurs subsequent passes. The course of the microstructural change as a function of the deformations is different, however. In this case, the largest change occurs not during the first pass, but during the second and third pass. Like the mechanical behavior, a gradual change in the microstructures can be observed during subsequent passes. Observation of the data from the orientation image maps revealed that the microstructures of processed material evolve quite rapidly. The following paragraphs describe how this evolution takes place during successive deformation.

The inverse pole figure which is taken from non-deformed sample reveals large grains with around 1mm grain diameter. These grains are quite big and nearly free of defects. Both ED and TD sections investigated for non-ECAPed sample. Orientation image maps are given in Fig. 5.7 and Fig. B.2.

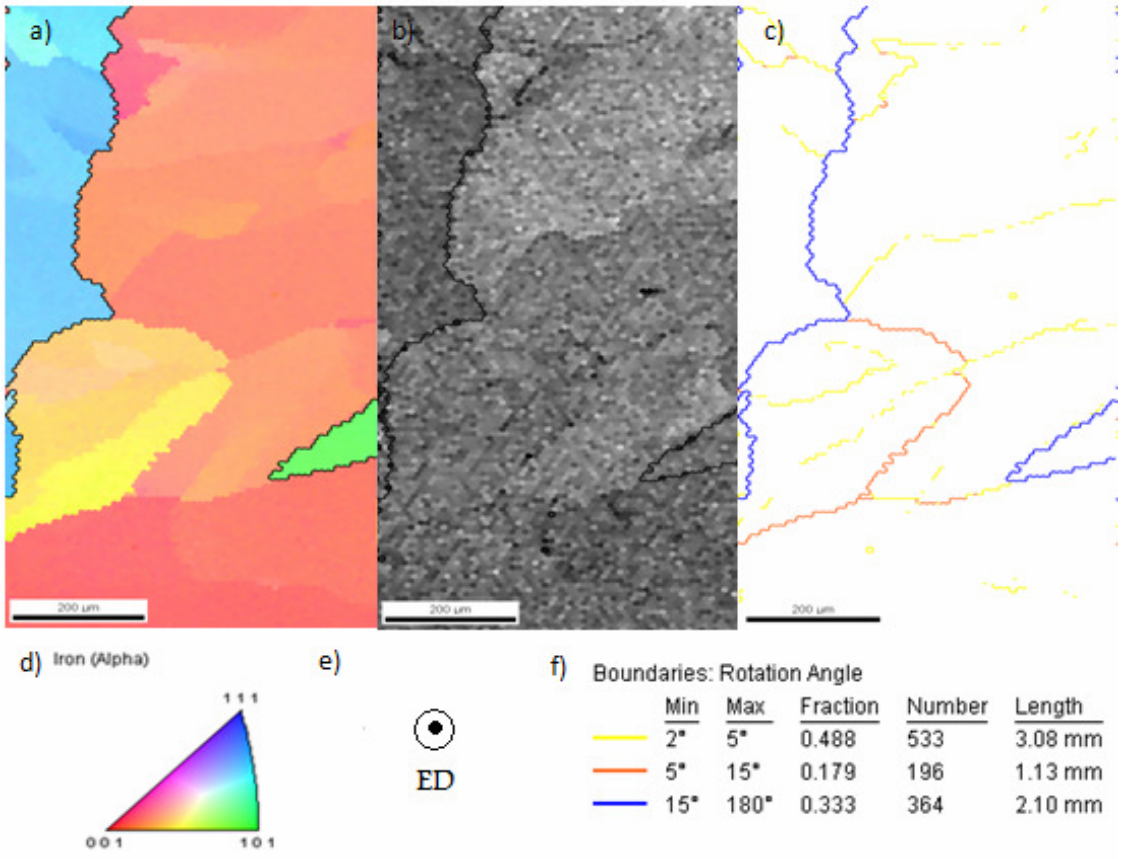

Figure 5.7: EBSD scan of ULC steel after 0 ECAP pass in ED section a) Inverse pole figure map, coloured according to the scale in d, b) Image quality map, c) Boundary map, high angle boundaries (>15^0) indicated with a blue line, medium angle boundaries indicated with orange line (5^0-15^0) and low angle boundaries indicated with yellow (2^0-5^0) line according to the scale in f. ND direction is the reference direction for inverse pole figure.

After the first ECAP pass grains are heavily deformed because of the high deformation. Sample pressed through the ECAP die at moderate homologous temperature (172^0 C or T_h =0,246). Fig 5.8 and Fig. B.3 show maps of an EBSD scan partially covering several deformed grains in two cross sections. In both sections localized shearing by micro bands and shear bands are visible in certain grains.

The boundary maps in Fig 5.8 and Fig. B.3 shows the low angle boundaries with a misorientation between 2^0 -5^0 and 5^0 - 15^0, in addition to the high angle boundaries which were already shown in Fig 5.8 and Fig. B.3.The low angle boundaries are more uniformly distributed in some parts of the sample. Some new high angle grain boundaries have already developed.

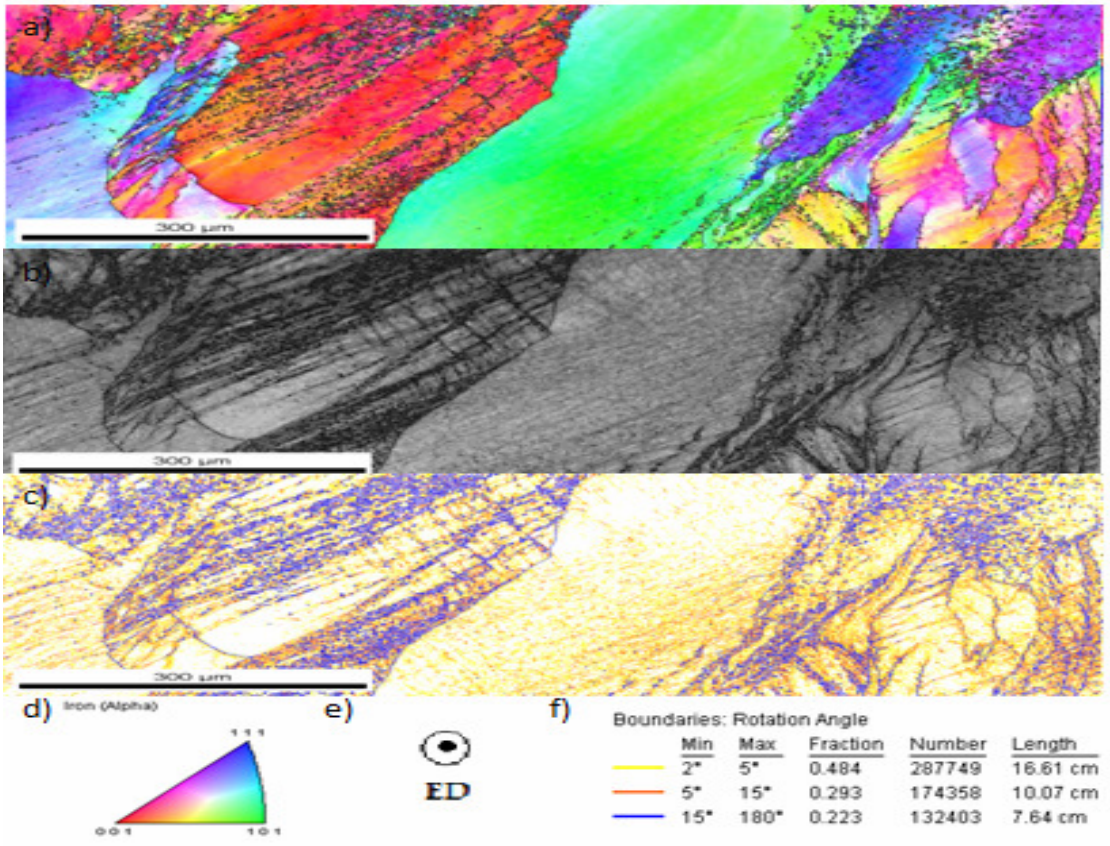

Figure 5.8: EBSD scan of ULC steel after 1 ECAP pass in ED section a) Inverse pole figure map, coloured according to the scale in d, b) Image quality map, c) Boundary map, high angle boundaries (>15^0) indicated with a blue line, medium angle boundaries indicated with orange line (5^0-15^0) and low angle boundaries indicated with yellow (2^0-5^0) line according to the scale in f.

There is a large difference in fragmentation behavior between different regions in the material. Strongly fragmented parts of the sample have point to point internal misorientations up to 25^0 and an average misorientation of about 10^0. Figure 5.9 shows the distribution of misorientations above 2^0 after 1 ECAP pass, including the original grain boundaries. About %50 of the boundaries have a misorientation between 2^0 and 5^0.

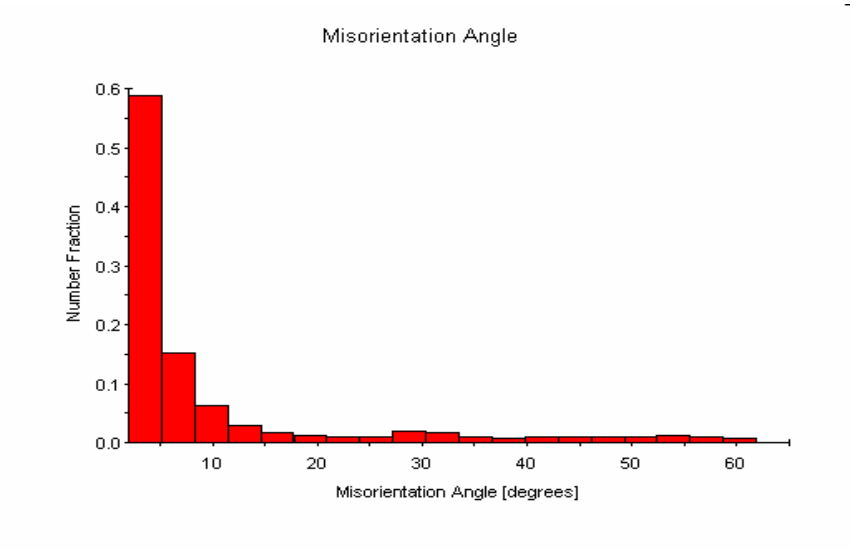

Figure 5.9: Misorientation distribution after 1 ECAP pass in ED section.

In general sub-grains with low angle grain boundaries (GB) form inside the original grains after the first ECAP pass. These boundaries are not clearly defined indicating an instable state. With the increase in number of passes, these low angle GBs evolve into well defined high angle GBs and the level of grain refinement increases.

Both cross sections of this sample have been scanned in detail. These areas are indicated in Fig. B.5 with rectangles. A detailed scan of sample ULC 1 pass ECAP perpendicular to the ED direction is shown in Fig. 5.10. The localized shear band is clearly visible by the high angle grain boundaries that surround it. The width of the band is 20 +/-3µm. The misorientation between the band and the surrounding matrix is about 30^0.

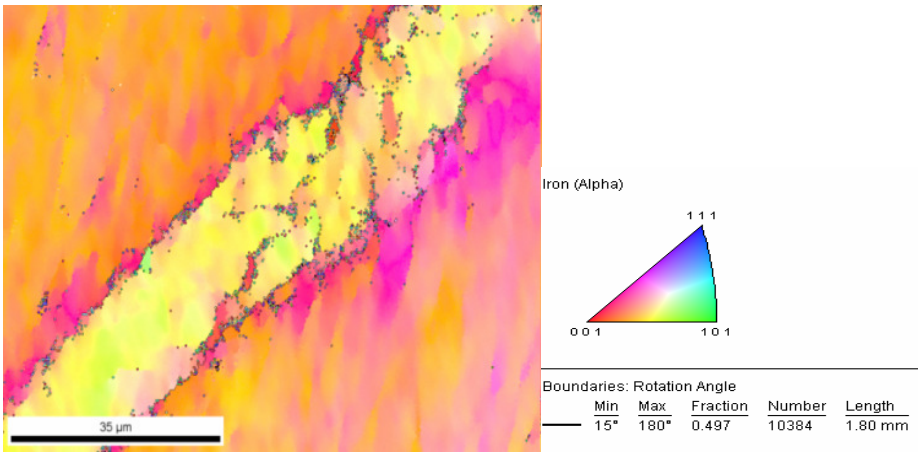

Figure 5.10: A Detailed EBSD data scan, collected with a step size of 0.3 µm, of 1 pass ECAPed ULC Steel.

After the second pass, more complex deformation structures are observed. The scans made over ED and TD sections of the sample, are shown in Fig. 5.11 and Fig. B.6.

The ED section shows a smooth structure crossed by bands. Shear bands are visible as bands in different morphology. There is 28+/- 15µm spacing between shear bands and the bandwidth is around 9 +/- 5 µm. The misorientation between the band and the surrounding matrix is about 40^0.

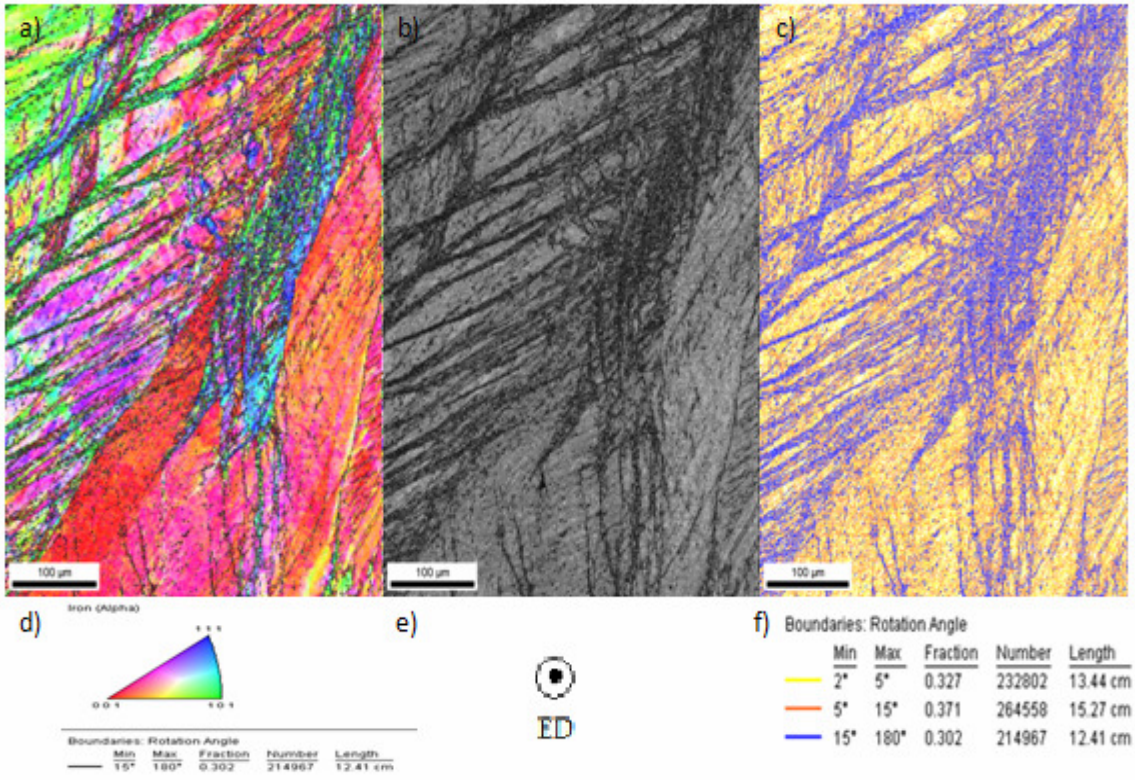

Figure 5.11: EBSD scan of ULC steel after 2 ECAP pass in ED section a) Inverse pole figure map, coloured according to the scale in d, b) Image quality map, c) Boundary map, high angle boundaries (>15^0) indicated with a blue line, medium angle boundaries indicated with orange line (5^0-15^0) and low angle boundaries indicated with yellow (2^0-5^0) line according to the scale in f.

Large differences of fragmentation continue to exist between regions in the material. In the ED section the region at the bottom right of the maps shows many low angle boundaries and only a few high angle boundaries. On the other hand the middle part of the maps contains only a few low angle boundaries and it has a fairly uniform orientation. In this region different crystal orientations are more intimately mixed. In the TD section fragmentation differences also continue to exist.

In the region at the bottom right of the maps it is obvious to see how different subdivision occurs in the grain. The grains are elongated and are cut by shear bands in two different directions. From literature it is known that at the onset of the deformation in the second pass by route B the critical shear stress on the activated slip systems is slightly higher than at the end of the first pass due to the cross change of strain path. After glide on these systems is initiated, the critical shear stress temporarily drops and slip localizes on a few slip planes cutting through the previously established dislocation structure. Obviously such slip contributes to the refinement of the fragment size.

The misorientation distribution after 2 pass via route B is shown in Fig. 5.12, together with the distribution in both cross sections. In the second pass the fraction of the boundaries with a misorientation angle of 5^0 has considerably decreased in favor of new medium and high angle boundaries.

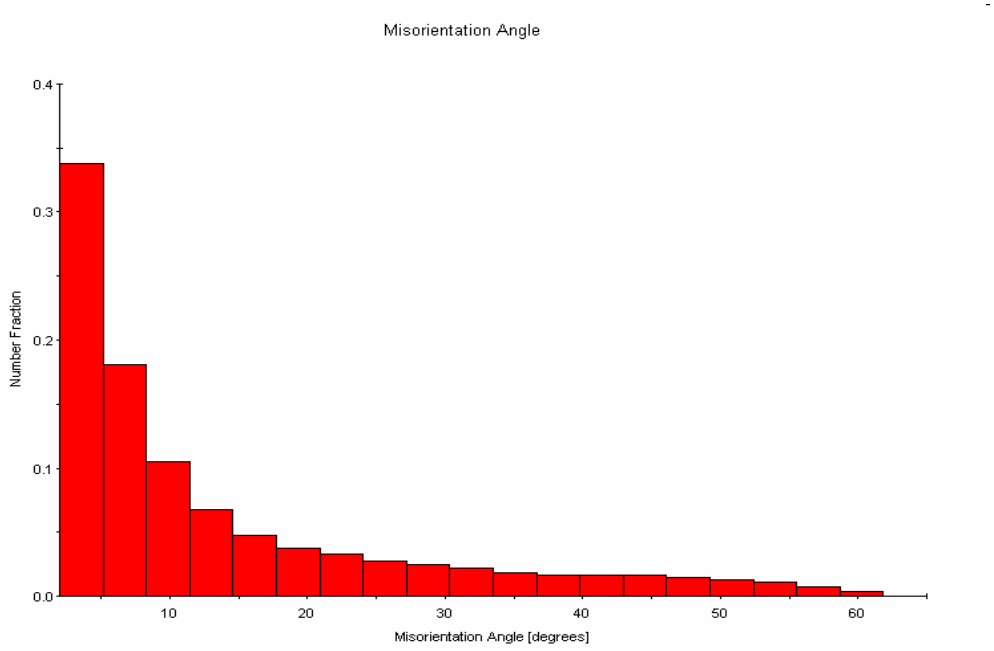

Figure 5.12: Misorientation distribution after 2 ECAP pass in ED section.

A detailed scan of the TD section consist of three grains with a different orientation. The evolution of the substructure is different for the two grains. It may be an indication of orientation dependent subdivision which is shown in Fig. B.8. A detailed scan of ULC 2 passes ECAPed sample perpendicular to the ED direction is shown in Fig. 5.13.

The shear bands and sub-grains are clearly visible. A difference in fragmentation between two grains is clearly visible. The upper part of the grain is strongly subdivided but the lower part of the grain is not subdivided yet and banding because of the deformation can be seen inside of the grain.

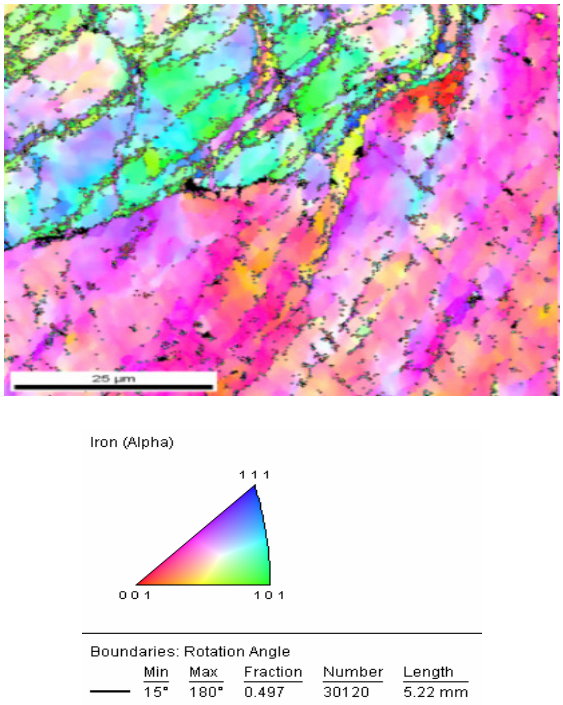

Figure 5.13: A Detailed EBSD data scan, collected with a step size of 0.3 µm, of 2 pass ECAPed ULC Steel.

Comparing the microstructures of the ULC steel taken after the second and the third pass, it is immediately noticed that the microstructure of the there times deformed material has clearly undergone a substantial change. Contrarily, the microstructure of the sample after two passes is clearly not fragmented. Band structure dominates the microstructure. EBSD maps of the microstructure after 3 passes via route B_c are shown in Fig. 5.14.This ECAP pass is very important because it bridges the drastic microstructural change between the 2^{nd} and the 4^{th} pass. In this pass original grains have disappeared and new small cells become visible.

The structure is completely deformed and the substructure continues to exist. It was necessary to apply a recovery heat treatment to the samples for 2 hours at 400°C in a salt bath. The images were collected with a step size 0.3µm, spot size 5 at 20kv voltage.

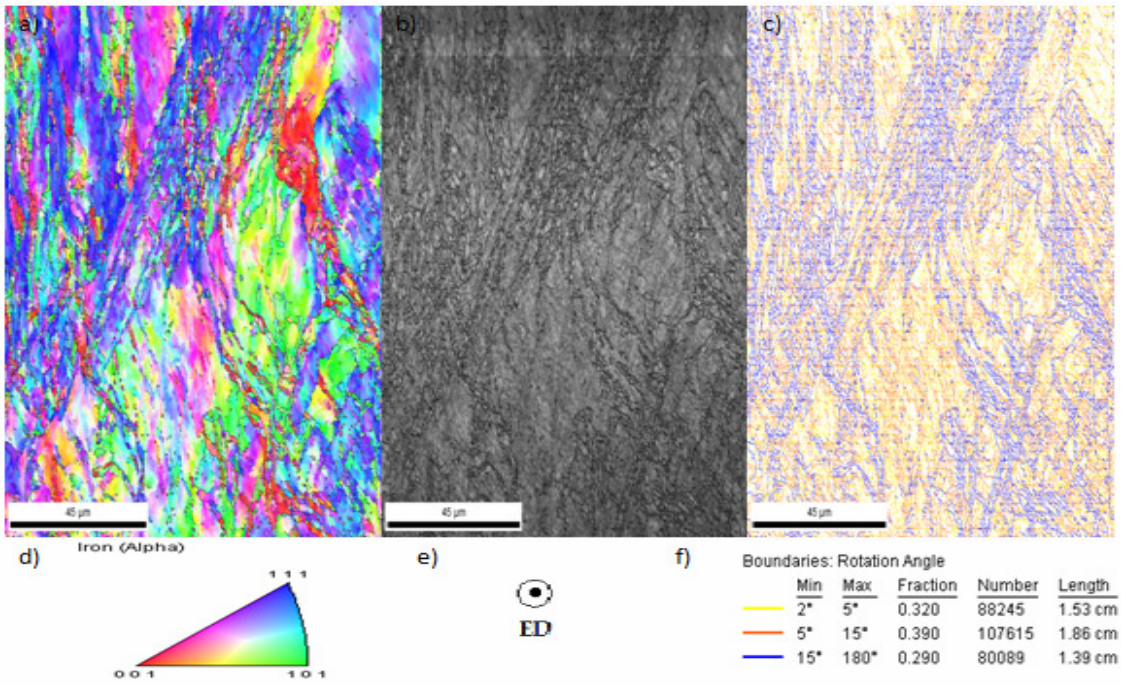

Figure 5.14: EBSD scan of ULC steel after 3 ECAP pass in ED section a) Inverse pole figure map, coloured according to the scale in d, b) Image quality map, c) Boundary map, high angle boundaries (>15^0) indicated with a blue line, medium angle boundaries indicated with orange line (5^0-15^0) and low angle boundaries indicated with yellow (2^0-5^0) line according to the scale in f.

The misorientation distribution after 3 passes is shown in Fig. 5.15. The difference after 2 passes is fairly small, but the fraction of high angle boundaries, are higher after 3 passes.

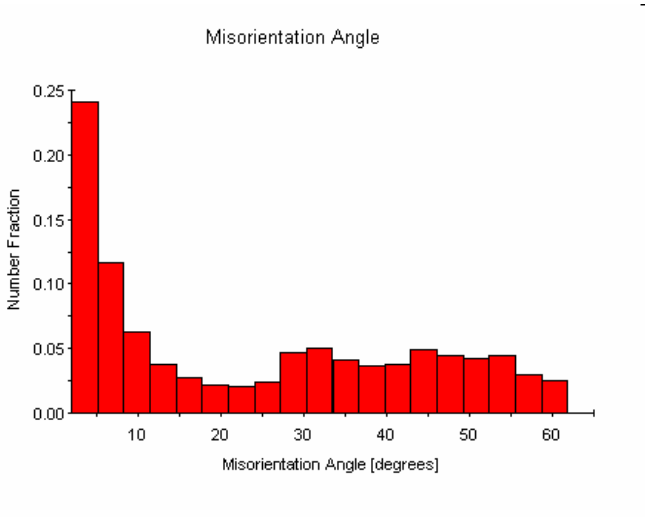

Figure 5.15: Misorientation distribution after 3 ECAP pass in ED section.

A detailed scan of the ED section consists of shear bands with a different orientation. The evolution of the shear bands is in different directions which is due to the cross change of strain path between two passes,is activating new slip systems. One can see elongated shear bands with small cell blocks in it. With a line scan accross these bands we can have information about the width of the bands, the width of the space between two bands and the misorientation of the bands. In the ED section the image collected with a step size of 0.1µm, shows an inhomogeneous microstructure. There is 3µm spacing between the shear bands and the band width is around 0,6 +/- 0,2 µm. The misorientation between the band and the surrounding matrix is about 12^0 +/-5^0. The misorientation inside of the band 8^0 + / - 2^0. The detailed images were collected with a step size 0, 1µm, spot size 5 at 20kV voltage which is given in Fig. 5.16.

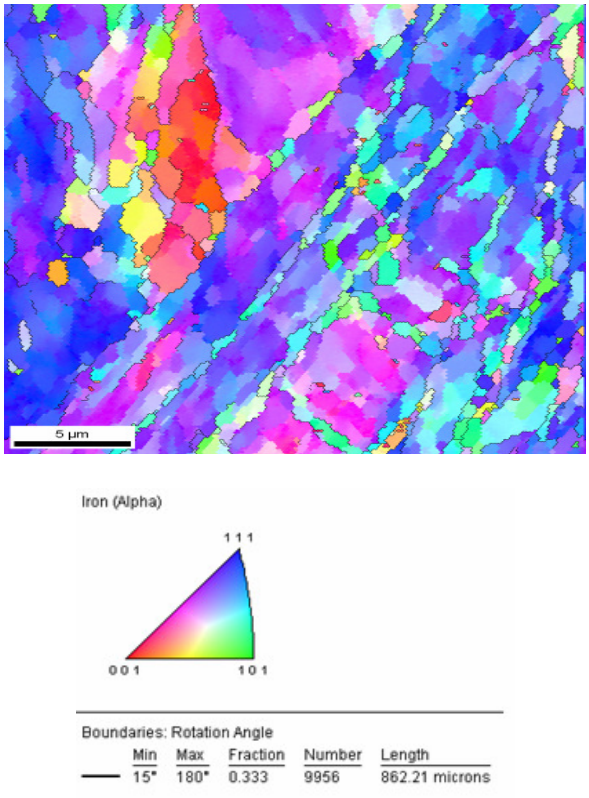

Figure 5.16: A Detailed EBSD data scan, collected with a step size of 0.3 µm, of 3 pass ECAPed ULC steel.

After four passes, the microstructure of the ULC steel is almost fully fragmented. On the other hand, there are still some regions can be observed not fully fragmented.

The scans made on a sample that is pressed 4 times through the ECAP die, are shown in Fig. 5.17 and Fig. B.10.

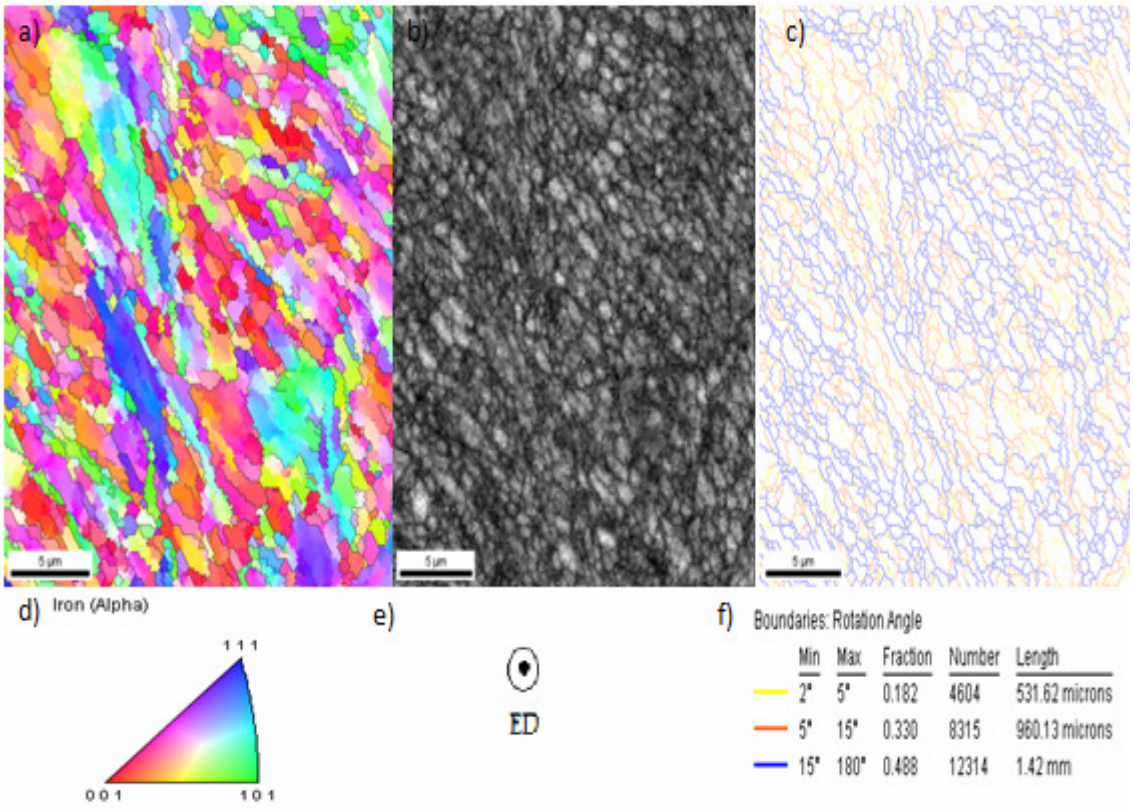

Figure 5.17: EBSD scan of ULC steel after 4 ECAP pass in ED section a) Inverse pole figure map, coloured according to the scale in d, b) Image quality map, c) Boundary map, high angle boundaries (>15^0) indicated with a blue line, medium angle boundaries indicated with orange line (5^0-15^0) and low angle boundaries indicated with yellow (2^0-5^0) line according to the scale in f.

In both section images are collected with a step size of 0.15µm and a spot size 5 with 20kv voltage. The step size is very small because of the presence of new small grains. It was necessary to apply a recovery heat treatment to the samples for 2 hour. Subdivision differences still exist. In both sections it is clear that the less fragmented areas are still present and visible in the EBSD maps.

For instance, in Fig. B.10 the green region mostly at the lower part is clearly less fragmented. In the misorientation distribution the fraction of low angle boundaries continues to decrease and high angle boundaries continue to increase in a big range.

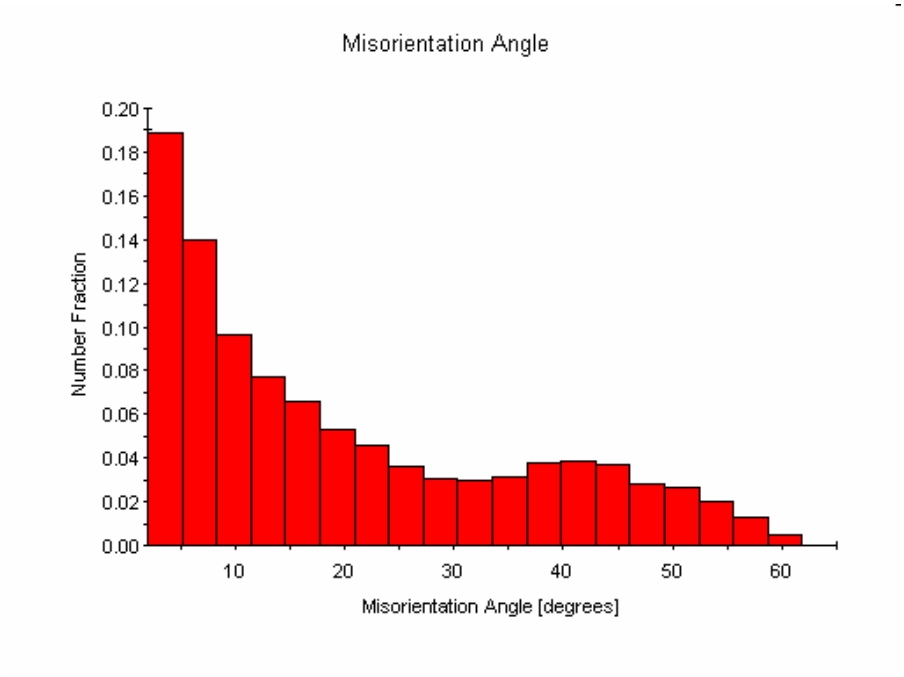

Figure 5.18: Misorientation distribution after 4 ECAP pass in ED section.

Sample pressed through the ECAP die at moderate homologous temperature (172^0 C or T_h =0,246) 5 times, is performed to investigate the substructural difference between 4 and 8 passes. This step not gives an crucial information about structural aspect during deformation process. It was necessary to apply a recovery heat treatment to the samples for 2 hours at 400°C.

The images were collected with a step size 0.3µm, spot size 5 at 20kv voltage. and Orientation image maps are shown in Fig. B.12 and B.13. for both sections. After 8 ECAP passes the microstructure is completely different from the previous passes. It is more homogeneous and equiaxed grains become visible in this stage. The grain size is approximately 0.8µm. It can also be noticed that some of the grains didn't finish the evolution yet.

The scans, which were taken in both-section, show equiaxed and elongated grains together. It was necessary to apply a recovery heat treatment to the samples for 2 hours at 300°C. The images were collected with a step size of 0, 15µm, spot size 5 at 20kv voltage. Fig 5.19 and Fig. B.14 show maps of an EBSD scan and fully fragmented structure are visible for two cross sections.

A line scan option was performed in some areas of the scan to have an idea about misorientation distribution and grain size. There is a high misorientation in between new grains which is around 50^0+/- 10^0, whereas the misorientation inside of the both equiaxed and elongated grains is around 8^0+/-5^0.

Line scan data gives also information about the grain size. For elongated grains the width is 0,8 +/- 0.5 µm and length is around 10µm +/- 7µm. Equiaxed grains are as it mentioned before, around 0,8µm large.

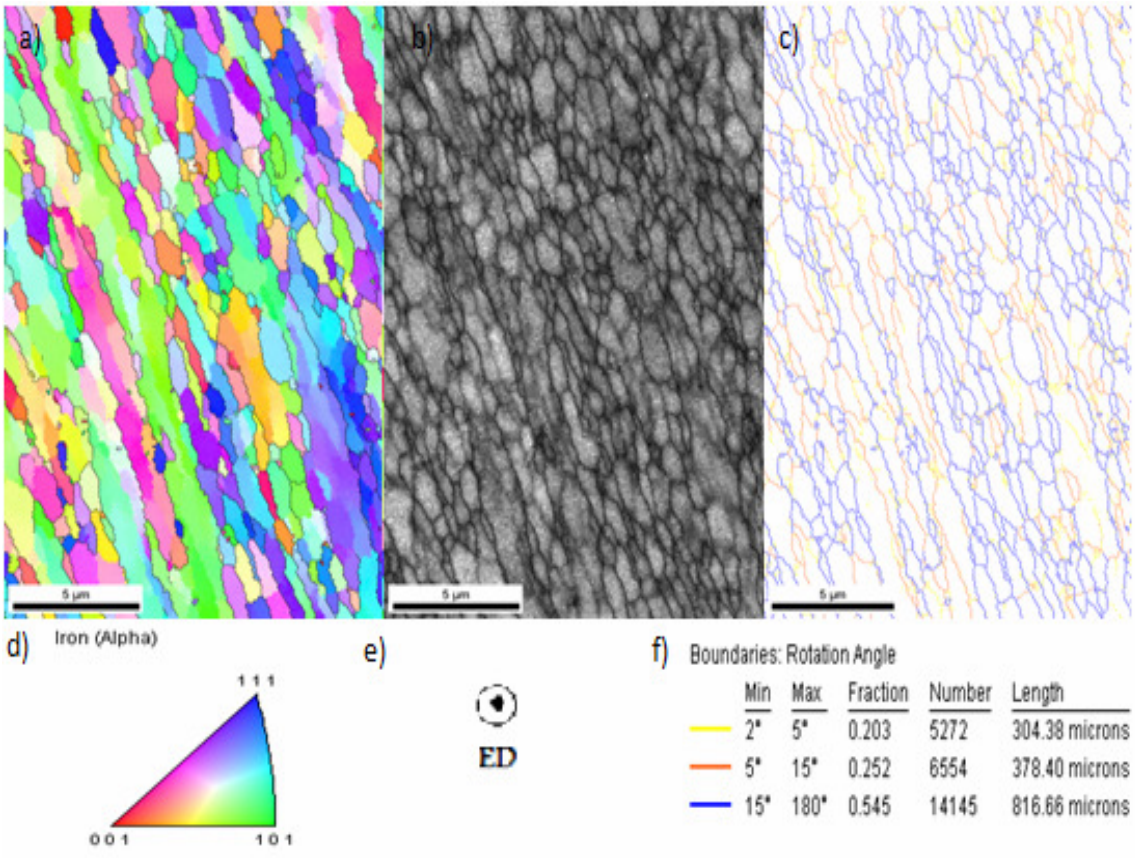

Figure 5.19: EBSD scan of ULC steel after 8 ECAP pass in ED section a) Inverse pole figure map, coloured according to the scale in d, b) Image quality map, c) Boundary map, high angle boundaries (>15^0) indicated with a blue line, medium angle boundaries indicated with orange line (5^0-15^0) and low angle boundaries indicated with yellow (2^0-5^0) line according to the scale in f.

The scans which were collected with a step size of 0, 1 µm from a TD section, give about the same results as the scans collected from the ED section. But this cross section has more equiaxed grains than the ED section with a 0, 9 +/- 0, 1 µm grain size.

Many new high angle boundaries are formed after 8 ECAP passes. Due to this fact the misorientation distribution fraction of high angle boundaries increased.

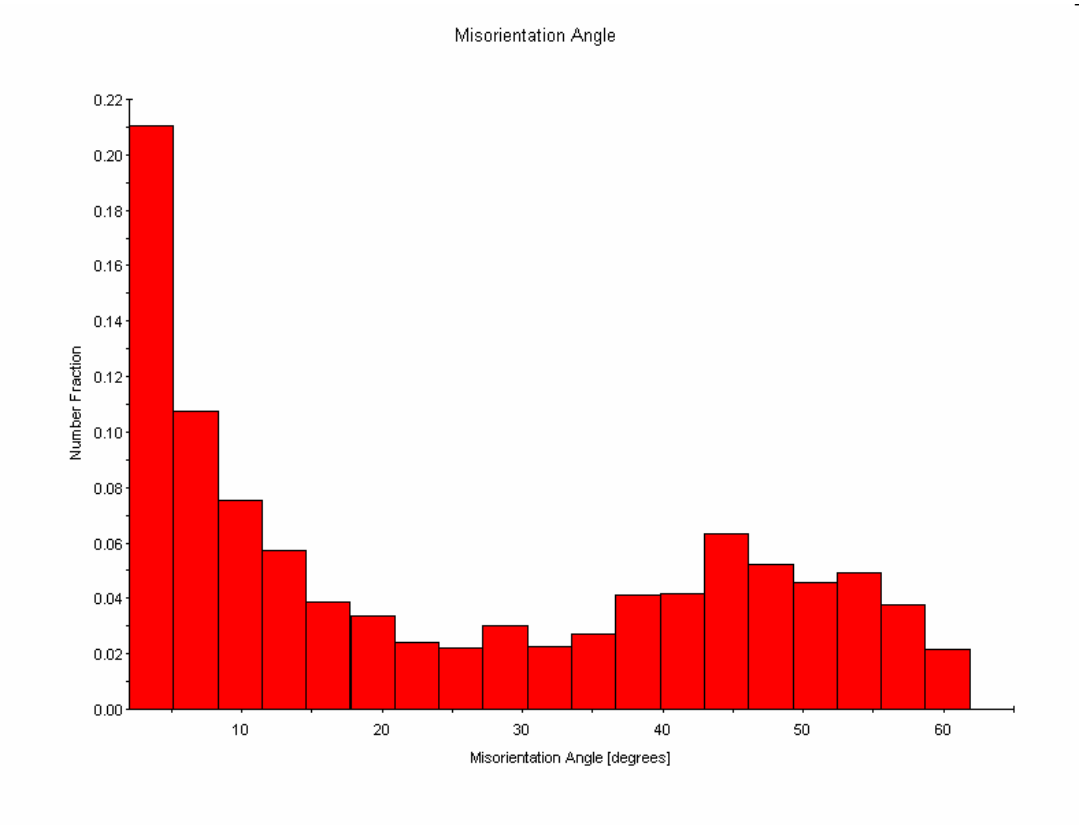

Figure 5.20: Misorientation distribution after 8 ECAP passes in ED section.

5.2.2.1 Misorientation differences through the ECAP passes

Misorientation distribution data give an overview of the structural evolution so it is important to compare the misorientation distribution of all ECAP passes. The values are compared for both cross sections in different graphs to see the correlation between the two sections.

The huge decrease is between 1 and 2 passes. And it can also be deduced from the graph that the large fraction of high angle boundaries can be seen after 5 and 8 passes.

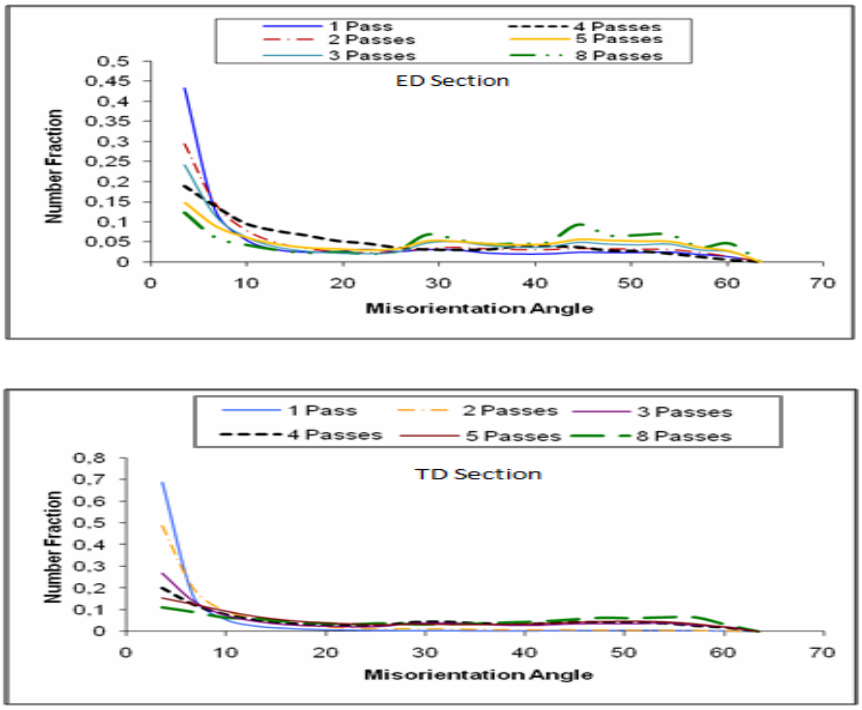

Figure 5.21: Misorientation distribution after all ECAP passes in both cross sections.

It is obvious from Fig. 5.22, that with an increasing ECAP pass; the fraction of the low angle boundaries between 2^0-5^0 is decreasing and the fraction of the high angle boundaries between 15^0-180^0 is increasing.

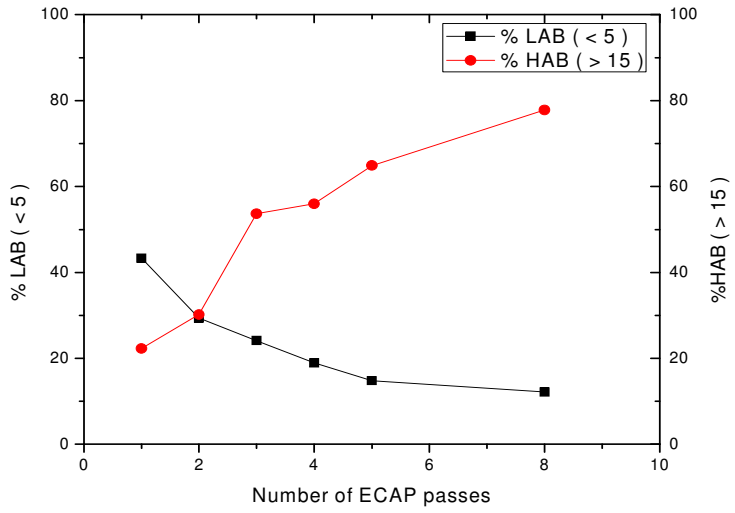

Figure 5.22: Variation of angle boundary through ECAP passes in ED section.

5.2.2.2 Evolution of micro structural parameters through the ECAP passes

The microstructural parameters measured by EBSD after ECAP are given in Table 5.1. The fraction of average boundary misorientation and percentage of high angle boundaries increasing is observed with augmented strain. The distinct morphology of the elongated micro shear bands starts to get replaced with cell blocks after 3 passes of ECAP. It is apparent from Table 5.1 that the fraction of high angle boundaries increases noticeable. The most drastic grain size decrease happens in between the 0 and 1 pass of ECAP. After 1 ECAP pass the grain size is around 200-250 µm as different from the initial material. Eventually after 8 passes of ECAP, very fine grains can be seen in the microstructure with a grain size around 0, 8 µm.

Table 5.1: Microstructural parameters obtained from EBSD measurements after 1, 2, 3, 4, 5, 8 ECAP passes via route B_c. The approximate equivalent strain ε_{eq}, Grain size d (µm), average boundary misorientation η (°) and percentage of high angle boundaries %HAB (%) are given for both section.

ED Sec.	**ε eq**	**d (µm)**	**η (°)**	**%HAB (%)**
1 Pass	1.15	~250µm	12.43	22.3
2 Pass	2.3	~70µm	18	30.2
3 Pass	3.45	~10µm	22.4	53.7
4 Pass	4.6	~5µm	23	56
5 Pass	5.75	~3µm	27.8	64.9
8 Pass	9.2	~0.8µm	33.6	77.8
TD Sec.	**ε eq**	**d (µm)**	**η (°)**	**%HAB (%)**
1 Pass	1.15	~275µm	13	24
2 Pass	2.3	~75µm	16	32.6
3 Pass	3.45	~15µm	21.3	46.5
4 Pass	4.6	~6µm	23	53.3
5 Pass	5.75	~3µm	24.29	55.31
8 Pass	9.2	~0.9µm	31.1	71.8

The microstructural parameters, which is measured from the ED section has values very close to those from the TD section. It is observed that both cross-section shows similarity to each other. It can be shown that from Fig. 5.23.

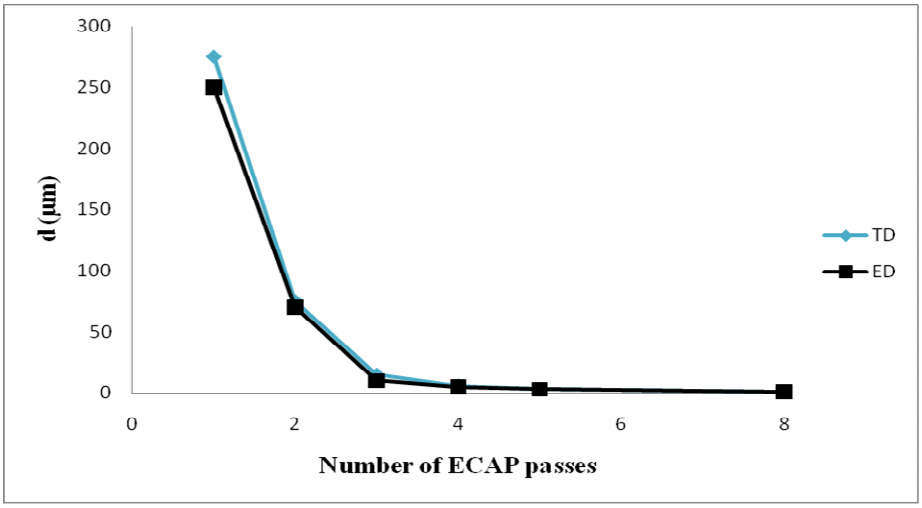

Figure 5.23: Grain size distribution as a function of ECAP passes

6. CONCLUSIONS

Ultra low carbon steel was processed by Equal Channel Angular Pressing (ECAP) with a sample rotated by 90^0 in the same direction between each pass in processing route Bc. The results reveal an evolution in the microstructure and mechanical properties. The results, is achieved throughout this research is compared with the results from a Phd. Thesis of Joke De Messemaeker and it is obtained that microstructural parameters which is given in previous part is close to each other with IF steel after ECAP process .In the present study, according to results the following conclusions can be made;

- ✓ The compression tests show a continuous strengthening of the samples pressed throughout the ECAP die. The explanation of the strength increase can be the decreasing grain size and increasing amount of dislocations inside of the grains with severe plastic deformation.
- ✓ The Micro hardness tests show there is a remarkable increase of hardness value between 0 and 8 passes but the drastic increments is achieved after the first pass. The reason of this big hardness increase between pass 0 and 1, is the uniform matrix before ECAP where the mean free path of the dislocations is very long.
- ✓ The interesting features occur after three ECAP passes, cell blocks start to replace the banding structure in this step.
- ✓ The fraction of the high angle boundaries increases with increasing strain on the other hand the fraction of low angle boundaries and grain size is decreasing simultaneously.
- ✓ At the end of pass 8 the microstructure is completely different from the initial material with equiaxed and elongated new fragments.

REFERENCES

[1] **Gleiter H.**, 1981. Deformation of Polycrystals: Mechanisms and Microstructures, Roslilde, Denmark.

[2] **Tsuzaki K.**, 2002. Preface to the Special Issue on Advanced Structural Steels, *ISIJ International*, **42**, 1325-1326.

[3] **Shin D.H., Park K.T.**, 2005. Ultrafine Grained Steels Processed by Equal Channel Angular Pressing, *Material Science and Engineering: A,* **410-411**, 299-302.

[4] **Zrnik J. et al**, 2007. Low carbon steel processed by equal channel angular warm pressing, *Metalurgija,* **46**, 21-27.

[5] **Shin D.H. et al**, 2000. Refinement mechanism during equal channel angular pressing of low carbon steel, *Acta Materialia*, **49**, 1285-1292.

[6] **Valiev R.Z., Islamgaliev R.K. and Alexandrov I.V.**, 2000. Bulk nanostructured materials from severe plastic deformation, *Prog. Material Science*, **45**, 103-189.

[7] **Horita Z., Fujinami T. and Langdon T.G.,** 2001. The potential for scaling ECAP: effect of sample size on grain refinement and mechanical properties, *Mater. Sci. Eng. A*, **318**, 34-41.

[8] **De Messemaeker J., Verlinden B. and Van Humbeeck J.,** 2004. On the strength of boundaries in submicron IF steel, *Material Letters*, **58**, 3782-3786.

[9] **Langdon T.G.**, 1993. The role of grain boundaries in high temperature deformation, *Material Science Engineering A*, **166**, 67-79.

[10] **Langdon T.G.**, 1994. A unified approach to grain boundary sliding in creep and superplasticity, *Acta Materialia,* **42**, 2437-2443.

[11] **Gholinia A., Humpreys F.J. and Prangnell P.B.**, 2002. Processing to ultrafine grain structures by conventional routes, *Mater. Sci. Tech.*, **16**, 1251-1255.

[12] **Sanders P.G., Fougere G.E., Thompson L.J., Eastman J.A. and Weertman J.R.**, 1997. Improvements in the synthesis and compaction of nanostructured materials, *Nanostruct. Mater.* , **8**, 243-252.

[13] **Koch C.C.**, 1997. Synthesis of nanostructured materials by mechanical milling: problems and opportunities, *Nanostruct. Mater,* **9**, 13-22.

[14] **Rigney D.A.**, 1988. Sliding wear of metals, *Ann. Rev. Mater. Sci*. **18**, 141-163.

[15] **Valiev R.Z., Korznikov A.V. and Mulyukov R.R.**, 1993. Structure and Properties of Ultrafine-Grained Materials Produced by Severe Plastic Deformation, *Mater. Sci. Eng. A*, **168**, 141-148.

[16] **Huang J. Y., Zhu Y. T., Jiang H. and Lowe T. C.**, 2001**.** Microstructures and dislocation configurations in nanostructured Cu processed by repetitive corrugation and straightening, *Acta Materialia,* **49**, 1497-1505.

[17] **Kim H. S.**, 2001. Finite element analysis of high pressure torsion processing, *Journal of Materials Processing Technology,* **113**, 617-621.

[18] **Ghosh A. K.**, 1988. Method of producing a fine grain aluminium alloy using three axes deformation, *U.S.Patent*, No: 4,721,537, USA.

[19] **Cherukuri B.**, 2004. Multi Axial Compression/Forging of AA6061, *M.Sc Thesis*, Wright State University, Dayton OH, USA.

[20] **Tsuji N., Saito Y., Utsunomiya H. and Tanigawa S.,** 1999. Ultra-fine grained bulk steel produced by accumulative roll-bonding (ARB) process, *Scripta Materialia,* **40**,795-800.

[21] **Saito Y., Utsunomiya H., Suzuki H. and Sakai T.**, 2000. Improvement in the r-value of aluminum strip by a continuous shear deformation process, *Scripta Materialia*, **42**, 1139-1144.

[22] **Segal V.M., Reznikov V.I., Drobyshevskiy A.E. and Kopylov V.I.**, 1981. *Russian Metall*., **1**, 99-105.

[23] **Segal V.M., Reznikov V.I., Kopylov V.I., Pavlik D.A. and Malyshev V.F.**, 1994. Process of Structure Formation During Straining, Scientific and Technical Publishing, Minsk, Belarus.

[24] **Segal V.M.,** 2002. Ultrafine Grained Materials II, *The Minerals, Metals & Materials Society,* Warrendale, PA, USA, April 19-23.

[25] **Farukawa M., Ohishi K., Komura S., Utsunomiya A., Horita Z., Nemoto M. and Langdon T.G.**, 1999. *Mater. Sci. Forum*, **97**, 304-306.

[26] **Nishida Y., Arima H., Kim J.C. and Ando T.**, 2001. Rotary-die equal-channel angular pressing of an Al – 7 mass% Si – 0.35 mass % Mg alloy, *Scripta Mater*., **45**, 261-266.

[27] **Segal V.M.**, 1997. *USSR Patent*, No: 575892.

[28] **Valiev R.Z., Krasilnikov N.A. and Tsenev N.K.**, 1991. Plastic deformation of alloys with submicron-grained structure, Institute for Metals Superplasticity Problems, *Mater. Sci. Eng. A*, **137**, 35-40.

[29] **Berbon P.B.**, 1998. Processing of ultrafine grained materials using the Equal channel angular pressing technique and optimization of the parameters to obtain superplasticity, *Doctorate Thesis*, University of Southern California, USA.

[30] **Wu Y. and Baker I.**, 1997. An experimental study of equal channel angular extrusion, *Scripta Materialia*, **37**, 437-442.

[31] **Korb G.**, 2008. Severe plastic deformation, *ARC Research Report*, Seibersdorf.

[32] **Zehetbauer M.J.**, 2008. Publishing jointly with Russian colleagues experiences in the field of Nanostructured Materials, *Rusera Exe Training course*, Vienna, Austria.

[33] **A. Rosochowski et al**, 2005. Methods of fabricating metals for nano-technology, *Bulletin Of The Polish Academy Of Sci.*, **53-4**, 413- 423.

[34] **Saito N.**, 2002. Production of Fine-Grained metals by rotary die Equal-Channel Angular Pressing, *AIST Today*, **2**, 10-28.

[35] **Raab G.I.**, 2005. Plastic flow at equal channel angular processing in parallel channels, *Mater Sci Eng. A*, **410-411**, 230-233.

[36] **Lee J.C.**, **Seok H.K. and Suh J.Y.**, 2002. Microstructural evolutions of the Al strip prepared by cold rolling and continuous equal channel angular pressing, *Acta Mater.*, **50**, 4005-4019.

[37] **Raab G.J, Valiev R.Z., Lowe T.C. and Zhu Y.T.**, 2004. Continuous processing of ultrafine grained Al by ECAP–Conform, *Materials Science and Engineering A,* **382**, 30-34.

[38] **Valiev R.Z. and Langdon T.G.**, 2006. Principles of equal-channel angular pressing as a processing tool for grain refinement, *Progress in Material Science,* **51**, 881-981.

[39] **Furukawa M. et.al**, 1997. The shearing characteristics associated with equal-channel angular pressing, *Mat. Sci. and Eng. A,* **257**, 328-332.

[40] **Furukawa M.**, 2001. Processing of metals by equal-channel angular pressing, *Journal of Materials Science,* **36**, 2835-2843.

[41] **Langdon T.G.**, 2007. The principles of grain refinement in equal-channel angular pressing, *Materials Science and Engineering A,* **462**, 3-11.

[42] **Furukawa M. et.al**, 2002. Factors influencing the shearing patterns in equal-channel angular pressing, *Materials Sci. and Eng. A,* **332**, 97-109.

[43] **Suh J.Y. et.al**, 2001. Finite element analysis of material flow in equal channel angular pressing, *Scripta Materialia,* **44**, 667-681.

[44] **Moss M.**, 2006. Novel Solid State Processing Route for the Development of Nanostructure Mg. Alloys, *ARC Research Report*, Australia.

[45] **Hansen N.**, 1990. Cold deformation microstructures, *Materials Science and Technology*, **6**, 1039-1040.

[46] **Hughes D.A. and Hansen N.**, 1996. High angle boundaries formed by grain subdivision mechanisms, *Acta Materialia*, **45-9**, 3871-3886.

[47] **Kulhman W.D. and Hansen N.,** 1991. Geometrically necessary, incidental and subgrain boundaries, *Scripta Metallurgica et Materialia*, **25**, 1557-1562.

[48] **Hughes D.A.**, 1993. Microstructural evolution in a non-cell forming metal Al-Mg, *Acta Metallurgica et Materialia*, **41**, 1421-1430.

[49] **Iwahashi Y., Horita Z., Nemoto M. and Langdon T.G**., 1997.An investigation of microstructural evolution during equal-channel angular pressing, *Acta Materialia*, **45**, 4733-4741.

[50] **Valiev R.Z., Ivanisenko Yu.V., Rauch E.F. and Baudelet B.**, 1996. Structure and deformation behavior of Armco iron subjected to severe plastic deformation, *Acta Materialia*, **44**, 4705-4712.

[51] **Wang Z.C. and Prangnell P.B.**, 2002. Improvement of mechanical property of polyimide blends with ^{60}Co-irradiation, *Radiation Physics and Chemistry*, **65**, 87-92.

[52] **Terhune S.D. et. al,** 2002. An investigation of microstructure and grain-boundary evolution during ECA pressing of pure aluminum, *Metallurgical and Materials Transactions A, **33-7**, 2173-2184.*

[53] **Li B.L. et.al**, 2004. Microstructural evolution of IF-steel during cold rolling, *Acta Materialia*, **52**, 1069-1081.

APPENDIX A

Table A.1: Microhardness over ED and TD sections, of Initial and ECAP samples.

	0 Pass	1 Pass	2 Pass	4 Pass	8 Pass
Hv (ED Sec.)	83.77 +/2.35	199.97 +/-24.4	218.95 +/-8.39	237.63 +/-13.9	261.64 +/-18.4
Hv (TD Sec.)	88.24 +/4.04	199.44 +/-8..97	219.30 +/- 13.9	241.59 +/-25.9	256.34 +/- 15.0

Table A.2: Micro-Indentation Harness values in different loading conditions, of Initial and ECAP samples.

	50g	100g	200g	300g	400g	500g
0 Pass	119.66	99.763	98.76	97.706	96.608	95.149
1 Pass	276.82	262.53	254.74	241.98	236.12	226.31
3 Pass	321.46	308.51	287.02	280.05	275.73	259.74
5 Pass	336.89	310.24	301.85	288.86	279.89	272.62
8 Pass	344.34	319.35	303.4	298.04	295.99	293.8

Table A.3: Micro-Indentation Harness values which is calculated with energy method, of Initial and ECAP samples.

	50g	100g	200g	300g	400g	500g
0 Pass	106,31	85,83	92,96	90,6	93,35	92,61
1 Pass	237,51	250,30	246,90	234,50	241,90	219,30
3 Pass	312,30	285,30	264,10	251,41	254,50	252,60
5 Pass	326,90	300,70	275,70	288,10	273,30	267,80
8 Pass	345,30	299,50	289,90	295,06	284,16	283,37

APPENDIX B

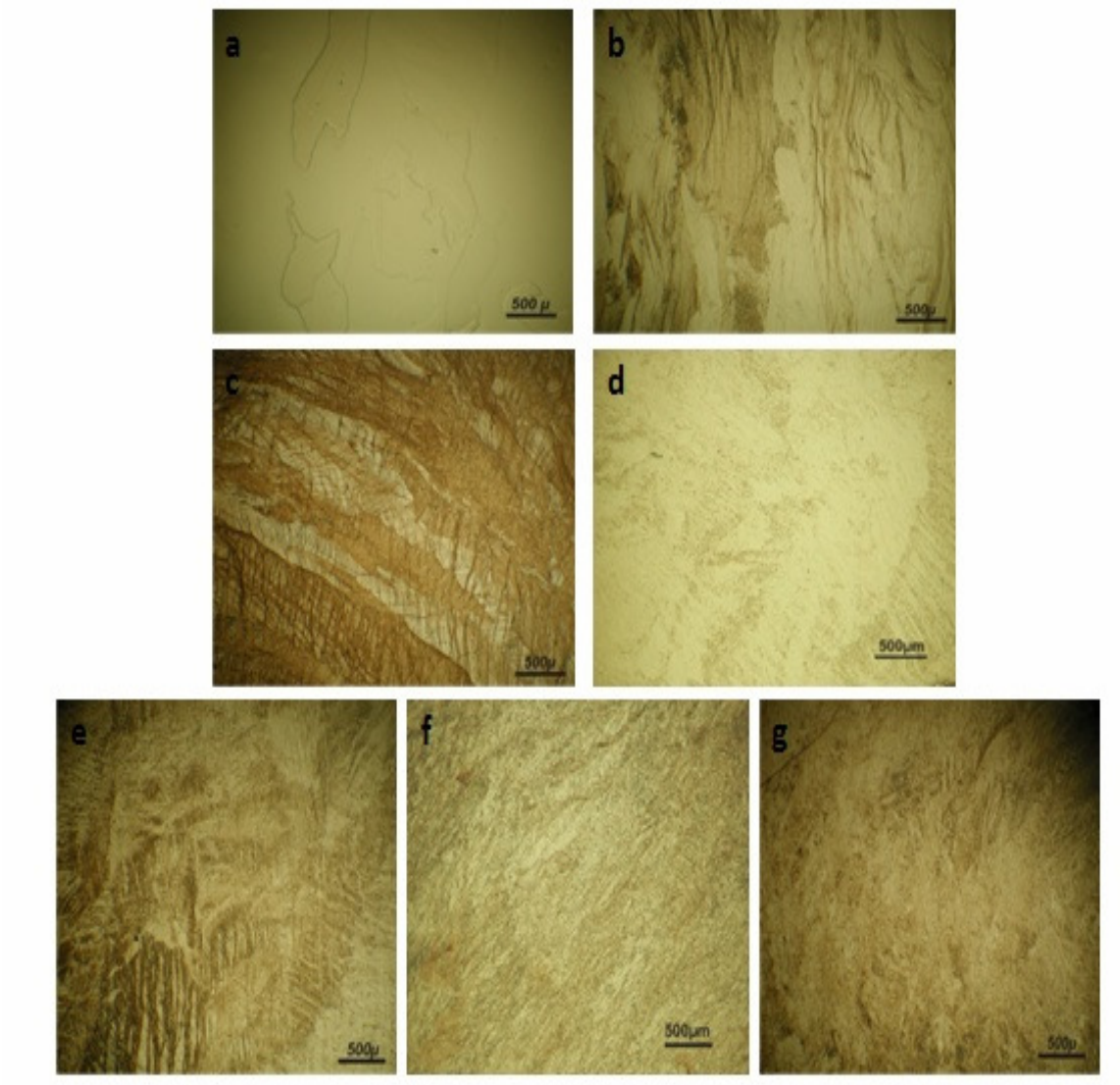

Figure B.1: Microstructure, obtained by optical microscopy on the TD section of the samples a) As received ULC steel b) 1 pass ECAP ULC steel c) 2 pass ECAP ULC steel d) 3 pass ECAP ULC steel e) 4 pass ECAP ULC steel f) 5 pass ECAP ULC steel g) 8 pass ECAP ULC steel.

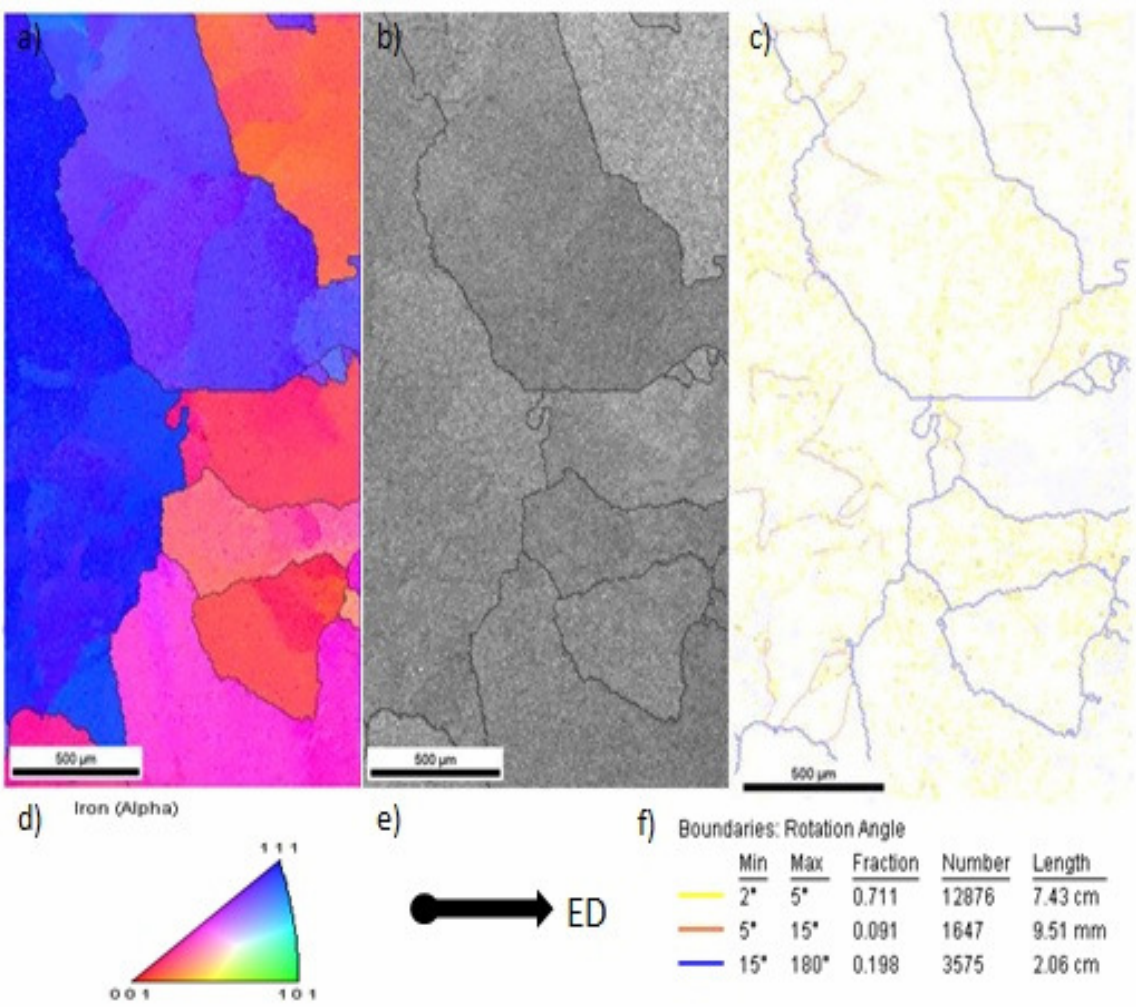

Figure B.2: EBSD scan of ULC steel after 0 ECAP pass in TD section a) Inverse pole figure map, coloured according to the scale in d, b) Image quality map, c) Boundary map, high angle boundaries (>15^0) indicated with a blue line, medium angle boundaries indicated with orange line (5^0-15^0) and low angle boundaries indicated with yellow (2^0-5^0) line according to the scale in f. ND direction is the reference direction for inverse pole figure.

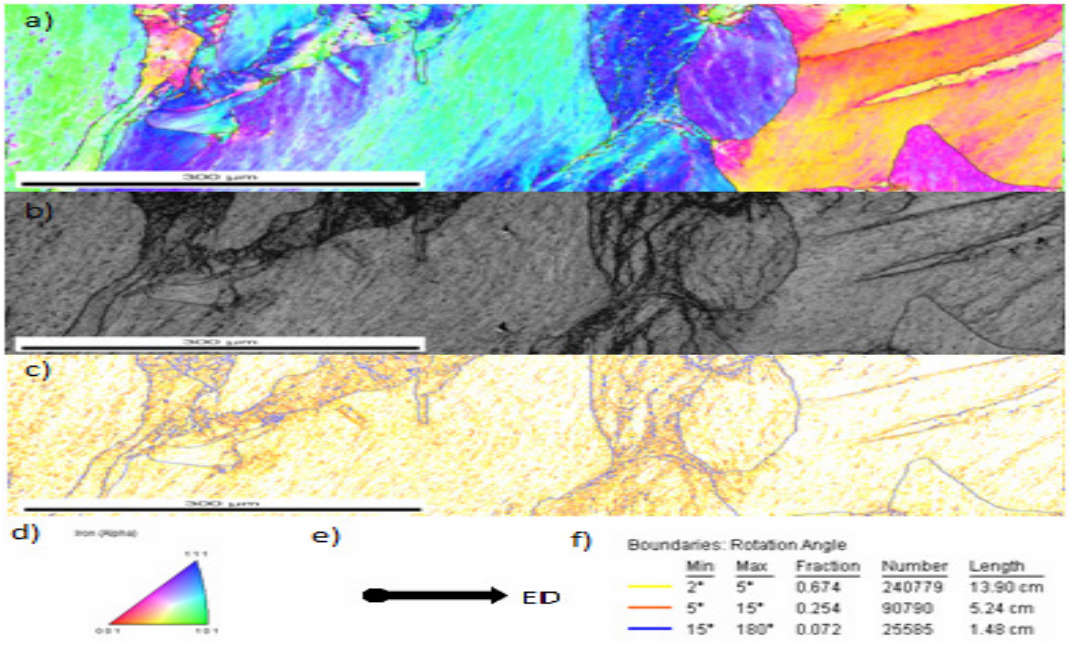

Figure B.3: EBSD scan of ULC steel after 1 ECAP pass in TD section a) Inverse pole figure map, coloured according to the scale in d, b) Image quality map, c) Boundary map, high angle boundaries (>15^0) indicated with a blue line, medium angle boundaries indicated with orange line (5^0-15^0) and low angle boundaries indicated with yellow (2^0-5^0) line according to the scale in f.

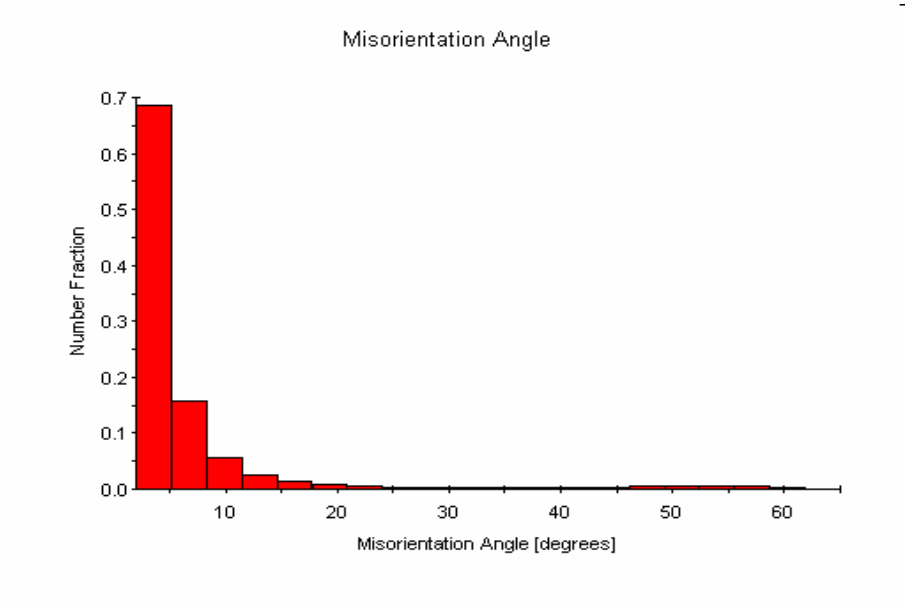

Figure B.4: Misorientation distribution after 1 ECAP pass in TD section.

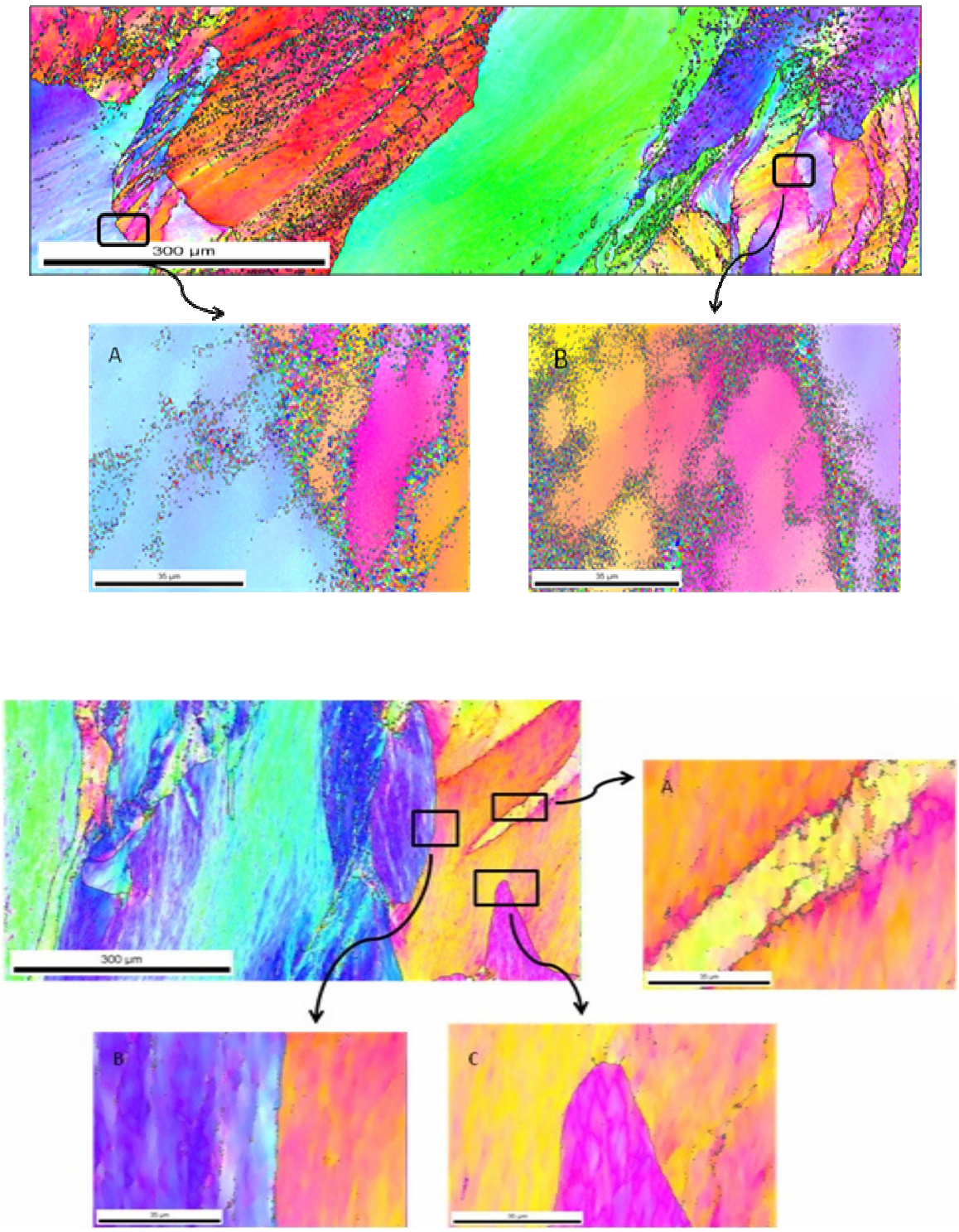

Figure B.5: The black boxes indicate the detailed scan areas after 1 ECAP pass ULC steel for ED and TD sections. The step size, to collect the EBSD data, is 0.3 µm.

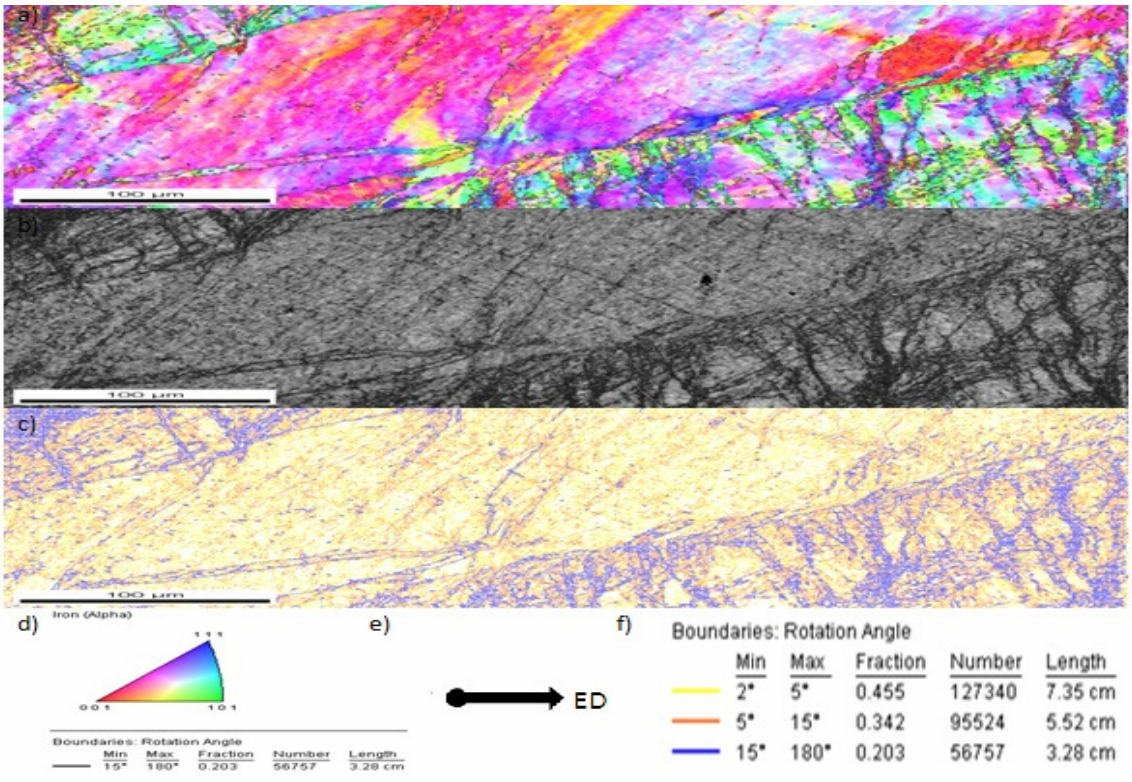

Figure B.6: EBSD scan of ULC steel after 2 ECAP pass in TD section a) Inverse pole figure map, coloured according to the scale in d, b) Image quality map, c) Boundary map, high angle boundaries (>15^0) indicated with a blue line, medium angle boundaries indicated with orange line (5^0-15^0) and low angle boundaries indicated with yellow (2^0-5^0) line according to the scale in f.

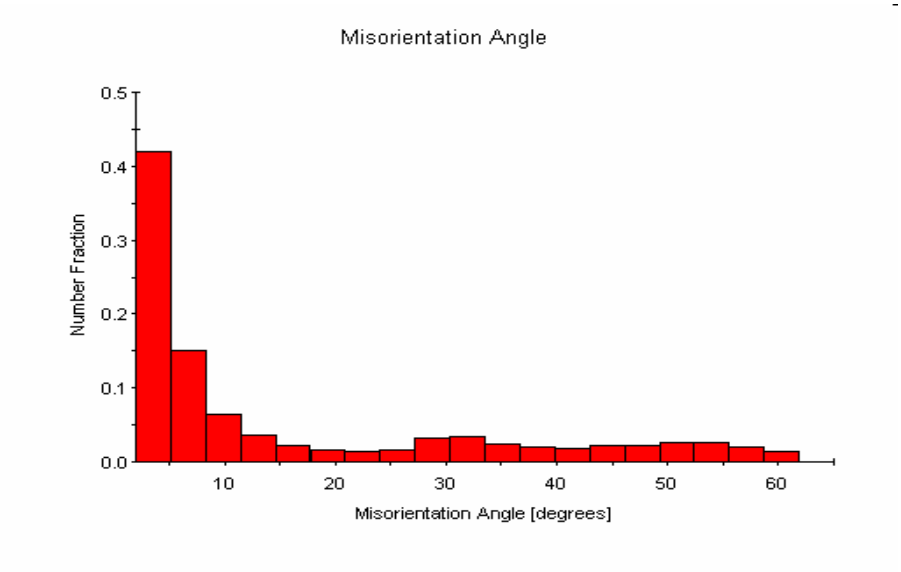

Figure B.7: Misorientation distribution after 2 ECAP pass in TD section.

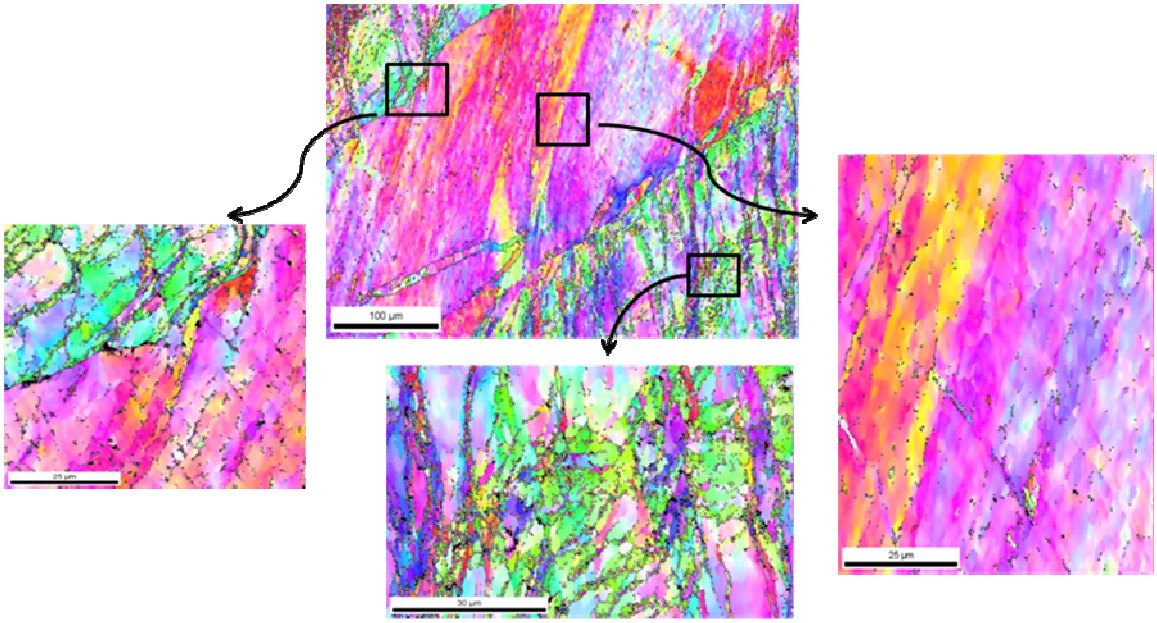

Figure B.8: The black boxes reveal the detailed scan areas after 2 ECAP pass ULC steel for TD section. The step size, to collect the EBSD data, is 0.3 µm.

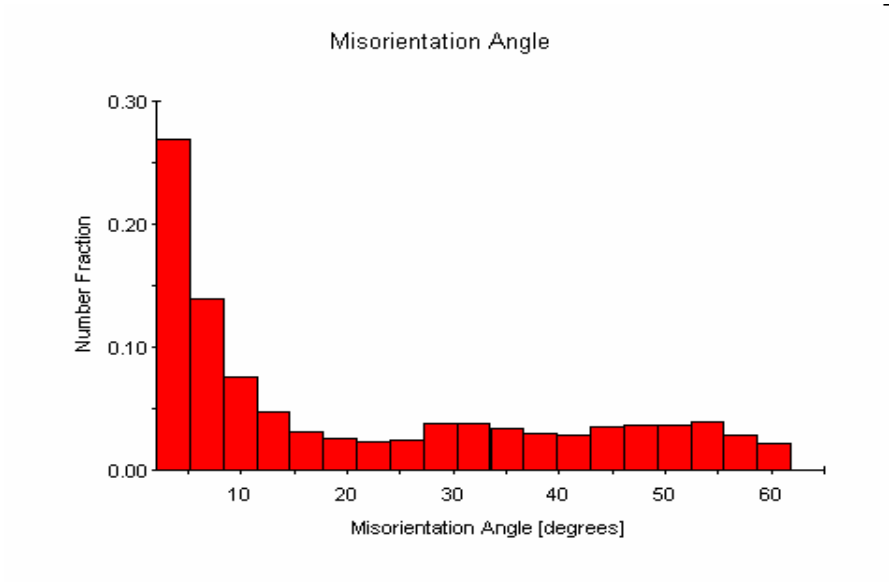

Figure B.9: Misorientation distribution after 3 ECAP pass in TD section.

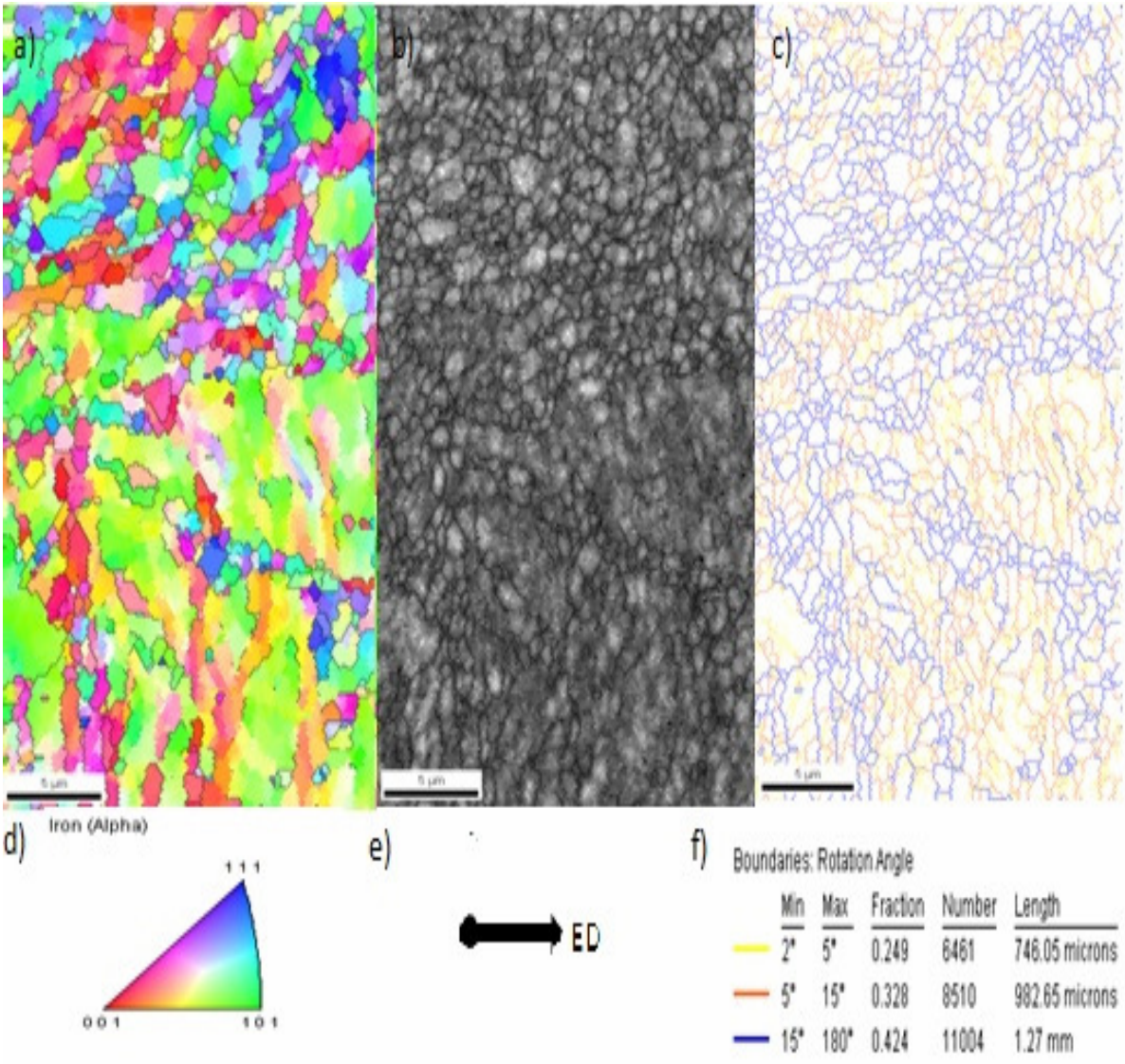

Figure B.10: EBSD scan of ULC steel after 4 ECAP pass in TD section a) Inverse pole figure map, coloured according to the scale in d, b) Image quality map, c) Boundary map, high angle boundaries (>15^0) indicated with a blue line, medium angle boundaries indicated with orange line (5^0-15^0) and low angle boundaries indicated with yellow (2^0-5^0) line according to the scale in f.

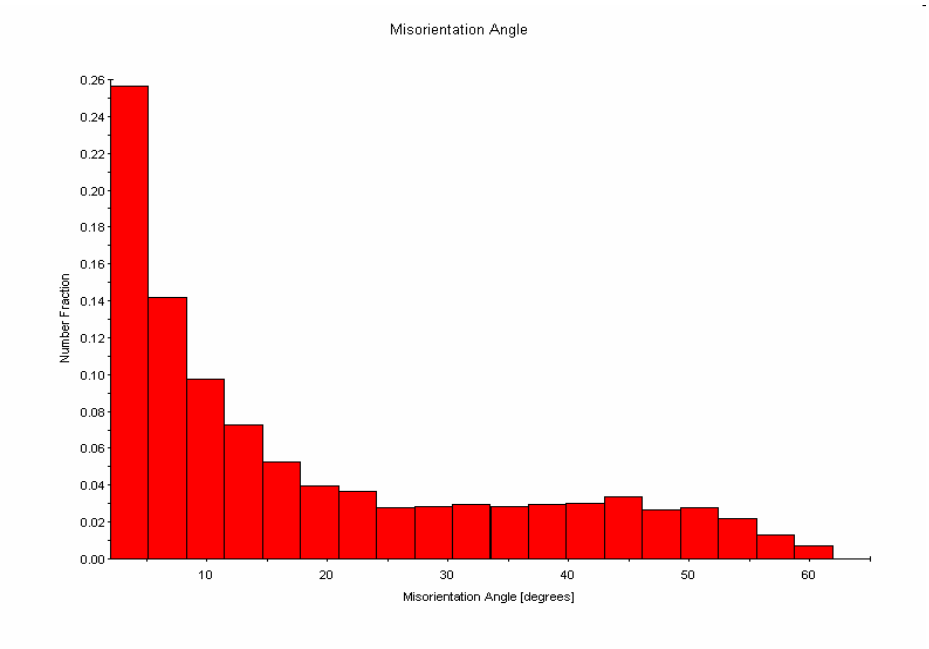

Figure B.11: Misorientation distribution after 4 ECAP pass in TD section.

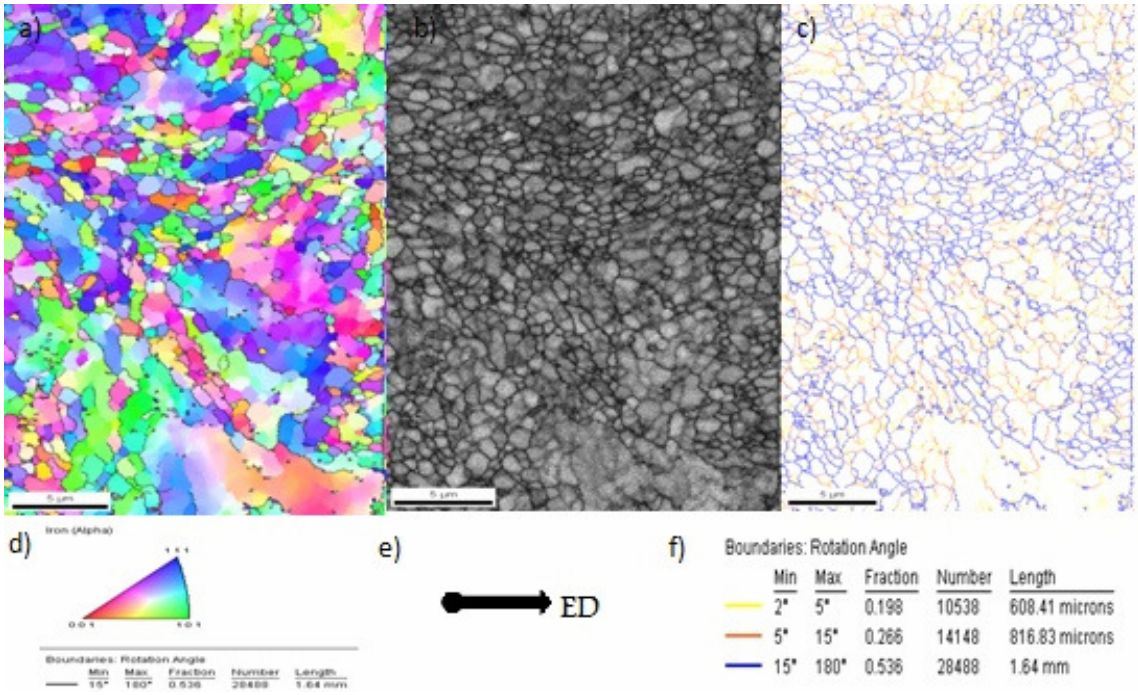

Figure B.12: EBSD scan of ULC steel after 5 ECAP pass in ED section a) Inverse pole figure map, coloured according to the scale in d, b) Image quality map, c) Boundary map, high angle boundaries (>15^0) indicated with a blue line, medium angle boundaries indicated with orange line (5^0-15^0) and low angle boundaries indicated with yellow (2^0-5^0) line according to the scale in f.

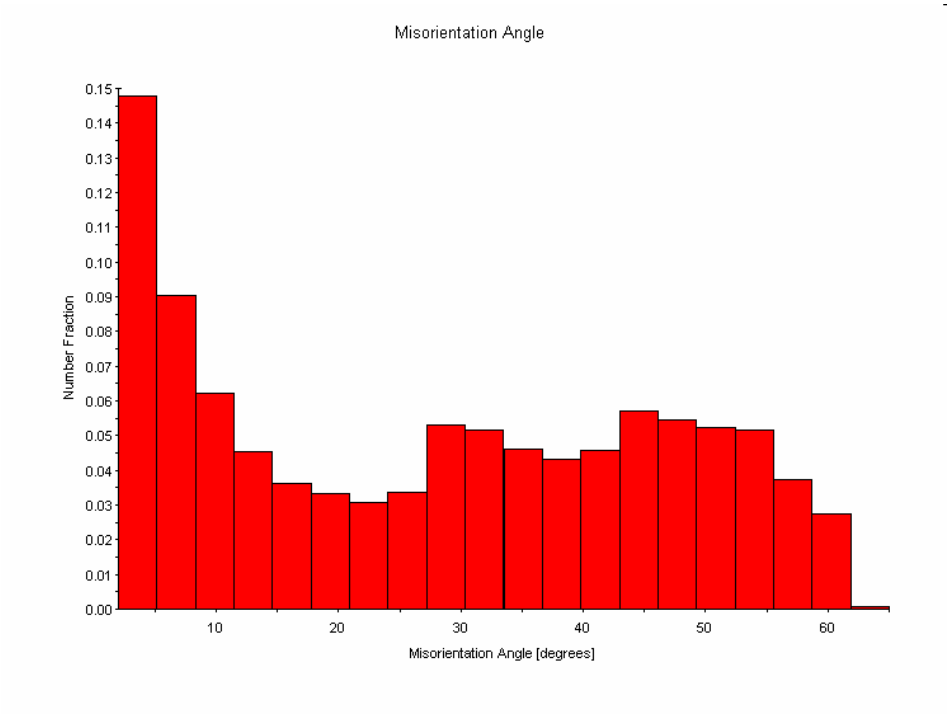

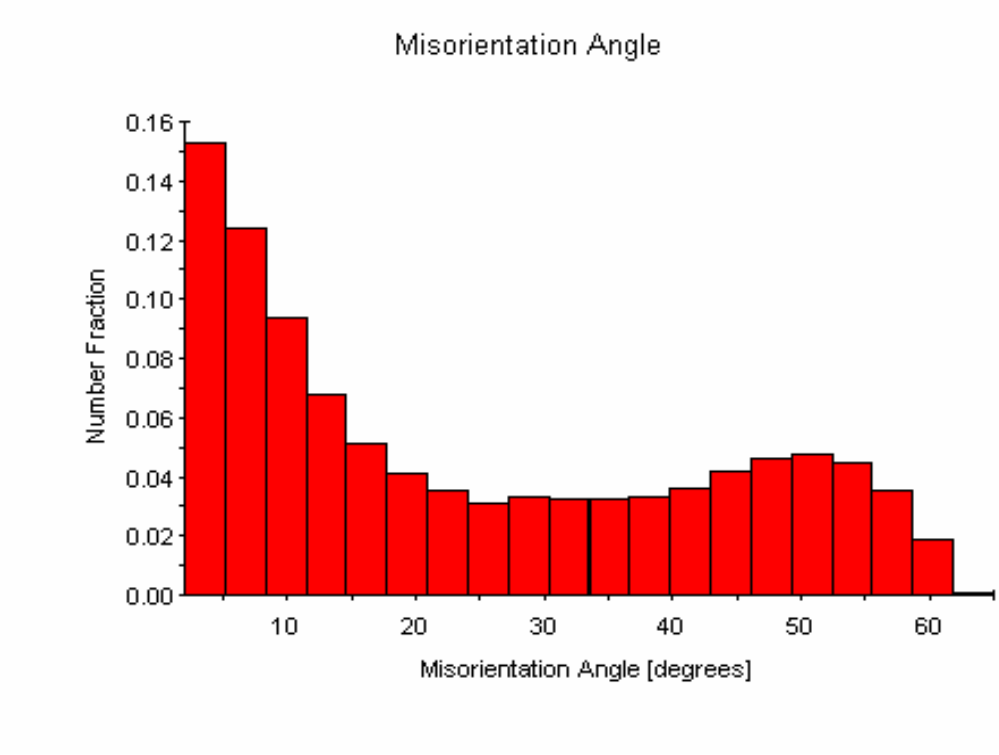

\

Figure B.13: Misorientation distribution after 5 ECAP pass in both cross sections.

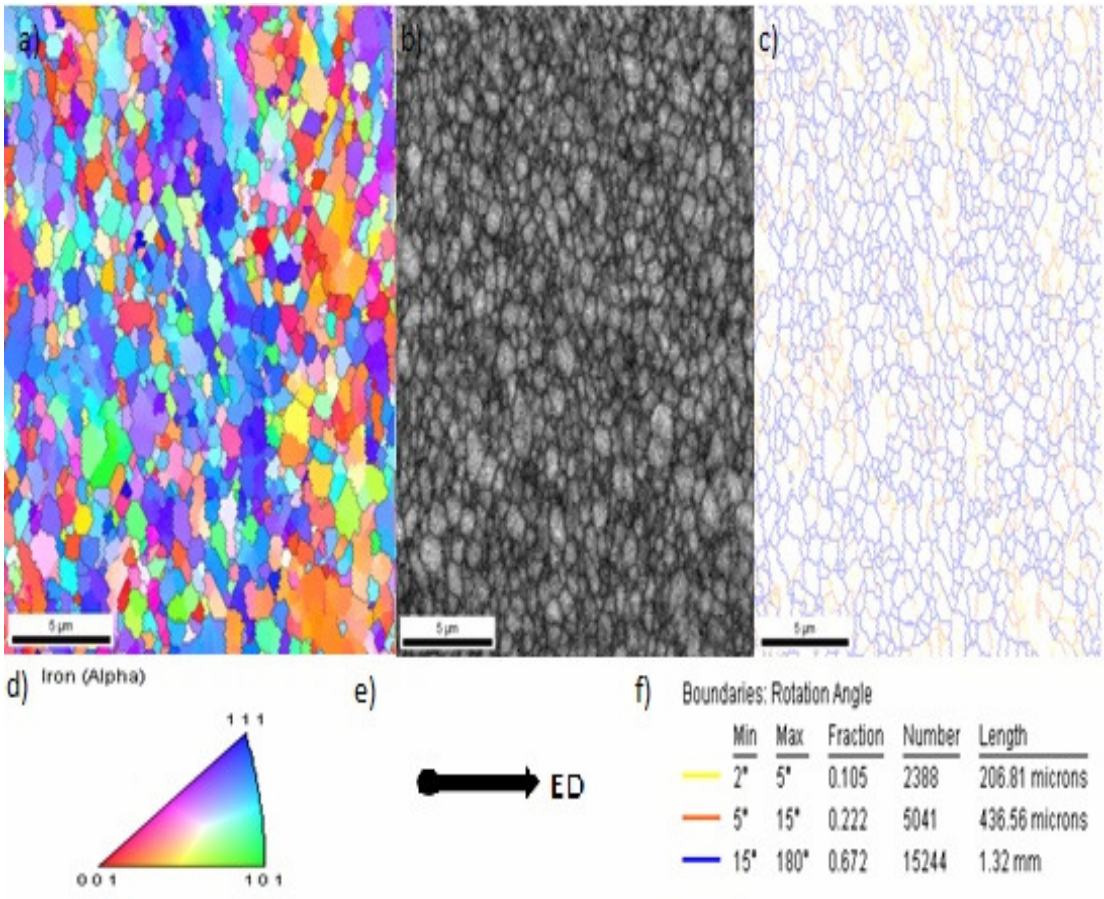

Figure B.14: EBSD scan of ULC steel after 8 ECAP pass in TD section a) Inverse pole figure map, coloured according to the scale in d, b) Image quality map, c) Boundary map, high angle boundaries (>15^0) indicated with a blue line, medium angle boundaries indicated with orange line (5^0-15^0) and low angle boundaries indicated with yellow (2^0-5^0) line according to the scale in f.

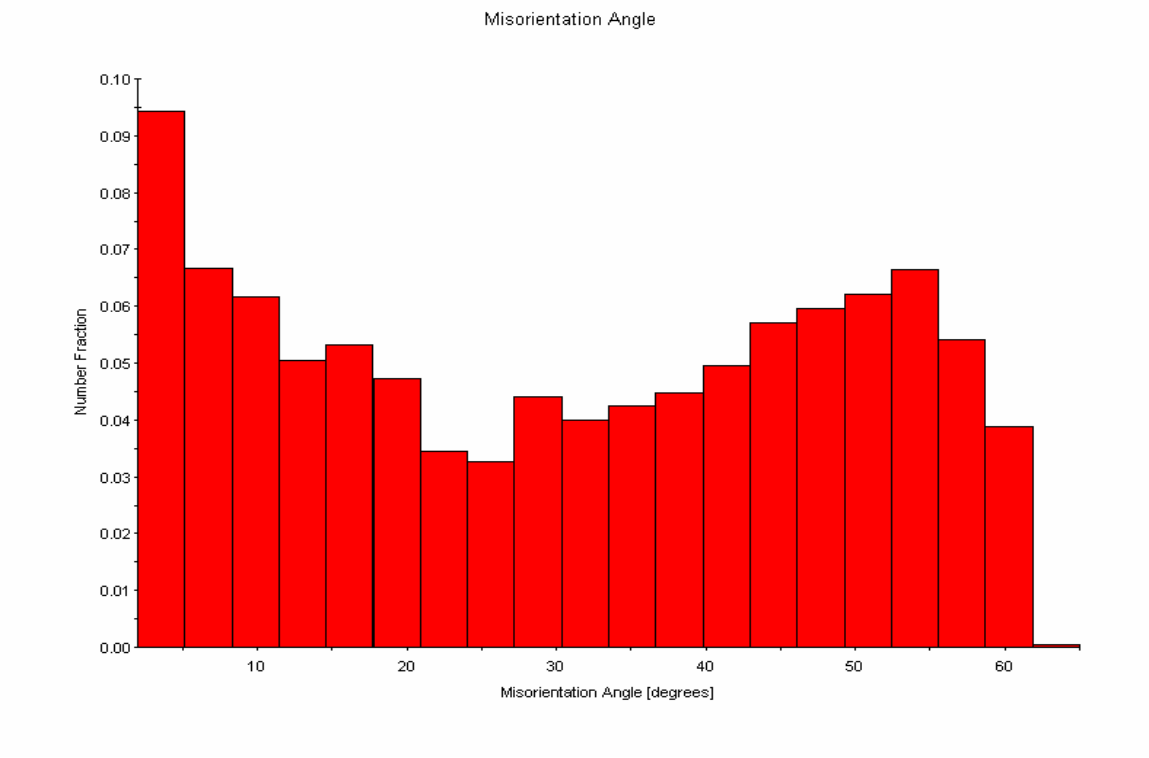

Figure B.15: Misorientation distribution after 8 ECAP pass in TD section.

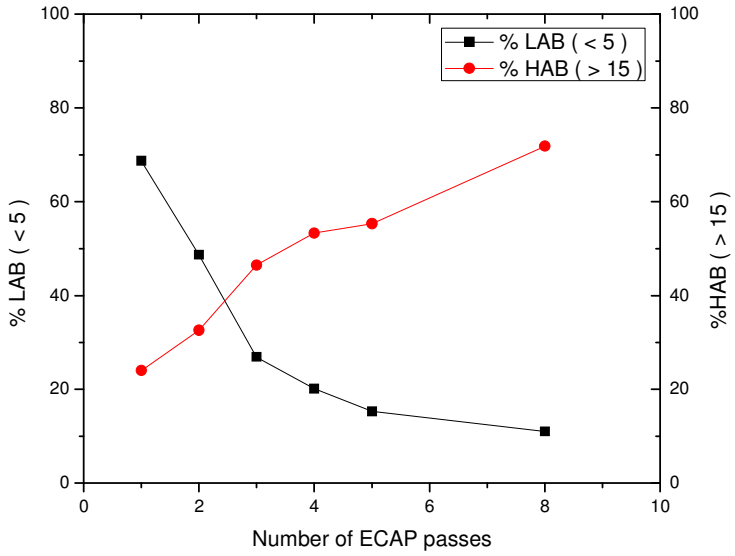

Figure B.16: Variation of angle boundary through ECAP passes in TD section.

BIOGRAPHY

Fatih UYSAL was born in June, 2 1984 in Kdz. Eregli. Following his high school graduation from Alaplı Anadolu Lisesi in 2002, he attended to Sakarya University to pursue a Bachelor of Science Degree in Metallurgy and Materials Engineering. After receiving his B. Sc. Degree in 2006, he was admitted to the department of Metallurgy and Material Engineering, Materials Engineering programme for his M. Sc. Studies.